The effects of future climate-induced adaptation of root zone storage capacity on modelled streamflow dynamics

by
Magali Ponds

January 5, 2022

A thesis presented for the degree of
Master of Science in
Water Management & Environmental Engineering

Student number: 4355792
Project duration: February 14, 2021 – January 13, 2022
Thesis committee:

Dr. M. Hrachowitz,	TU Delft, Chair
Dr. G. Schoups,	TU Delft
Dr. M. ten Veldhuis,	TU Delft
Dr. H. Zekollari	TU Delft

The effects of future climate-induced adaptation of root zone storage capacity on modelled streamflow dynamics

for obtaining a masters degree in Water Management & Environmental Engineering, TU Delft
Magali Ponds 4355792

Abstract. Hydrological models are often used to evaluate future changes in streamflow. Despite the strong awareness of non-stationarity in hydrological system characteristics, model parameters are often assumed stationary and obtained through calibration on past conditions. The representation of system change in hydrological models is challenging, as a lot of uncertainty abounds on changes in future climate and ecosystems. However, it is shown that ecosystems co-evolve with the prevailing climate conditions. There is increasing evidence that vegetation adapts its root zone storage capacity - considered as a key parameter in any hydrological model - corresponding to moisture deficits in the root zone. This is the main assumption underlying the water balance method. In combination with long-term water budget estimates from the Budyko framework, this method has the potential to meaningfully describe future climate-vegetation interactions within the context of process-based hydrological models. Accordingly, this study provides an exploratory analysis for six catchments in the Austrian Alps to investigate future changes in root zone storage capacity and their impact on modelled streamflow in the past and under two emission scenarios in the future. Our findings show that, although parameter ranges of the root zone storage capacity significantly narrow-down for climate-based estimates, modelling performance on past streamflow is similar when using the calibrated and climate-based parameter sets. Following climate projections from 14 climate models, adaptive climate-based parameter estimates are predicted to increase by 10-100% in all catchments in the future. However, little to no dissimilarity in modelled future streamflow is found when adaptation in root zone storage capacity is included in the hydrological model. Modelled differences in annual mean, maximum, and minimum flows remain within 5%, with slight increases for monthly streamflow and runoff coefficients. Thereby, little to no evidence is found that time-dynamic representation of root zone storage capacity significantly alters modelled future streamflow and suggests limited necessity for its inclusion in hydrological models to obtain reasonable descriptions of future streamflow in the investigated Alpine catchments.

1 Introduction

Climate change is expected to further increase global temperature and precipitation extremes in the future and thereby cause the hydrological cycle to accelerate (IPCC, 2021). Additionally, land cover is affected, amongst others through adjustments in plant biomass, species distribution, water use efficiency, photosynthesis and respiration rates (Stephens, Lall, Johnson, & Marshall, 2021). In turn, changes in land cover also impact the hydrological response, in some cases even more than climate change (Seibert & van Meerveld, 2016; Savenije & Hrachowitz, 2017). However, little is known about how ecosystems will change, due to the complex feedbacks between soils, vegetation and climate (Stephens et al., 2021). This complicates the modelling of emerging future hydrological processes under change, which is recognized as a major challenge in hydrology (Boschl, 2010; Berghuijs, Gnann, & Woods, 2020).

Hydrological models are often employed in change impact studies on both short- and long-term hydrological responses. These models link forcing (input) to streamflow (output) and can be distributed with regard to different hydrological response units (Savenije, 2010). The processes occurring in and between these units are largely represented through equations of physics. But, as data of sufficient detail and coverage is unavailable for several system properties, parameterization is commonly applied to complete the equations and thereby approximate system conditions. The required parameter values often result from calibration to streamflow observations or from literature (Boschl, 2010; Coron et al., 2012; Seibert & van Meerveld, 2016).

Despite the context of a changing climate, many models work with stationary system parameters. Although this assumption holds for predictions on shorter timescales, assuming long-term system stationarity under a changing climate is incorrect. Not the least, because ecosys-

tems can adapt towards prevailing climate conditions and thereby drastically alter a catchment water balance (Fenicia, Savenije, & Avdeeva, 2009; Jaramillo & Destouni, 2014; Nijzink et al., 2016; Savenije & Hrachowitz, 2017; Hrachowitz et al., 2020; Levia et al., 2020).

There is increasing evidence that vegetation dynamically adapts its root systems to the prevailing climate in order to guarantee water supply to the canopy (Schenk, 2002; Jochen Schenk, 2005). This is inherent to changes in the root zone storage capacity, which is the amount of water within reach of the root zone that can be used by vegetation to bridge droughts. As sub-surface water flow is mainly gravity-induced outside the root zone area, the root zone storage capacity is determining in the partitioning of water fluxes, i.e. the ratio between drainage and transpiration water fluxes, and an important regulator in runoff dynamics (Hrachowitz et al., 2020; de Boer-Euser, McMillan, Hrachowitz, Winsemius, & Savenije, 2016; Hrachowitz et al., 2020; de Boer-Euser et al., 2016). Therefore, changes in the root zone storage capacity are also reflected in transpiration and runoff rates and thus in the hydrological cycle (H. Gao et al., 2014; Zhang, Dawes, & Walker, 2001; Bouaziz et al., 2021). In current hydrological models, the root zone storage capacity is represented by model parameter (S_R). Its value is traditionally based on soil characteristics and root zone estimates or determined through calibration (Andréassian, Parent, & Michel, 2003). However, required observations of soil characteristics and the rooting system are scarce in both space and time and are difficult to extrapolate to the catchment scale, due to heterogeneity of the landscape (Wagener, 2007; Dueth-mann, Bloschl, & Parajka, 2020). Alternatively, the parameter can be calibrated on past streamflow. Still, none of these methods considers the dynamic nature of the root zone and its dependency on climate, ecosystems and land cover change. Hence, a better understanding and representation of vegetation responses towards changing climate conditions are needed to make more robust simulations of hydrological runoff evolution in the future. (Coron et al., 2012; Keenan et al., 2013).

The importance of including hydrological system changes, and hence non-stationarity, in hydrological models has been increasingly recognized over the past years (P. C. Milly et al., 2008; Merz, Parajka, & Blöschl, 2011; Bouaziz et al., 2021). Yet, the underlying interactions and feedback mechanisms between climate, vegetation, soils, ecosystems and humans are complex, not entirely understood and hence hard to represent. Besides that, changes often occur gradually and simultaneously with other changes (Seibert & van Meerveld, 2016; Stephens, Marshall, & Johnson, 2019; Bouaziz et al., 2021). The main methods to explain the relationship between catchment change and hydrological functioning are based on paired watershed methods and hydrological modelling studies (Andréassian et al., 2003). In hydrological modelling, system evolution is often reflected by changing one or more parameters values based on a combination of literature with adapted land-cover maps (Buytaert & Beven, 2009; J. Gao, Holden, & Kirkby, 2015). Although this is valuable for testing the sensitivity of hydrological response towards change (Seibert & van Meerveld, 2016), these approaches require an understanding of how catchment characteristics relate to model parameters. As such, a-priori estimations and regionalization approaches of catchment characteristics face considerable uncertainty (Wagener, 2007). The required data (e.g. future land-use maps or vegetation indices) may also be unavailable in the context of a changing climate (Duethmann et al., 2020).

This illustrates the need for an alternative approach that could rigorously upscale or downscale soil-vegetation hydrological interactions, whilst accounting not only for spatial heterogeneity but also for temporal dynamics (Stephens et al., 2021).
A solution can be found in approaches that are based on large-scale optimality principles and consider the co-evolution of climate, soil and vegetation in a holistic way (Boschl, 2010). Accordingly, several studies evidenced that the root zone storage capacity - a key parameter in any hydrological model - can be derived from annual water deficits (H. Gao et al., 2014; de Boer-Euser et al., 2016; Wang-Erlandsson et al., 2016; Nijzink et al., 2016; Bouaziz et al., 2021). Following the water balance method, the root zone storage capacity of vegetation is estimated based on the assumption that vegetation adapts its root zone in order to bridge droughts. Thereby vegetation maximizes water accessibility and minimizes waste of water resources (H. Gao et al., 2014; Gentine, D'Odorico, Lintner, Sivandran, & Salvucci, 2012). The water-balance method requires only precipitation and evaporation data, which are available for the past. However, evaporation time-series are subjective to complex climate-vegetation interaction, which makes them subjective to uncertainty and hard to predict (P. C. D. Milly & Dunne, 2011).
However, despite the complexity and heterogeneity of landscapes in different climates, the Budyko framework manages to reasonably describe the long-term (»1 year) mean partitioning of water fluxes at the catchment scale. According to this framework, the proportion of precipitation that evaporates, defined as the evaporative index ($\frac{E_a}{P}$), is mainly controlled by climate, expressed in the aridity index ($\frac{E_p}{P}$). Changes in climate are reflected by horizontal shifts in the Budyko space, along the Budyko curve. In addition, the influence of catchment characteristics, including topography, vegetation and soils, is

reflected by vertical shifts in the Budyko space. This results in a systemic scatter around the curve, which could mean that partitioning of water fluxes is not solely climate-controlled, but instead results from the co-evolution of catchment properties and climate characteristics. Troch, Carrillo, Sivapalan, Wagener, and Sawicz (2013) further evidence this hypothesis, showing catchment to deviate from the Budyko curve when exchanging climates across different catchments in a modelling experiment. Parametric Budyko equations combined these other influences in a catchment specific parameter and hence a catchment specific Budyko curve (Fu, 1981; Zhang et al., 2004). As such, both changes in future climate and vegetation can be accounted for in the partitioning of water fluxes.

1.1 Case study description

Hence, combining the water balance method with long-term water budget estimates of a parameterized Budyko framework could serve as a robust way to investigate how climate change influences hydrological system characteristics and, as a result, streamflow (Zhang et al., 2001; Bouaziz et al., 2021). This approach answers the need of adopting a process-based method, that accounts for the inter-dependency of climate, soil and landscape, whilst requiring only little, but available, input data.
This study provides an exploratory analysis of the method first proposed by Bouaziz et al. (2021), in six catchments in the Austrian Alps. The main aim is to (i) gain a broader and more robust understanding of how climate change induces dynamics in the root zone storage capacity and (ii) investigate how model response changes accordingly in the past and (iii) in the future.
To answer these research objectives, three successive phases are conducted. Firstly climate-based estimates of the root zone storage capacity for the past and future are derived through complimentary use of the Budyko framework and the water balance method. Next, the use of climate-based parameter values is validated based on model performance on observed streamflow using the FLEX-topo model, as proposed by Hanus (2020). Lastly, this model, using either stationary or adaptive climate-based parameters root zone storage capacity, is deployed to investigate the effect on future runoff predictions.

2 Study Area & Data

This study aims to predict past and future streamflow for six catchments in the Austrian Alps. The therefore deployed catchment and climate data are elaborated upon in this section.

2.1 Study Area

The six selected catchments in the Austrian Alpine region (Figure 1) are of additional relevance as high elevation areas are particularly vulnerable to climate change (IPCC, 2019). Together, the study areas cover a broad spectrum of climates, sizes, environments and topography (Table 1).
The Pitztal has the highest mean altitude of 2558m and features a nivo-glacial discharge regime. It is located in the center of Austria and is largely bare (70%, with 18% glacial coverage). The lowest catchment is the Feistritztal, with a mean altitude of 917m. It is located in the east of Austria, features a nivo-pluvial discharge regime and a relatively dense vegetation cover (72% forest and 25% grass). All other catchments have a nival regime but differ in mean elevation between 1315m (Paltental) and 2233m (Defreggental). The land cover varies in correspondence with altitude: The dominant land cover in high altitude catchments is bare rock and grassland, whereas lower elevation catchments are mainly covered by forest. The most west located catchment is the Silbertal, whereas the Feistritztal has the most easterly location.

2.2 Data

This study provides a past-future analysis for modelled streamflow, using different models. The past and future time frames cover a period of 30 years, respectively between 1981-2010 and 2071-2100. The deployed datasets are elaborated upon below.

2.2.1 Historical data

Firstly, historical discharge, land cover and topography data were used to set up the hydrological model. Daily discharge sums are used from the Hydrographic Service Austria (https://ehyd.gv.at). Land cover data of the catchments is derived from observations of the CORINE Land Cover dataset (https://land.copernicus.eu/pan-european-corine-land-cover, 2018) (Table 1). The riparian zone was determined based on a 10 $\times$ 10 height-above-nearest-drainage map (HAND) (Prenner, Hrachowitz, & Kaitna, 2019). Topographic information is derived from a 10 $\times$ 10 digital elevation model (DEM) of Austria (https://www.data.gv.at/katalog/dataset/dgm). Daily gridded snow cover data from satellites (MOD10A1) was utilized for the calibration (Hall & Riggs, 2016). Historic glacier outlines between 1997-2006 were available at the Austrian Glacier Inventory (https://www.uibk.ac.at/acinn/research/ice-and-climate/projects/austrian-glacier-inventory.html.en)

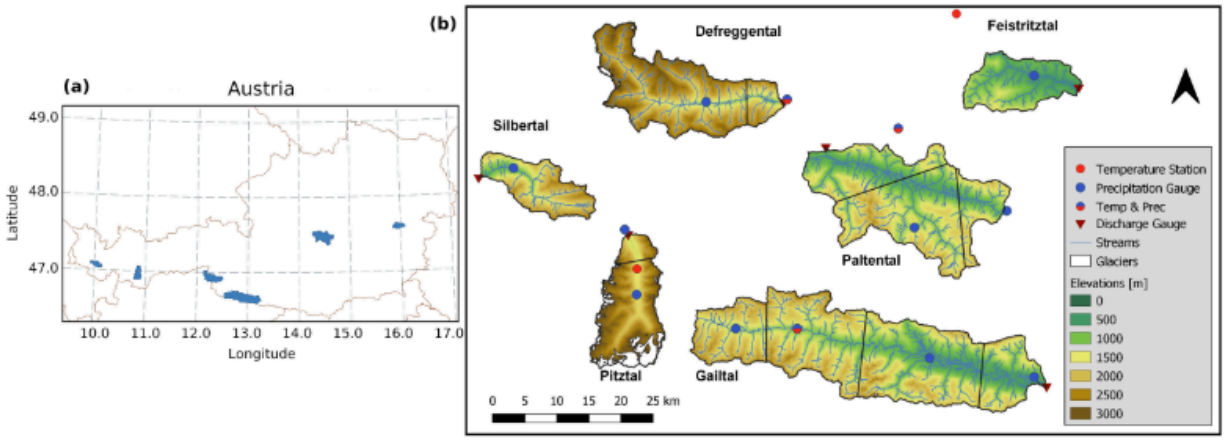

Figure 1: **(a)** Location of the catchments in Austria. **(b)** Catchment outlines indicating altitude, different precipitation zones and the location and number of Precipitation Gauges and Temperature Stations (Right) (Hanus, 2020)

Table 1: Catchment characteristics, land cover data & discharge regimes based on Mader et al. (1996)

	Feistritztal	Gailtal	Paltental	Silbertal	Defreggental	Pitztal
Characteristics						
Mean Altitude [m]	917	1476	1315	1776	2233	2558
Elevation [m]	449-1595	596-2778	633-2447	671-2764	1096-3763	1339-3763
Area [km^2]	116	587	370	100	267	166
Prec. Gauges [#]	1	4	3	1	2	2
Discharge Regime	Nivo-pluvial	Autumn nival	Moderate nival	Nival	Nival	Nivo-glacial
Land cover						
Bare (Glacier) [%]	0 (0)	8 (0)	4 (0)	20 (0)	43 (1.5)	70 (18)
Grass [%]	25	33.5	32	46	32	23
Forest [%]	72	56.6	61	32	23	6
Riparian [%]	3	2	3	2	2	1

(Lambrecht & Kuhn, 2007; Abermann, Fischer, Lambrecht, & Geist, 2010). Linear interpolation between observation years has been applied to extrapolate changes in glacier outlines up to 2015.

Subsequently, to simulate past streamflow the model is forced with observed climate data. Temperature and precipitation data is retrieved from the Austrian Central Institute for Meteorology and Geodynamics (ZAMG) and the Hydrographic Service Austria. The location of the consulted precipitation and temperature stations is indicated in Figure 1. All data has been normalized to daily resolution. For each catchment, the plausibility of the datasets was checked according to correspondence with the long-term water balance. A mismatch was found for the Defreggental and Silbertal, where long-term precipitation exceeded long-term discharge. Hence, past discharge measurements of these catchments are scaled to match long-term water balance estimates of the Budyko framework.

2.2.2 Projected data

The prediction of future streamflow requires time-series of climate data, snow cover and glacier outlines. Future precipitation and temperature data are generated from 14 high-resolution climate projections, based on the EURO-CORDEX data (Table 2). Each regional climate model employs two emission scenarios, respectively RCP 4.5 and RCP 8.5 (Switanek et al., 2017). All future climate datasets are retrieved at the station scale and cover the period from 1950-2100.

The future evolution of glaciers in the Pitztal under different emission scenarios is represented by model outputs of Zekollari, Huss, and Farinotti (2019).

Table 2: EURO-CORDEX projections used in this study

ID	GCM	RCM
1	CNRM-CM5 r1i1p1	CCLM4-8-17
2		ALADIN53
3		RCA4
4	EC-EARTH r1i1p1	RACMO22E
5	EC-EARTH r3i1p1	HIRHAM5
6	EC-EARTH r12i1p1	CCLM4-8-17
7		RCA4
8	CM5A-MR r1i1p1	WRF361H
9		RCA4
10	HadGEM2-ES r1i1p1	CCLM4-8-17
11		RCA4
12		RACMO22E
13	MPI-ESM-LR r1i1p1	CCLM4-8-17
14		RCA4

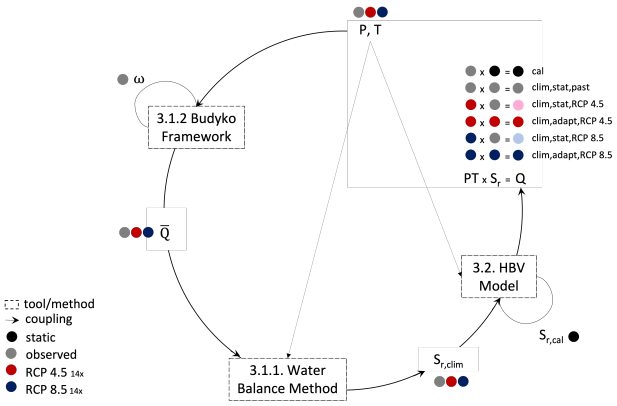

Figure 2: Process scheme of step wise approach. Steps followed are (3.1.2) Estimate long term runoff coefficient from the Budyko framework. (3.1.1) Determine climate-based root zone storage capacity values. (3.2) Implement climate-based and calibrated S_R to predict past and future streamflow. Respective indices refer to sections numbers.

3 Methods

This study adopts the top-down and process-based approach as is shown in Figure 2, with the main aim to describe the interactions between changes in climate and vegetation (3.1) and the potential impacts thereof on streamflow in the past and future (3.2). Therefore, the following step-wise approach is adopted: Firstly, short-term water balances (3.1.1) are combined with long-term water balance estimates (3.1.2) to describe corresponding developments in the root zone storage capacity of vegetation (3.1.3). This results in climate-based estimates of root zone storage capacity $S_{R,clim}$, that are subsequently verified by implementation in a FLEX-topo hydrological model (3.2.2). On the condition that the climate-based parameter model can reasonably describe past streamflow signatures, the model is subsequently deployed to investigate potential changes in future streamflow characteristics (3.2.3).

3.1 Climate change induced adaptation of the root zone storage capacity of vegetation

The root zone storage capacity is the amount of water stored in the unsaturated zone that can be held against gravity, which is accessible to the roots of vegetation for transpiration. Hence, it is a key controlling factor in the partitioning of precipitation into evapotranspiration and runoff in a catchment. Since vegetation co-evolves with a changing climate, the partitioning of water fluxes alters accordingly. This dynamic should hence be considered to match long-term future evaporation and runoff in a changing climate. To describe future adapted root zone storage capacities in a changing climate, this study combines short-term and long-term runoff estimates, respectively derived from the water balance method and the Budyko framework.

3.1.1 Using short-term water balances to quantify vegetation root-zone storage capacity

The water balance method describes climate-induced dynamics in the root zone of vegetation, based on the assumption that vegetation adapts its root-zone storage capacity to offset future hydroclimatic seasonality, by building a buffer large enough to bridge dry spells (Gentine et al., 2012; Donohue, Roderick, & McVicar, 2012; H. Gao et al., 2014). Hence, the water balance method estimates the amount of excess transpiration over effective precipitation ($(P_E - E_R)$, which is assumed to originate only from the water stored in the unsaturated zone. Daily deficits are then accumulated over the total the period of water shortage ($T_0 - T_1$), to estimate the total water buffer stored in the root zone (Equation 1). Thereby, T_0 marks the first day at which transpiration exceeds effective precipitation ($(P_E - E_R) < 0$) and T_1 represents the day at which the root zone storage deficit is restored to zero ($S_{R,def} = 0$). Previous studies have shown that different vegetation types develop root systems that can bridge droughts of different return periods. Following this assumption, the root zone storage capacity of grass and forest would develop to endure droughts with a return period of respectively 2 and 20 years (H. Gao et al., 2014; Nijzink et al., 2016; de Boer-Euser et al., 2016; Wang-Erlandsson et al., 2016; Hrachowitz et al., 2014). As the rooting

depth of riparian vegetation is limited by high groundwater levels, the root zone storage capacity is assumed to equal that of grass. Corresponding root zone storage capacities for grass, forest and riparian vegetation can be retrieved from the Gumbel extreme value (GEV) distribution, using a time series of annual maximum deficits.

$$S_{R,def}(t) = \min \int_{T_0}^{T_1} \left(P_E(t) - E_R(t)\right) dt \quad (1)$$

To determine yearly maximum storage deficits, daily time series of transpiration and effective precipitation are required. Daily transpiration series are obtained from daily time series of precipitation, potential evaporation, and a long-term runoff coefficient. Effective precipitation, defined as the liquid water input from snowmelt (M) and remaining precipitation after interception ($-\frac{dS_I(t)}{dt} - E_I$), is estimated from the water balance of the canopy storage (Equation 2). To minimize the influence of the unknown interception storage capacity (I_{max}) of the interception storage (S_I), a random sample of 300 different I_{max} values, ranging between 1-3mm has been used. A set of 300 values showed to be the threshold for obtaining a stable range in effective precipitation values (P_E) and hence root zone storage deficits ($S_{R,def}$) (Appendix A.2).

$$P_E(t) = P(t) + M(t) - E_I(t) - \frac{dS_I(t)}{dt} \quad (2)$$

The long term transpiration ($\overline{E}_R$) is derived from the long-term water balance (Equation 3, all in $mmyr^{-1}$), under the assumption that the long-term inter-catchment groundwater flows and storage changes are negligible ($\overline{E}_A = \overline{P} - \overline{Q} < \overline{E}_P$). The long-term transpiration is subsequently scaled to daily transpiration estimates, using the daily signal of potential evaporation minus interception evaporation (Equation 4). Note that this transpiration estimate also includes soil evaporation, as these fluxes could not be separated using the available data.

$$\overline{E}_r \approx \overline{P}_E - \overline{Q} \quad (3)$$

$$E_R(t) = (E_P(t) - E_I(t)) \cdot \frac{\overline{E}_R}{(\overline{E}_P - \overline{E}_I)} \quad (4)$$

However, to complete the water balance method for the future, a long-term mean runoff coefficient is required and obtained from the Budyko framework.

3.1.2 Long term water balance framework for estimating changes in future runoff

The Budyko framework is consulted to obtain a well-founded estimate of the long-term mean runoff coefficient. This relationship describes how climate - expressed as the aridity index ($\frac{\overline{E}_P}{\overline{P}}$) controls the long term partitioning of precipitation ($\overline{P}$) into evaporation ($\overline{E}_a$) and runoff ($\overline{Q}$). Thereby, the Budyko space is bounded by the (i) supply limit, as no more water can evaporate than is available, and the (ii) demand limit, as long-term evaporation cannot exceed potential evaporation. (Zhang et al., 2001; Xing, Wang, Zou, & Deng, 2018; Mianabadi, Davary, & Pourreza-bilondi, 2020; Berghuijs et al., 2020). Despite its relatively simple outlook and low requirement for input data, the Budyko curve manages to reasonably capture the partitioning of water fluxes in virtually every catchment around the world (Berghuijs et al., 2020).

However, the original Budyko relationship does not explicitly consider the combined influence of soil, topography and vegetation. This is an likely explanation for the systemic scatter found around the Budyko curve (Troch et al., 2013). In response, parameterized Budyko equations, such as the Fu equation, account for catchment biophysical features through the catchment specific parameter(ω) (Equation 5) (Fu, 1981).

$$\frac{\overline{E}_A}{\overline{P}} = 1 - \left(\frac{\overline{Q}}{\overline{P}}\right) = 1 + \left(\frac{\overline{E}_P}{\overline{P}}\right) - \left(1 + \left(\frac{\overline{E}_P}{\overline{P}}\right)^{\omega}\right)^{\frac{1}{\omega}} \quad (5)$$

Despite several attempts, it remains difficult to constitute a value for ω from individual influencing factors, due to the heterogeneity and interdependency of catchment-specific influences. Therefore the relationship between changing vegetation dynamics and changed catchment specific parameter is likely also catchment specific (Dwarakish & Ganasri, 2015; Sankarasubramanian, Wang, Archfield, Reitz, & Vogel, 2020; Jaramillo et al., 2018; Berghuijs et al., 2020; Jaramillo & Destouni, 2014; Jaramillo et al., 2018; Van der Velde et al., 2014). Alternatively, the value of ω can be determined by solving Equation 5, using observed climate and discharge data, averaged over a 30-year time period (1981-2010), (P_{obs}, T_{obs},Q_{obs}). The resulting parameter value (ω_{obs}) hence represents historical catchment conditions.

To investigate how solely changes in climate influence the future long-term mean runoff in the catchment, it is assumed that soil, topographic and vegetative conditions remain unchanged over time. Hence, the ω_{obs}-parameterized Budyko curve can be used to derive changes in the future partitioning of water fluxes in response to the changing climate.

Thereby, future changes in climate reflect in an altered aridity index, as a consequence of changed precipitation rates ($\Delta\overline{P} = \overline{P}_{fut} - \overline{P}_{obs}$), temperature and hence potential evapotranspiration ($\Delta\overline{E}_P = \overline{E}_{P,fut} - \overline{E}_{P,obs}$) (Figure 3a). Here, the Thornthwaite formula is adopted

to calculate potential evaporation from temperature input, as several studies declare adequate performance in humid regions (Yates, 1994; Li, Yang, Kan, & Hong, 2018). Changes in climate cause a horizontal shift in the Budyko space, moving a catchment from initial position (p_{obs}), along the ω_{obs}-parameterized Budyko curve to a new position (p_{fut}) (Equation 6). The new location thereby indicates the future evaporative index and hence runoff coefficient ($\overline{Q}_{fut}$).

$$\left(\frac{\overline{E}_P}{\overline{P}_{fut}} = \frac{\overline{E}_{P,obs} + \Delta\overline{E}_P}{\overline{P}_{obs} + \Delta\overline{P}}\right) \tag{6}$$

$$\begin{aligned}\left(\frac{\overline{Q}}{\overline{P}}\right)_{fut} &= \left(\frac{\overline{Q}_{obs} + \Delta\overline{Q}}{\overline{P}_{obs} + \Delta\overline{P}}\right) \\ &= -\left(\left(\frac{\overline{E}_P}{\overline{P}}\right)_{fut} - \left(1 + \left(\frac{\overline{E}_P}{\overline{P}}\right)^{\omega}\right)^{\frac{1}{\omega}}\right)\end{aligned} \tag{7}$$

3.1.3 Combining the long- and short-term water balances to describe future changes in the root zone storage capacity

By combining the Budyko framework and the water balance method, future changes in root zone storage capacity can be quantified. Drawing upon the Budyko framework, runoff coefficients are estimated for the past and future. Thereby respectively observed meteorological data (1981-2010) and future climate projections (2071-2100) of 14 RCMs and 2 different RCPs are used to estimate a total of 29 runoff coefficients per catchment. Through implementation in the water balance equations, 29 root-zone storage capacity estimates were derived for each vegetation type. Note that the use of a range of 300 values of I_{max} values results in parameter ranges instead of single parameter values.

To account for potential biases in the projected climate data, the respective modelled future ($S_{R,clim,fut}$) values are scaled to the difference between observed and modelled past root zone storage parameters, according to Appendix A.3 (Bouaziz et al., 2021). A second correction is applied to account for the respective area share of vegetation. Initially, the found $S_{R,clim,fut}$ values represent root zone storages in a catchment entirely covered by either forest, grass or riparian vegetation, which results in too large estimates of the actual root zone storage capacity of the vegetation types in the catchment.

3.2 Hydrological model

The influence of a climate-based root zone storage capacity parameter on modelled streamflow is tested using a process-based, semi-distributed hydrological model, as utilized and employed by Hanus (2020). This hydrological model represents the dominant rainfall-runoff processes in the catchments based on topography and land cover classes. It thereby acknowledges the importance of landscape on runoff behavior, whilst retaining a simplistic model approach (Savenije, 2010). The model structure is depicted in Figure 4, and considers four hydrological response units (HRUs): bare rock, forested hillslope, grassland hillslope and riparian zone. In each timestep, all units are first run separately. Afterward, the total runoff is generated as the weighted sum of the runoffs of the individual units. The model includes the storage components of interception, unsaturated root zone and a fast and slow storage component, i.e. groundwater. All relevant equations are displayed in Table 3, whereas a more detailed model description is provided in Hanus (2020). The model code is written in Julia (`https://julialang.org/`) and available on GitHub (`https://github.com/magaliponds/Thesis-model`).

3.2.1 Calibration & Evaluation

In total, the model features 20 parameters that are initially calibrated on observed streamflow data and are hereafter referred to as the stationary parameter set. For the Pitztal an additional loss parameter was included that accounts for water divergence from the catchment. Following the work of Hanus (2020, Appendix B), all parameters have been constrained a-priori based on literature (Brenner et al., 2019; H. Gao et al., 2014). Additional constraints are provided to ensure that parameter combinations match the perceptions of the system, e.g. the interception capacity of forest is larger than that of grass (Gharari, Hrachowitz, Fenicia, Gao, & Savenije, 2014).

The model has been calibrated using 8 objective functions to ensure correct process representation (Table 4), (Efstratiadis & Koutsoyiannis, 2010). These functions cover the timing of high and low flows, the magnitude of flows, the memory of the catchment and the partitioning between evaporation and runoff. All functions are equally weighted, as the calibrated model aims to represent overall system dynamics. The overall model performance was assessed using the Euclidian Distance (D_E) from the perfect model fit (Hrachowitz et al., 2014).

For each catchment, a random Monte Carlo Sampling of 1.000.000 realizations was performed, resulting in the same amount of possible parameter combinations. These are subsequently called parameter sets. Calibration was run for each parameter set over 20 years (Oct 1985 - Oct 2005), with a 3-year warm-up period. Only the best performing 0.01% has been selected, corresponding to a Euclidean Distance equal to or below 0.2. Thereby ill-performing parameter combinations are excluded and constraints parameter uncertainty due to the

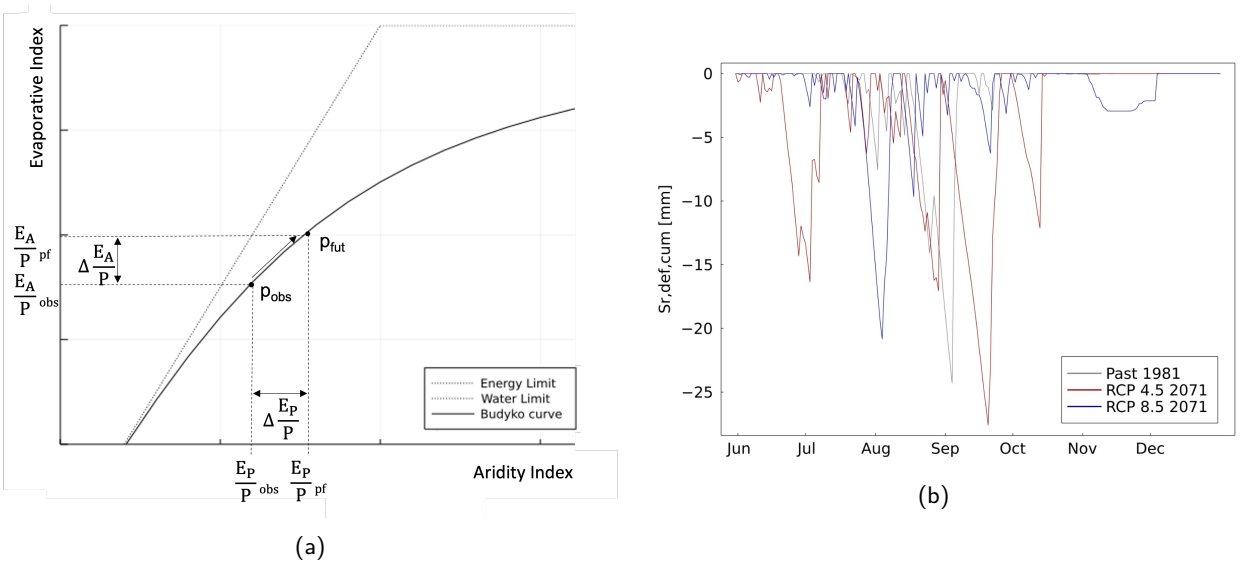

Figure 3: **(a)** Representation of the Budyko space, showing the Evaporative Index $\frac{E_A}{P}$ and the Aridity Index $\frac{E_P}{P}$ and the energy and water limit. Using observed climate data, $\frac{E_A}{P}_{obs}$ and $\frac{E_P}{P}_{obs}$ respectively, a catchment plots on position p_{obs} on the parametric Budyko curve with parameter ω_{obs}. A changed climate, and hence altered input data, results in an altered Aridity Index ($\frac{E_P}{P}_{fut}$). This causes the catchment to move along the Budyko curve ($\frac{E_P}{P}_{\Delta}$) towards position p_{fut}, that corresponds with a future Evaporative Index ($\frac{E_A}{P}_{fut}$). **(b)** Cumulative storage deficits ($S_{R,def}$), derived from effective precipitation (P_E) and transpiration (E_R) using the observed past data and climate projections for RCP 4.5 and RCP 8.5

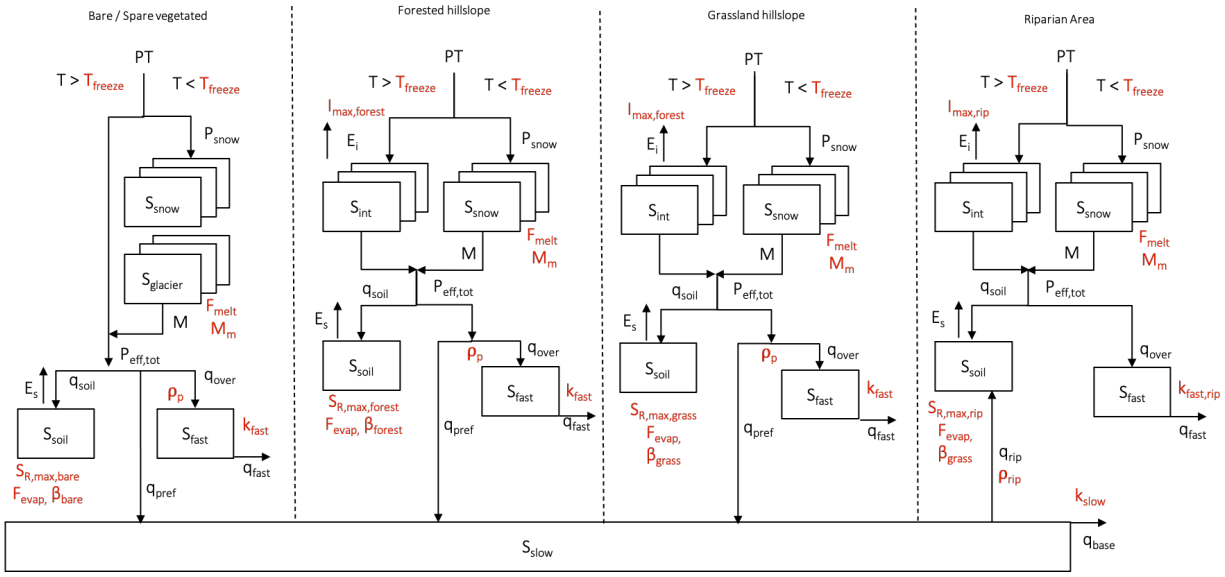

Figure 4: Schematization of model structure per precipitation zone. Based on topography, the model is distributed with regard to four Hydrological Response Units. Boxes represent states, black arrows are fluxes and Red indicates parameter

concept of equifinality - the phenomenon that different combinations of parameters can acceptably reproduce observed runoff (Beven & Binley, 1992). The selected 300 parameter sets are subsequently evaluated using the same objective functions as described before (Table 4) over a period of 8 to 10 years, from 2005 to 2013 (2015), depending on data availability. Subsequently, these 300 parameter sets are called calibration parameter sets. The

Table 3: List of equations used in the hydrological model. An more extensive description can be found in Hanus (2020)

Reservoir	Water balance Equation	Constitutive functions
Interception	$\frac{dS_{int}}{dt} = P_{rain} - E_{int} - P_{eff}$	$P_{eff} = \max(S_{int} - I_{max}, 0)$ $E_{int} = \min(0.5 \cdot E_{pot}, S_{int})$
Snow	$\frac{dS_{snow}}{dt} = P_{snow} - M_{snow}$	$M = F_{melt} \cdot M_M \left(\frac{T - T_{tresh}}{M_M} + \ln\left(1 + \exp\left(-\frac{T - T_{tresh}}{M_M}\right)\right)\right)$ $M_{snow} = \min(M, S_{snow})$ $M_{glacier} = M$ $M_{tot} = M_{snow} \cdot (1 - A_{gl}) + M_{glacier} + A_{gl}$
		$P_{eff,tot} = \sum_{i=1}^{Elevations} P_{eff} + \sum_{i=1}^{Elevations} M_{tot}$
Unsaturated Zone	$\frac{dS_{soil}}{dt} = P_e - E_{soil} - R$ $\frac{dS_{soil,rip}}{dt} = P_e Q_{rip} - E_{soil} - R$	$q_{soil,rip} = P_{eff} + Q_{rip} - R$ $q_{soil} = P_{eff} + Q_{rip} - R$ $S_{R,m} = (1+\beta) S_{R,max} \left(1 - \left(1 - \frac{S_R}{S_{R,max}}\right)^{1/(1+\beta)}\right)$ $R = P_{eff} - S_{R,max} + S_R + S_{R,max} \cdot \left(1 - \frac{P_{eff} + S_{R,m}}{(1+\beta) S_{R,max}^{1+\beta}}\right)$ $Perc = Perc_{max} \frac{S_R}{S_{R,max}}$ $E_{soil} = (E_{pot} - E_{int}) \cdot \min\left(\frac{S_{Soil}}{S_{soil,max} \cdot F_{evap}}, 1\right)$ $S_{soil} = S_{Soil} + P_{eff} - E_{Soil} - R$ $S_{soil,rip} = S_{Soil} + P_{eff} - E_{soil} - R$
Fast Reservoir	$\frac{dS_{fast}}{dt} = q_{overland} - q_{fast}$	$q_{overland} = (P_{eff,tot} - q_{soil}) \cdot \rho_p$ $q_{overland,rip} = P_{eff,tot} + q_{rip} - q_{soil,rip}$ $q_{fast} = k_{fast} \cdot S_{fast}$
Slow reservoir	$\frac{dS_{slow}}{dt} = \sum_{i=i}^{HRU} q_{pref} - q_{slow}$	$q_{pref} = (P_{eff,tot} - q_{soil}) \cdot (1 - \rho_p) + R$ $q_{slow} = k_{slow} \cdot S_{slow}$

depending on data availability. Subsequently, these 300 parameter sets are called calibration parameter sets. The main focus of this study is the catchment average root zone storage capacity parameter.

3.2.2 Testing climate-based root zone storage parameters for modelling past streamflow

To test the influence of inclusion of non-stationarity in the root zone on, streamflow predictions, modelled using climate-based and calibration parameter sets, are compared.

The climate-based parameter sets are constructed from the ensemble of calibration parameter sets. Thereby the calibration parameters $S_{R,cal,forest}$, $S_{R,cal,grass}$ and $S_{R,cal,rip}$ are replaced with a climate-based formulation, respectively $S_{R,clim,forest}$, $S_{R,clim,grass}$ and $S_{R,clim,rip}$. To include a certain level of equifinality in the climate-based parameter sets, for every calibration parameter set, 10 random samples have been taken from the water balance ranges. Hence, the ensemble of 300 calibrated parameter sets results in 3000 climate-based equivalents, for both past conditions as well as the two emission scenarios in the future. After implementation, models using calibration and climate-based parametersets are respectively referred to with subscription cal and clim.

The model performance of the climate-based model is tested and compared to results of the calibrated model based on the eight objective functions (Table 4).

3.2.3 Comparing the influence of future root zone development on streamflow

To investigate the influence of future dynamics of the root zone storage development on streamflow, a second analysis is made, comparing modelled future streamflow including $S_{R,climate,past}$ and $S_{R,clim,fut}$. The respective parameter sets hence represent climate-based stationary and climate-based adaptive model conditions. Thereby, hydrological change is evaluated over 30 years to decrease noise and allow for a robust comparison of streamflow. The analysis covers different streamflow characteristics and assesses changes in timing and magnitude. This includes changes in mean annual dis-

Table 4: Objective functions used for calibration

Signature	Symbol	Reference
Timeseries of flow	NSE	(Nash & Sutcliffe, 1970)
	NSE_{log}	(Nash & Sutcliffe, 1970)
	VE	(Criss & Winston, 2008)
Flow Duration Curve	FDC	(Euser et al., 2013)
Autocorrelation Curve	AC1	(Euser et al., 2013)
	AC90	(Hrachowitz et al., 2014)
Monthly Runoff Coefficient	RC	(Hrachowitz et al., 2014)
Snow Cover	Snow	(Finger, Vis, Huss, & Seibert, 2015)

charge, which indicates future water availability, mean monthly discharge and both annual and seasonal runoff coefficients. Furthermore, changes in extreme hydrological events are analyzed according to (Blöschl et al., 2017, 2019). As such, changes in the magnitude of high flows are assessed using a time series of Annual Maximum Flows (AMF). Changes in AMF are also analyzed in the context of different return periods, that are obtained through ranking average annual maximum flows. Changes in timing are assessed based on the method of circular statistics (Young, Round, & Gustard, 2000; Blöschl et al., 2017). This method provides correct timings of extreme events despite the turns of the year. However, a bi-model flood season would be hidden, as the average date of occurrence would be located in the middle of the flood season. For this case, also the relative frequency of AMF occurring in 15 days is studied. A 15day time frame allows for the co-occurrence of different events, whilst providing insight into relatively small changes in AMF over time.

Changes in low flows are assessed using a similar approach and are based on the annual minimum runoff throughout 7 consecutive days. As low flows mainly occur in winter, a moving average from June to May is used, to avoid complications with the turn of the year. Low flows are also analyzed in terms of Q90/P, which indicates the ratio of low flows, exceeded 90% of the time, to precipitation. Furthermore, droughts are assessed, which are defined as the summed deficit volume of days with streamflow under the Q90 threshold. This metric hence provides information on both the frequency and magnitude of low flows. Timings of low flows are again assessed using the method of circular statistics.

4 Results & Discussion

Temperature and precipitation are projected to increase in all catchments in the future, especially under RCP 8.5 (subsubsection 4.1.1). This is inherent to higher catchment dryness and evapotranspiration rates (subsubsection 4.1.2). Hence, when using climate data to estimate S_R, $S_{R,clim,past}$ parameter ranges are found to differ significantly per catchment, although parameter ranges significantly narrow-down for the climate-based estimates compared to calibration values. The implementation in the FLEX-topo model reveals that both calibration and climate-based parameters result in a reasonably good performance on modelling past streamflow (subsubsection 4.3.1). According to the increase in catchment dryness and evaporative index, higher climate-based S_R values are estimates for all catchments in the future (subsection 4.2). However, only a limited difference is found in modelled future streamflow, when accounting for climate-induced changes in S_R (subsection 4.4).

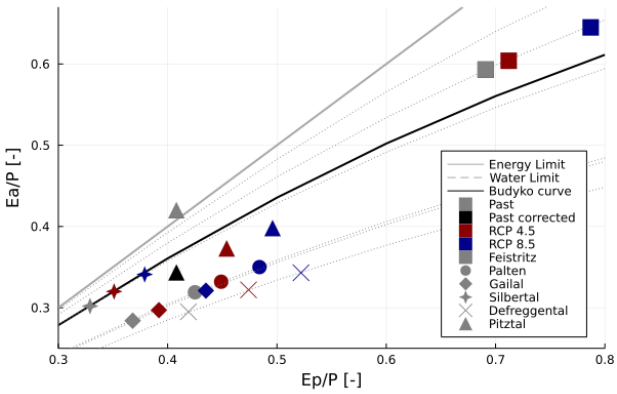

Figure 5: Mean location of the study catchments in the Budyko space in the past and under two emission scenarios at the end of the 21st century, averaged over 14 climate models. Dashed lines represent the Fu curves. For the Pitztal the position is indicated before and after correction of observed streamflow data.

4.1 Projected changes in climate

4.1.1 Hydroclimatic Change

Annual median temperature and precipitation, averaged over 30 years, are projected to increase in the future (Figure 6).

Similar temperature changes were found across all catchments, with median increases around 2-3 °C for RCP 4.5 and 4-5 °C for RCP 8.5. The highest median increases are found in the Defreggental and Pitztal.
Median precipitation increases for all catchments in the future and are most pronounced for RCP 8.5, where changes range between 4% in the Gailtal and 9% in the Defreggental. However, the sign of change depends on the climate model used as the spread in projected change ranges between -10% decrease and 20% increase.

4.1.2 Future changes in the long-term water balance

Figure 5 shows the changes in aridity and evaporative index of all catchments in the Budyko space, for the past and for two emission scenarios in the future. In the past, the Feistritztal and Silbertal show the highest and lowest aridity indices (AI) of respectively 0.691 and 0.231 (Table 5). This is likely related to their respective most west and east location, since climate dryness increases for more land inward catchments, resulting in higher aridity indices and vice versa.
The evaporative index (EI) ranges between 0.284 in the Gailtal and 0.593 in the Feistritztal. The higher evaporative indices can be explained by higher vegetation cover. The opposite applies to the runoff coefficients $(1 - \frac{\overline{E_a}}{\overline{P}})$. It can be seen that the Pitztal plots outside the energy limit, suggesting too little runoff. This likely results from water abstraction for hydropower uses in the area, which is corrected for in further calculations (Figure 5).
By solving the Budyko equation, using past aridity and evaporative indices as input, catchment-specific parameters (ω) are obtained for each catchment. Values for ω are found to range between 1.72 in the Defreggental and 3.025 in the Feistritztal. Higher values for ω for the same aridity index indicate more water use for evaporation and could be related to the increased water use by young vegetation as opposed to older forest (Fenicia et al., 2009), (Table 1 & 5). The second-lowest ω value of 1.834 is found in the Gailtal, which explains its lower evaporative index, despite relatively high vegetation cover.
As a result of increased aridity and evaporative indices in the future, all catchments move to the top right of the Budyko framework. This indicates that the catchments become dryer and have more available energy for evaporation. Hence, evaporation rates increase and runoff coefficients reduce in the future. On average, median aridity indices increase with ca. 0.03 in all catchments and increase up to twice as much for RCP 8.5 (Figure S5). However, the magnitude of change depends on the climate model, as is shown in Figure S4. In accordance with previous results, future lowest and highest aridity indices are found in the Silbertal (0.351) and Feistritztal (0.712), which further increase to 0.379 and 0.787 for RCP 8.5. The largest change is found in the Defreggental (0.1, RCP 8.5), corresponding to increases in temperature (Figure 6). In the Silbertal, the least change in AI is found (0.04, RCP 8.5), which is potentially caused by the offsetting effect of increases in precipitation rates, higher temperatures and hence increased potential evaporation.
Future evaporative indices increase with ca. 0.02 in all catchments for RCP 4.5 and range between 0.297 (Feistritztal) and 0.604 (Gailtal), with further increases for RCP 8.5. Only in the Pitztal, the evaporative index decreases in the future. This is especially pronounced for RCP 4.5, where the EI changes with -0.04. Changes in the evaporative index result from the combined influence of hydroclimatic changes and catchment characteristics, represented by ω, that can both amplify or offset each other's effect on evapotranspiration. Corresponding to changed evaporative indices, the highest and lowest runoff coefficients are found in the Gailtal (0.396, RCP 4.5) and Feistritztal respectively (0.296, RCP 4.5). The absolute long-term mean runoff is the lowest for the Feistritztal (0.993), which is likely the result of the high vegetation coverage, decreasing runoff and increasing evaporation. The highest runoff is found in the Silbertal (2.935), likely as a result of a more humid climate, corresponding to its relatively west location. As evaporation rates are relatively low, long-term mean runoff values are relatively high.

4.2 Climate based estimates of root zone storage capacity in the past and future

Figure 7 shows root zone storage capacity estimates derived with observed historical data and modelled future data of 14 climate models. Median values for the past climate based root zone storage capacity parameters are found to range between 5-27mm for $S_{R,clim,2years}$ and 5-155mm for $S_{R,clim,20years}$. For both grass and forest the respective lowest and highest $S_{R,clim}$ are found in the Pitztal and Feistritztal and show a relationship with the vegetation cover in the catchments. The low root zone storage capacities in the Pitztal are associated with shallow hydrologically active soil depths, which is realistic as bare rock covers a substantial portion of the catchment area. The opposite applies to the Feistritzal, where grass and forest are the dominant land cover types. Similar regional patterns in soil moisture storage capacities are demonstrated by Merz and Blöschl (2004) in a calibration experiment for 308 catchments in Austria. The spread in $S_{R,clim,past}$ is below 5mm in all catchments and directly results from the 300 different interception

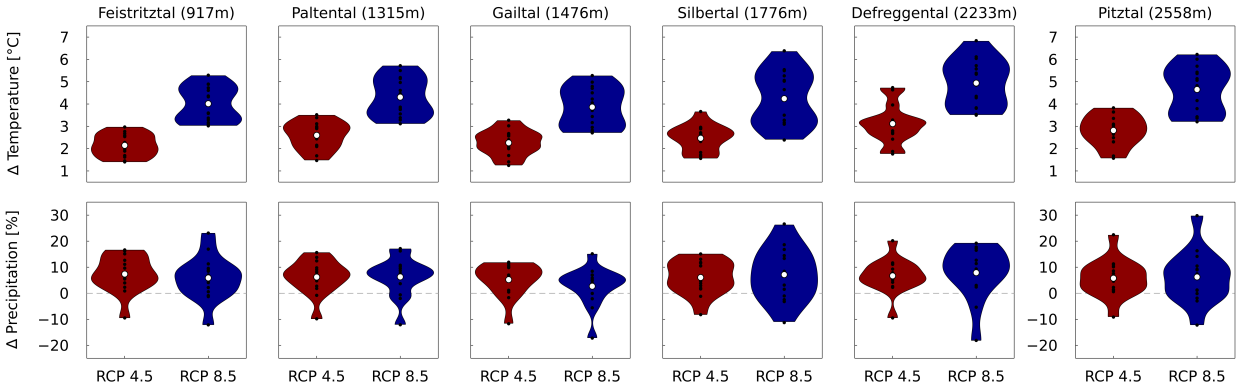

Figure 6: Absolute changes in mean annual temperature and relative changes in mean annual precipitation for all 14 climate simulations and two RCPs. RCP 4.5 is coloured in red and RCP 8.5 in blue.

Table 5: Derivation of Aridity Index, Evaporative Index and catchment specific parameter ω from mean observed climate data for all catchments. Subsequent calculation of future Aridity and Evaporative Indices, runoff coefficients and long term runoff estimates. All displayed values are averaged over 30 years and 14 climate projections for each emission scenario.

Catchment	$\frac{\overline{E_P}}{\overline{P}_{obs}}$	$\frac{\overline{E_A}}{\overline{P}_{obs}}$	ω	$\frac{\overline{E_P}}{\overline{P}_{rcp45}}$	$\frac{\overline{E_P}}{\overline{P}_{rcp85}}$	$\frac{\overline{E_A}}{\overline{P}_{rcp45}}$	$\frac{\overline{E_A}}{\overline{P}_{rcp85}}$	$\frac{\overline{Q}}{\overline{P}_{rcp45}}$	$\frac{\overline{Q}}{\overline{P}_{rcp85}}$	$\overline{Q_{rcp45}}$	$\overline{Q_{rcp85}}$
	[-]	[-]	[-]	[-]	[-]	[-]	[-]	[-]	[-]	[mm]	[mm]
Feistritztal	**0.691**	**0.593**	3.026	**0.712**	**0.787**	**0.604**	**0.645**	**0.396**	**0.355**	**0.983**	**0.876**
Paltental	0.425	0.319	1.851	0.449	0.484	0.332	0.35	0.668	0.65	2.326	2.272
Gailtal	0.368	**0.284**	1.834	0.392	0.435	**0.297**	**0.321**	**0.703**	**0.679**	2.622	2.474
Silbertal	**0.329**	0.302	2.445	**0.351**	**0.379**	0.32	0.341	0.68	0.659	**2.837**	**2.787**
Defreggental	0.419	0.295	**1.723**	0.474	0.522	0.322	0.343	0.678	0.657	1.814	1.778
Pitztal	0.408	0.42	**3.863**	0.454	0.496	0.373	0.398	0.627	0.602	1.655	1.597

capacities applied in the water balance method.

$S_{R,clim}$, estimated using modelled past data, are on average higher due to overestimation of precipitation in modelled climate data. This bias has been corrected for in the estimation of future climate-based parameters (Appendix A.3). Moisture deficits in the rootzone increase in the future as a result of increased dryness indices, higher evapotranspiration rates and decreased long-term mean runoff and hence increased $S_{R,clim}$ (Equation 1 & 4, Figure 5). $S_{R,clim,forest}$ increases with at least 10mm (100%, Defreggental) and maximum 30mm (75% Pitztal) for RCP 4.5, with further increases for RCP 8.5. Only in the Pitztal little to no increase is found in the future, which corresponds to the slight decrease in EI (Figure 3a & Appendix B.1). These results reveal a relationship between the magnitude of changes in the root zone and the area share of forest, which is resp. 6% and 61% in the Pitztal and Paltental. Plausibly, the applied correction for area share of forest and grass contributes to this, as increments in $S_{R,clim,forest}$ in low forested areas are significantly reduced and vice versa.
$S_{R,clim,grass}$ increases with 4-20mm (6-32mm, RCP 8.5) in all catchments in the future. This translates to relative changes of 14-125%, with the lowest increases in the Feistritztal and Pitztal and the largest increase in $S_{R,clim,grass}$ in the Silbertal. A similar pattern is found in grassland coverage, which is the lowest in the Feistritztal (25%) and Pitztal (23%) and increases up to 46% in the Silbertal.
The spread in $S_{R,clim}$ increases in the future for all vegetation types, mostly for RCP 8.5 and likely relates to uncertainty in the used climate models. In the past, parameter spread is limited to approximately 5-10mm for forest and 2-8mm for grass. The Silbertal shows the largest spread for both vegetation types. In the future, spread in $S_{R,clim,forest}$ ranges between 30-110mm (45-160mm, RCP 8.5), with respective minimum and maximum spread found in the Defreggental and Feistritztal. The Pitztal is an exception to this, as it shows almost no spread in $S_{R,clim,forest}$. The absolute spread in $S_{R,clim,grass}$ is relatively lower and lies between 18-60mm (28-36mm, RCP 8.5), with respective lowest and highest spread found in the Defreggental and Silbertal. Again a plausible explanation for the variety in the model spread is the coherence with the areal reduction factor applied, reducing spread for sparser vegetated areas. Still, the

spread in $S_{R,clim}$ is much smaller compared to the spread found in calibration parameters (Appendix B.2).

4.3 Modelled Hydrological Response

The found calibration and climate-based parameters are subsequently implemented in the FLEX-topo model to test the influence on modelled streamflow in the past and future.

4.3.1 Calibration & Evaluation

Figure 8 shows that both the calibrated and climate based models reproduce the main features of the observed hydrological response reasonably well in all study catchments. Overall model performance ranges between $Obj_{cal,tot}$ = 0.81-0.88 and $Obj_{clim,tot}$ = 0.80-0.87 during the calibration period (Figure 8, top row) and remains stable for the evaluation period, where $Obj_{cal,tot}$ = 0.78-0.89 and $Obj_{clim,tot}$ = 0.80-0.85 (Figure 8, middle row). Also for individual objective functions both models show an overall good performance during both the calibration and evaluation period. Thereby, the differences in model performance between the two models are close to zero (Figure 8, bottom row). For the calibration period ΔObj_{tot} ranges between -0.002 (Defreggental) and -0.056 (Silbertal), in favour of the model using the calibration parameter $S_{R,cal}$. For the evaluation period differences in model performance range between ΔObj_{tot} = -0.068 (Silbertal) and ΔObj_{tot} = 0.038 (Pitztal) in favor of the calibrated and climate based model respectively.

Likewise, the modelled hydrographs show that the short-term flow dynamics are generally adequately captured by the models, regardless of the used parameter set (Figure 9 & Appendix B.3.). In some cases, peak flows remain underestimated. This is likely associated with uncertainties in observations in very localized high-intensity convective rainfall events (Hrachowitz & Weiler, 2011). Likewise, the mean regime curves of flow show that the model matches observations rather well during both calibration and evaluation period (Figure 10).

Hence it can be concluded that both the calibrated and climate-based models adequately capture the general magnitudes and seasonality in all study catchments. The overall good model performance implies that the retained climate-based parameter sets can be used for modelling future streamflow.

4.4 Future streamflow predictions

The analysis of future streamflow predictions describes the found changes in streamflow between past and future. In this section the main focus lies on the comparison of models, which respectively use the climate-based stationary ($S_{R,clim,stat}$) and climate-based adaptive ($S_{R,clim,adapt}$) parameters (Figure 11. Hence, both models are climate-based and will be referred to as the stationary and adaptive model hereafter.

4.4.1 Annual discharges

In general, an increase in discharge is projected in all catchments in the future (Figure 11, Figure S18), especially for RCP 8.5. However, the direction of change depends on the catchment, hydrological model and climate projection used. For RCP 4.5, the stationary model predicts changes in discharge between -4% (Feistritztal) and 10% (Pitztal) for RCP 4.5. Hence, discharge is projected to increase in the future in all high elevation catchments, whereas the sign of change is less certain for the three lower elevation catchments. In comparison, discharges are 2-6% higher in all catchments for RCP 8.5. Only in the Feistritztal a larger difference is found,

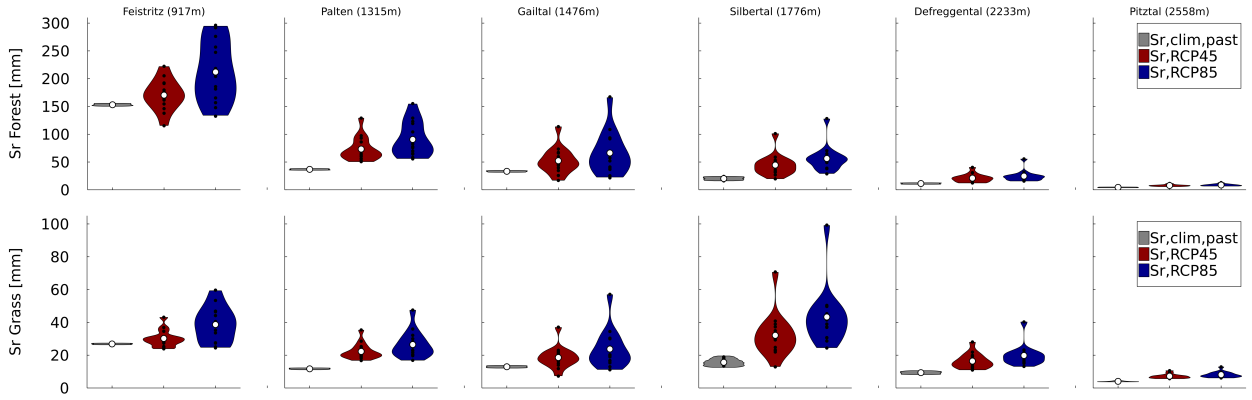

Figure 7: climate-based parameter ranges derived from observed past climate data and corrected future climate data. Results include 14 RCMs. RCP 4.5 is depicted in red and RCP 8.5 in blue.

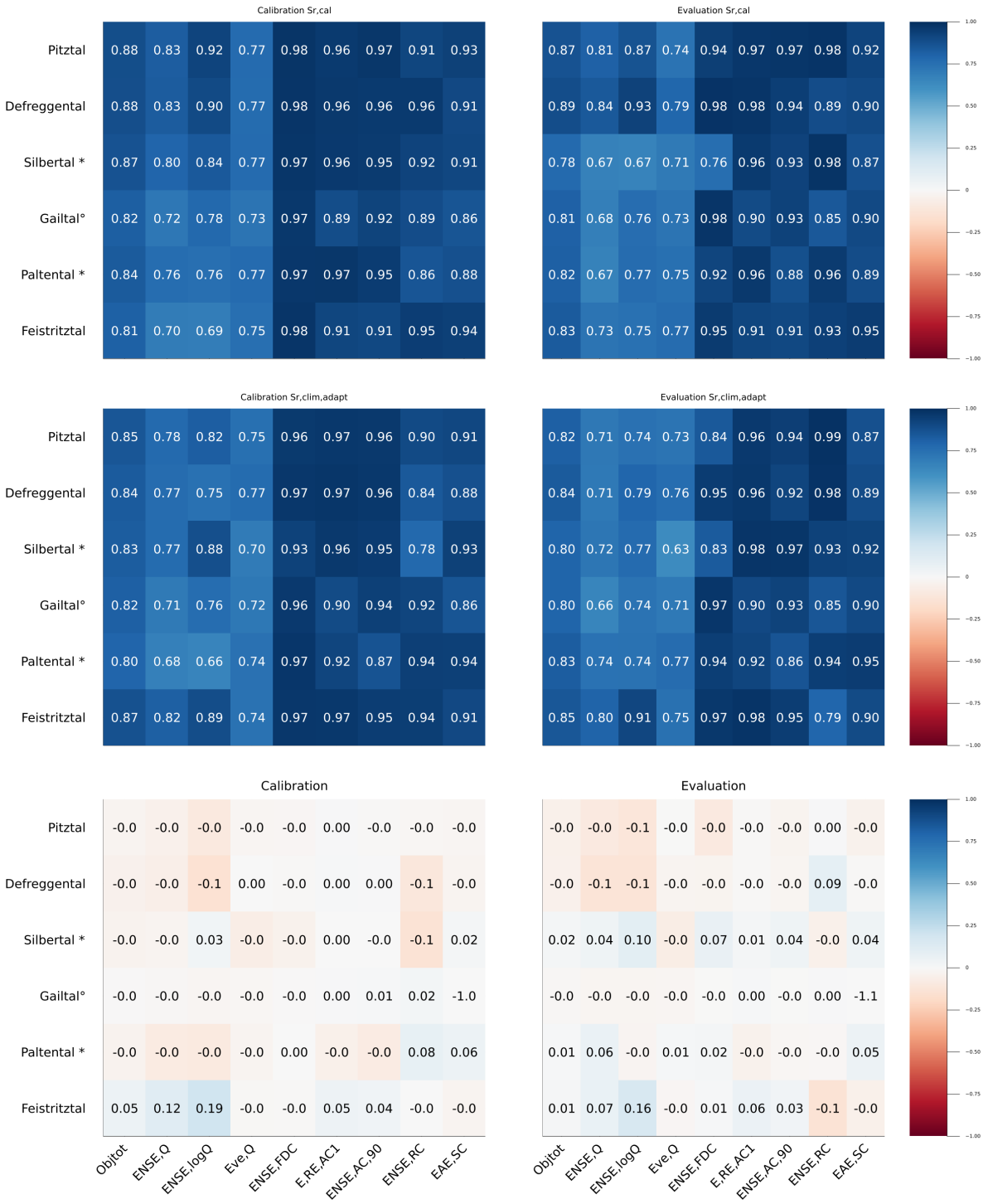

Figure 8: Mean model performance of best 300 calibration (top) and 3000 climate based parametersets (middle) during calibration (left) and evaluation (right) period. Obj_{tot} shows the overall model fit. The bottom row indicates relative model performance of climate based compared to calibration parameter sets in the respective periods, defined as $\Delta\text{Obj}_{\text{tot}} = \text{Obj}_{\text{clim,tot}} - \text{Obj}_{\text{cal,tot}}$. Hence, positive values indicate a better performance of climate based Parameter sets. 3 provides a description of objective functions. Catchments marked with an aterisk (*) use an evaluation period of 8 years instead of 10 years.

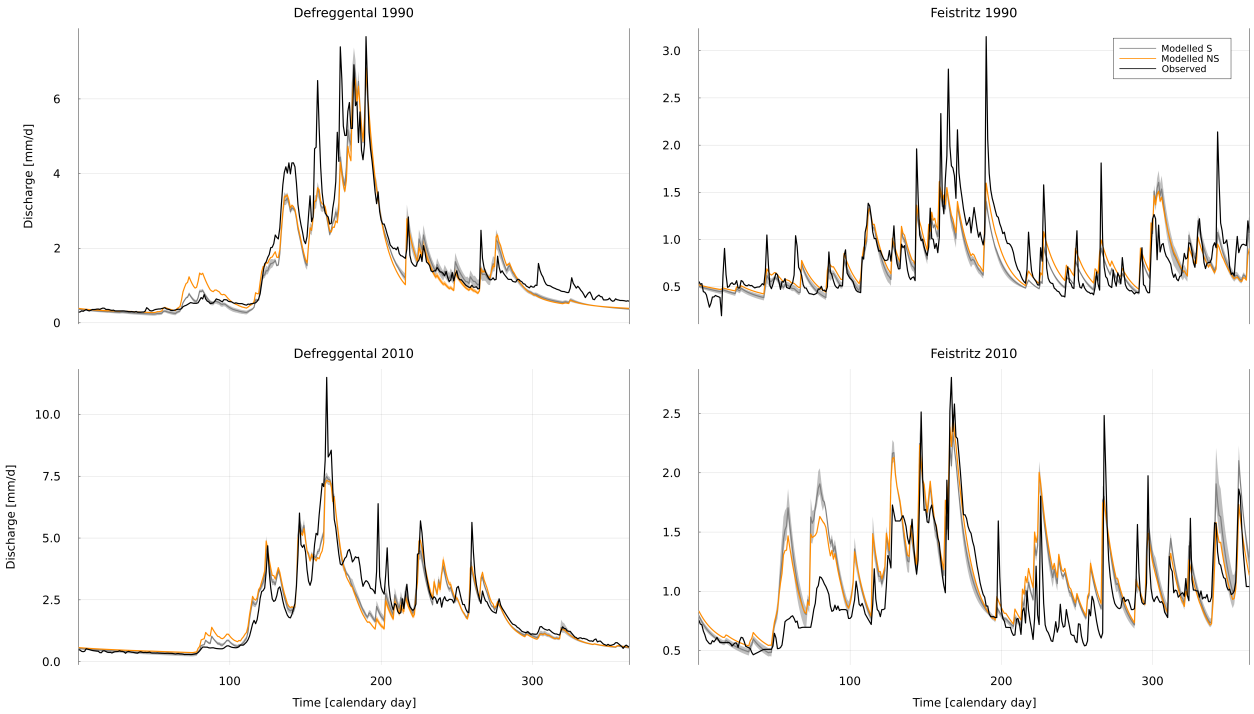

Figure 9: Comparison of measured (black) and calibrated (grey) and climate based (orange) modelled runoff for a year during calibration period (1990) and a year during the evaluation period (2010). The solid lines indicate mean modelled runoff using best parameter sets and the shaded area corresponds to the range of best parameter sets

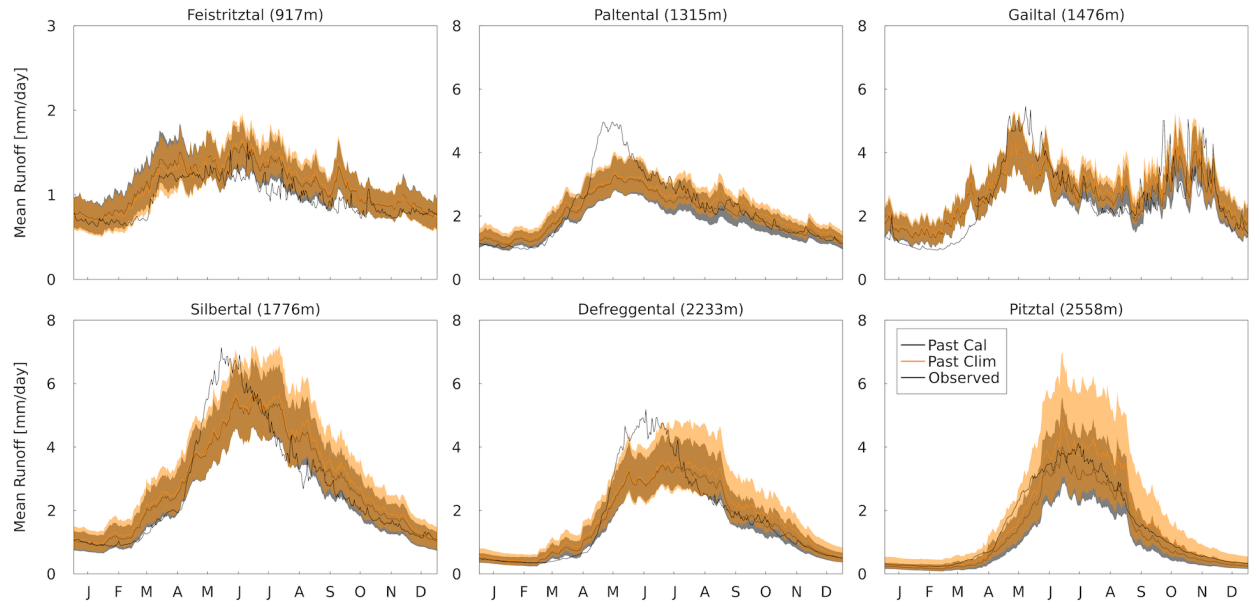

Figure 10: Annual mean regime curves for the six study catchments over a 30 year period in the past (1981-2010). Observed discharges are depicted in black, modelled discharge results from the calibrated model and the climate based model in grey and orange respectively. Solid lines represent mean runoff and shaded bands indicate ± 1 std.

where changes in discharge alter from -4% (RCP 4.5) to 10%. The Pitztal shows lower increases in discharge for RCP 8.5. Increases in discharge are likely the result of increasing annual precipitation in the future. However, this can be offset by higher future runoff coefficients as a consequence of increased evaporation (Figure 5).

The differences between median modelled discharge change using the climate-based stationary and adaptive model are close to zero, which is in line with findings of Bouaziz et al. (2021). All modelled discharges show relatively high uncertainty. For the stationary model, the spread varies between 30% (Paltental) 100% (Pitztal) for RCP 4.5 and even more for RCP 8.5. For the adaptive model, uncertainty ranges are between 50% (Paltental) and 120% (Pitztal), with higher increases in the negative direction of change.

4.4.2 Monthly Discharges

Changes in future monthly discharges reveal subtle differences between both the stationary and adaptive model (Figure 12 & S19). The stationary model predicts monthly discharge to increase by 20-90% (0-1mm, RCP 4.5) in the winter and spring months in all catchments, whereas a decrease of -10 to -20% (0 to -1mm) is projected in monthly summer discharges. An explanation for this is the projected future temperature increase, resulting in decreased snow storage and an earlier onset of the melting season. This increases discharges in winter and spring but results in decreases afterward. Summer discharges are further reduced by increased evaporation rates under higher summer temperatures. For RCP 8.5 changes are in general up to twice as high and plausibly relates to the projected higher mean increase in precipitation, temperature and therefore also snowmelt. Only the Feistritztal shows an increase in discharge of approximately 0.2 mm/day in summer for RCP 4.5, likely as increasing precipitation rates are dominant over temperature changes in these catchments. The opposite applies for RCP 8.5, as slightly negative changes are projected. Winter increases are similar under both scenarios, which could be due to the minor role of snow dynamics in the discharge regime.

The highest change in discharge is found in the Silbertal and Pitztal, where mean discharge changes with + 1.5mm/d in summer and - 1.5mm/d in winter (25%, RCP 8.5). The Feistritztal experiences the least change of 0.2mm/d (20%). An explanation for the larger changes encountered in higher elevation catchments could be the higher absolute increases in temperature. Additionally, a decrease in snow storage under higher emission scenarios leads to lower contributions of snow and glacier melt to discharge, further reducing summer flows.

The timing of the largest flow increase in winter occurs between February (0.4-0.6 mm/day, Gailtal) and May (1.0-1.4 mm/day, Pitztal) for all catchments. Only the Feistritztal and Paltental show no distinctive month with maximum change. A similar shift in timing is found for summer decreases in monthly discharge. The first low flows occur in May in the Feistritztal, Paltental, and Silbertal. Flow reductions are experienced the latest in July

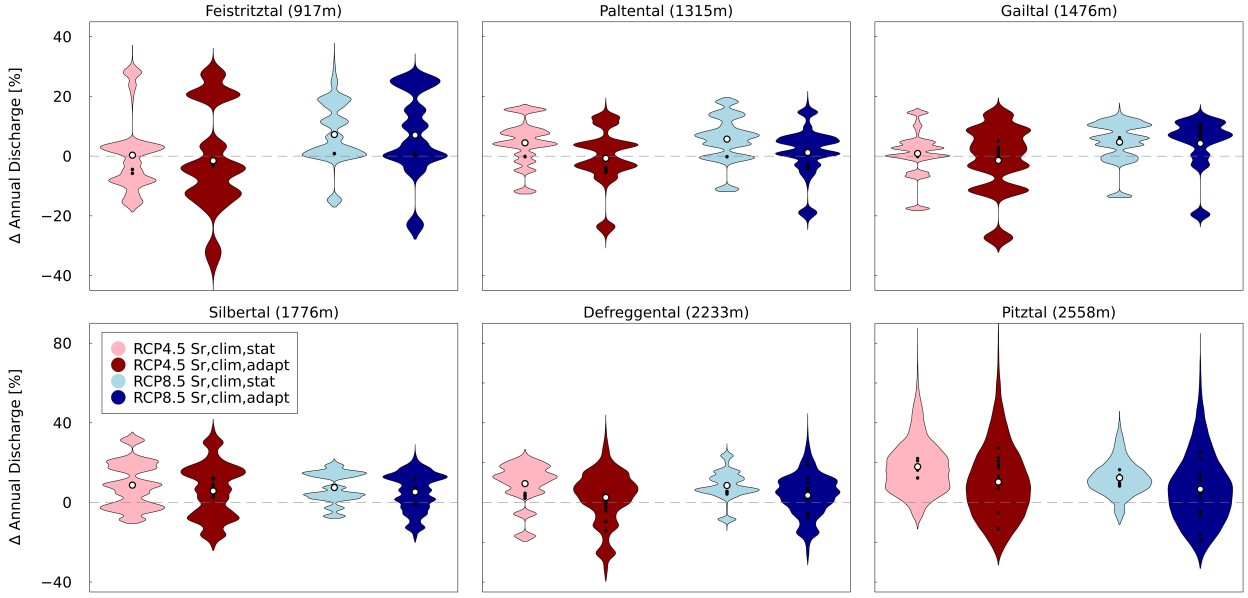

Figure 11: Relative changes in mean annual discharge for all catchments, using models featuring $S_{R,clim,stat}$ (light) and $S_{R,clim,adapt}$ (dark), for all 14 climate simulations and RCPs. RCP 4.5 is coloured in red and RCP 8.5 in blue.

in the Pitztal, whereas winter increases and summer decreases are experienced later. The difference in timings between catchments of different altitudes probably relates to the altitude-temperature gradient. Namely, the relatively lower temperatures at higher elevations lead to a postponement of the melting season and hence later timings for both changes in summer and winter (Bavay, Grünewald, & Lehning, 2013).

The absolute spread in monthly changes is the smallest in the Feistritztal (3mm, 90%), and increases for catchments that are subject to larger changes. The maximum model spread of 2.4mm is found in June and August in the Pitztal. The largest relative change is found in the Pitztal in March (180%). Uncertainty bands increase further for RCP 8.5, which corresponds to increased uncertainty in climate projections and $S_{R,clim}$ parameters.

The climate-based adaptive model shows a similar pattern in monthly discharge changes, although projected changes are around 0.1mm (10%) lower for all catchments year-round. Differences in model predictions slightly increase for the second half of the year, for higher altitude catchments and RCP 8.5. The maximum deviation is found in the Pitztal, where the adaptive model predicts 0.4mm/d (15%) lower summer reductions in July. This could relate to the higher storage capacities, leading to decreased runoff and decreased changes in runoff (Figure 13 & S20). In the Feistritztal almost no change (0-5%) between models is found. In all other catchments, the difference lies between 10-15%, with the largest differences occurring in the second half of the year. As compared to the stationary model, the spread in model results from the adaptive model is 0-8mm larger for RCP 4.5 and 0.2-14mm for RCP 8.5. Hence, estimates of changes can significantly differ depending on the climate model used.

4.4.3 Runoff Coefficient

Median annual runoff coefficients are predicted to increase for both models in all catchments for RCP 4.5, with further increases for RCP 8.5 (Figure 13). According to the stationary model, the maximum change of ca. 0.2 is experienced in the Pitztal and Defreggental under RCP 8.5, which corresponds to 12%, resp. 14%, change. The sign of change is highly dependent on the climate projection used. The model spread ranges between 0.3 (Paltental) and 1.1 (Pitztal) for RCP 4.5, with on average larger spread for the higher elevated catchments and the RCP 8.5 scenario.

The adaptive model predicts a similar pattern of change in annual runoff coefficients. However median estimates are around 0.05 (5%) smaller for RCP 4.5 and increase for RCP 8.5. This supports findings from Bouaziz et al. (2021) and could result from the relatively higher root zone storage capacities in the future and a related increased threshold for runoff activation. Also, evaporation rates, that increase due to reduced moisture stress, can contribute to lower runoff coefficients. The largest difference between adaptive and stationary model predictions is 0.1 (10%) difference in the Paltental (RCP

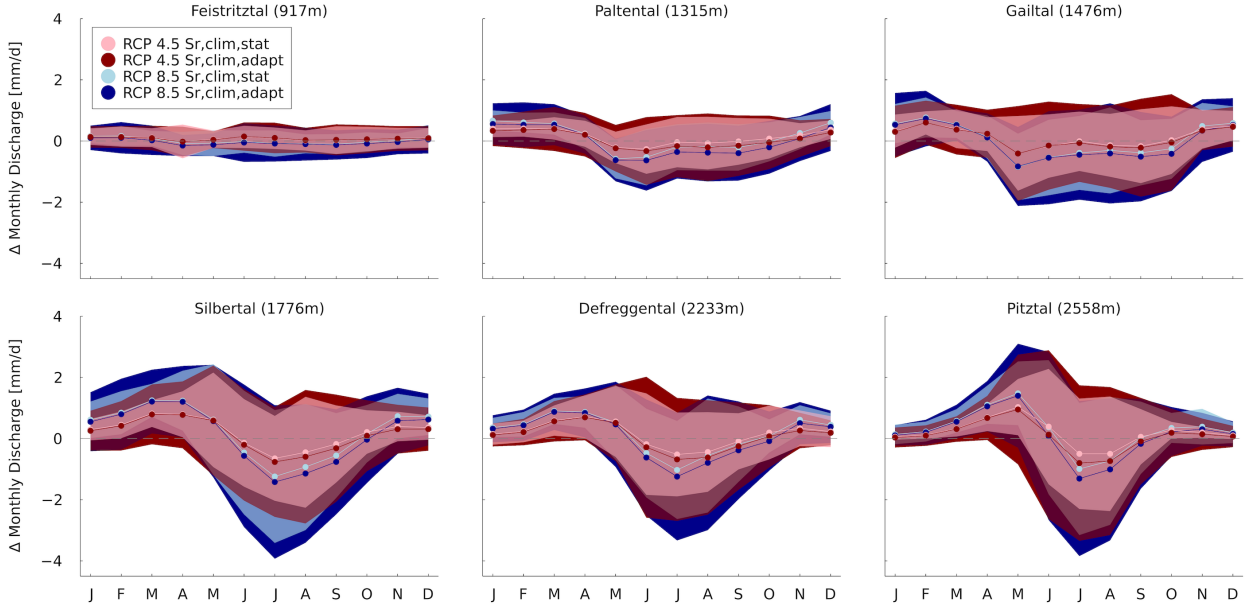

Figure 12: Absolute changes in mean monthly discharge, using data of 14 climate models and two RCPs of 30 years in the future (2071-2100). Results obtained from models featuring $S_{R,clim,stat}$ and $S_{R,clim,adapt}$ are respectively depicted in pink and red for RCP 4.5 and light blue and blue for RCP 8.5.

8.5), which is also the catchment showing the largest relative change in $S_{R,clim}$ between past and future.

Predictions of the absolute seasonal runoff coefficient correspond to predicted changes in monthly discharge. Especially in higher elevation catchments, runoff coefficients increase in the winter and spring and decrease in summer months, conceivably as a result of seasonality in snowmelt contributions. Lower elevation catchments show only limited change throughout the entire year. Increased runoff coefficients in winter range between -0.02 in the Feistritztal and 0.32 in the Pitztal. Summer reductions are between 0.0 and 0.15 for these same catchments. In autumn only limited changes in runoff coefficient are encountered in all catchments. Changes in runoff coefficient become more pronounced for RCP 8.5, as temperatures and consequently snowmelt further increase. A similar pattern is found for relative changes (Figure S20). The spread in model results differs per season and increases for higher estimates of change. On average the largest model spread is found in winter and ranges between 0.35 (70%, Silbertal) and 0.75 (65%, Gailtal).

The adaptive model results show similar seasonality as predicted by the stationary model, with again a slightly smaller magnitude of change in all catchments for both absolute and relative changes. The least difference in model results is found in the Feistritztal, where model predictions are 0.01 apart throughout the entire year. The largest offset is found in the Paltental, showing differences of 0.1 (12%) in Autumn for RCP 4.5 and increases up to 0.15 (16%) under scenario RCP 8.5. The model spread in the adaptive model is the same size or up to 0.3 (Pitztal) smaller than the stationary model. The maximum difference in relative model spread of 50% is found in the Defreggental. Hence, predictions of seasonal runoff coefficients can differ vastly depending on the time of the year and used climate model, although mean seasonal runoff coefficients are broadly consistent.

4.4.4 Timing of High Flows

The timing of Annual Maximum Flows (AMF) shifts substantially towards earlier occurrences in the future for all catchments except for the Gailtal (Figure 14, Table S1). This likely results from an earlier onset of the melting season. In the past, annual maximum flows occur on average in the summer, with an average timing in the first half of July for higher elevation catchments and in the second half of June for lower elevation catchments. The Gailtal experiences annual maximum flows on average at the end of September. For RCP 4.5, the stationary model results show timings of AMF to shift on average by +1 and -16 days in the Feistritztal and Silbertal respectively. The shifts become more pronounced for RCP 8.5 and range between -6 days in the Paltental and -23 days in the Silbertal. Only in the Defreggental, an opposite trend is encountered for RCP 8.5, predicting a change in timing of +2 days, in contrast to the -5 days predicted shift for RCP 4.5. On the contrary, the Gailtal shows substantial shifts towards later occurrences of on

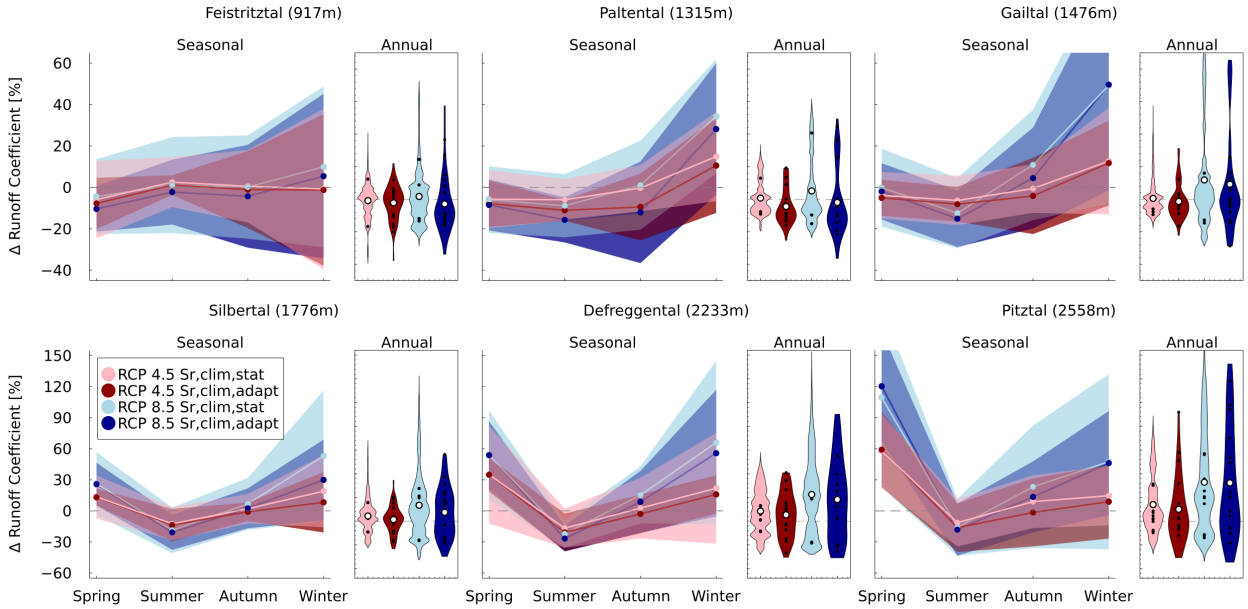

Figure 13: Absolute changes in 30 years average seasonal runoff coefficient, for 14 climate scenarios and 2 RCPs, using the climate based stationary and adaptive model. Results obtained from models featuring $S_{R,clim,stat}$ and $S_{R,clim,adapt}$ are respectively depicted in pink and red for RCP 4.5 and light blue and blue for RCP 8.5.

average +21 days and further increase to +35 days for RCP 8.5.

The climate-based adaptive model predicts slightly more pronounced shifts in timings in the same direction of change as the stationary model. The Defreggental is an exception to this, where the direction of change is reversed for the RCP 8.5 scenario. The magnitude of change in timing is in general 2-3 days larger (RCP 4.5) for the adaptive model for all catchments. For RCP 8.5 timings change in between 1-8 days, indicating a larger spread between model predictions. Only in the Paltental projected changes in timing are larger and shift with respectively -6 and -17 days for RCP 4.5 and RCP 8.5.

To account for a potential bimodal timing in Annual Maximum Flows, also the fraction of timing of occurrences within 30 years time period is investigated as it provides additional information on the intensity of seasonality.

Figure 15 reveals a bimodal seasonality of AMF for the Gailtal, that experiences AMF in the middle of May and end of September. This is characteristic for the autumnal flow regime, where a first flow maximum occurs in late spring due to snowmelt and a second maximum result from intensive precipitation in autumn (Mader et al., 1996; Blöschl et al., 2011).

Furthermore, a clear relationship between seasonality and altitude can be deducted (Figure S20). The lowest catchment (Feistritztal) shows widely spread AMF over the year and experiences maximum incidents in May, whereas the higher elevation catchments show the most pronounced seasonality and experience most incidents in the period from June to July, probably because snowmelt has a dominant role in flood generating processes.

In the future, the stationary model predicts a shift towards earlier timings for the three higher elevation catchments, with further advancements for RCP 8.5. Likely, this is related to the earlier onset of the snowmelt season in the future, as is shown in more detail by Hanus (2020). In the Feistritztal and Paltental, the first prevalence of AMF is shifted to half a month earlier for RCP 8.5. Hence, maximum discharges increase in January and February in the Feistritztal and in March in the

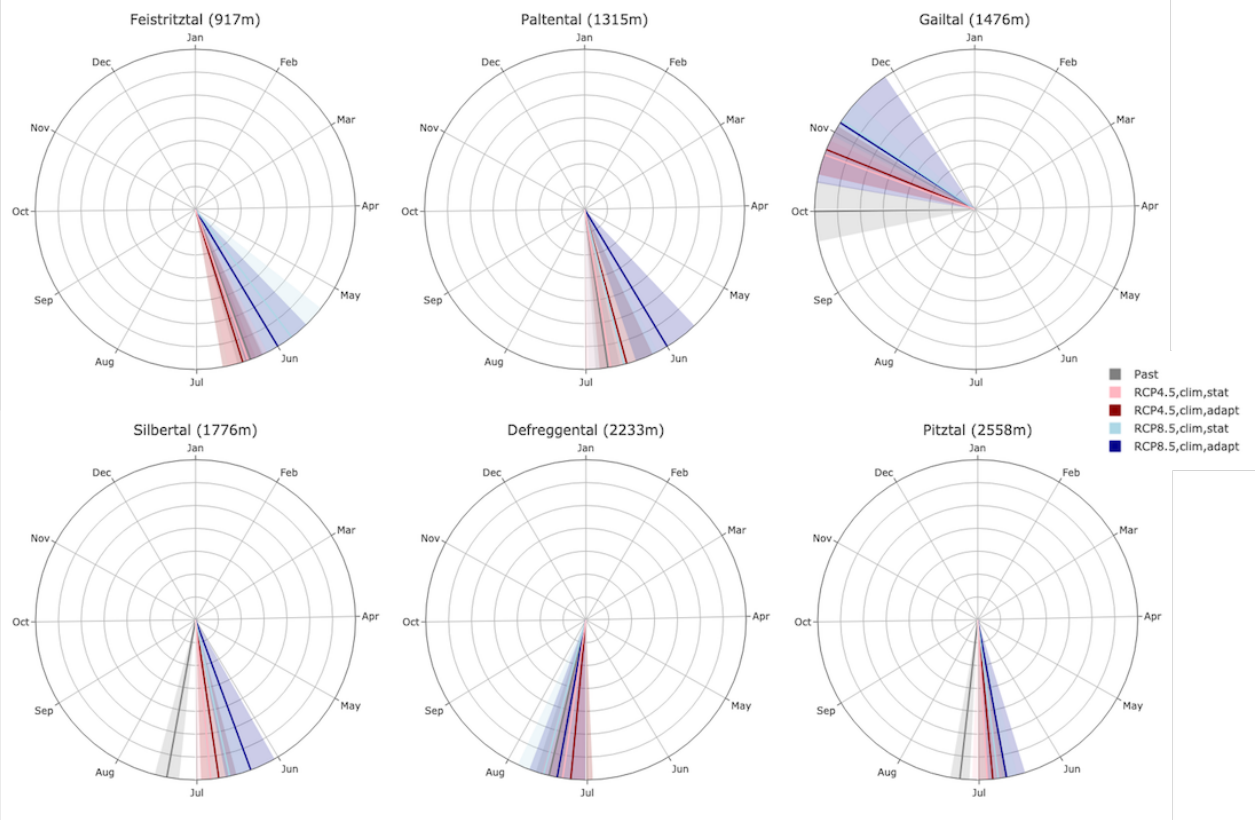

Figure 14: Simulation of mean occurrence of average timing of AMF over 30years, for 14 climate scenarios and 2 RCPs, using the climate-based stationary and adaptive model. Error bands indicate ±1 std. Results obtained from models featuring $S_{R,clim,stat}$ and $S_{R,clim,adapt}$ are respectively depicted in pink and red for RCP 4.5 and light blue and blue for RCP 8.5. Uncertainty bands of ±1 std are shaded and lines connecting 15 day periods are used to allow for better visualization.

Paltental. A possible explanation for this can be the unchanged precipitation rates for RCP 8.5 compared to RCP 4.5. This results in relatively lower summer discharges compared to other seasons, thereby reducing the fraction of occurrences of AMF in summer. Only in the Gailtal occurrences of AMF are delayed to November in the future, which could relate to a shift of flood generating processes from snowmelt to precipitation in the future(Vormoor, Lawrence, Heistermann, & Bronstert, 2015; Brunner, Melsen, Newman, Wood, & Clark, 2020; Hanus, 2020). The increased role of precipitation in flood generating processes, causes the flood season to move to the season with the highest precipitation and a decrease in AMF events during the snowmelt season. A shift in maximum precipitation from October to November, hence explains the shift in AMF timings in the Gailtal.
Also, the seasonality of AMF becomes less pronounced in the future and goes with an increased length of the potential flood season. Shifts are in between 0.5 to 1 month in the Paltental to 2-3 months in the Silbertal and Defreggental. Decreased seasonality in combination with an increased length of the flood season again points at the more dominant role of precipitation in flood generation processes in the future.

Concerning both magnitude and timing, no clear differences are found with predictions from the adaptive model. Hence timings of AMF in the future will continue to depend on snowmelt. As such, shifts in the timing of snowmelt will translate into shifts of AMF events. This illustrates the influence of temperature changes on alpine runoff dynamics. In lower elevation catchments with less pronounced seasonality, shifts in timing mainly occur due to the combination of changes in precipitation patterns, decreased flows in summer months and increased flows in winter months. However, these changes in timing are less clear than for high elevation catchments.

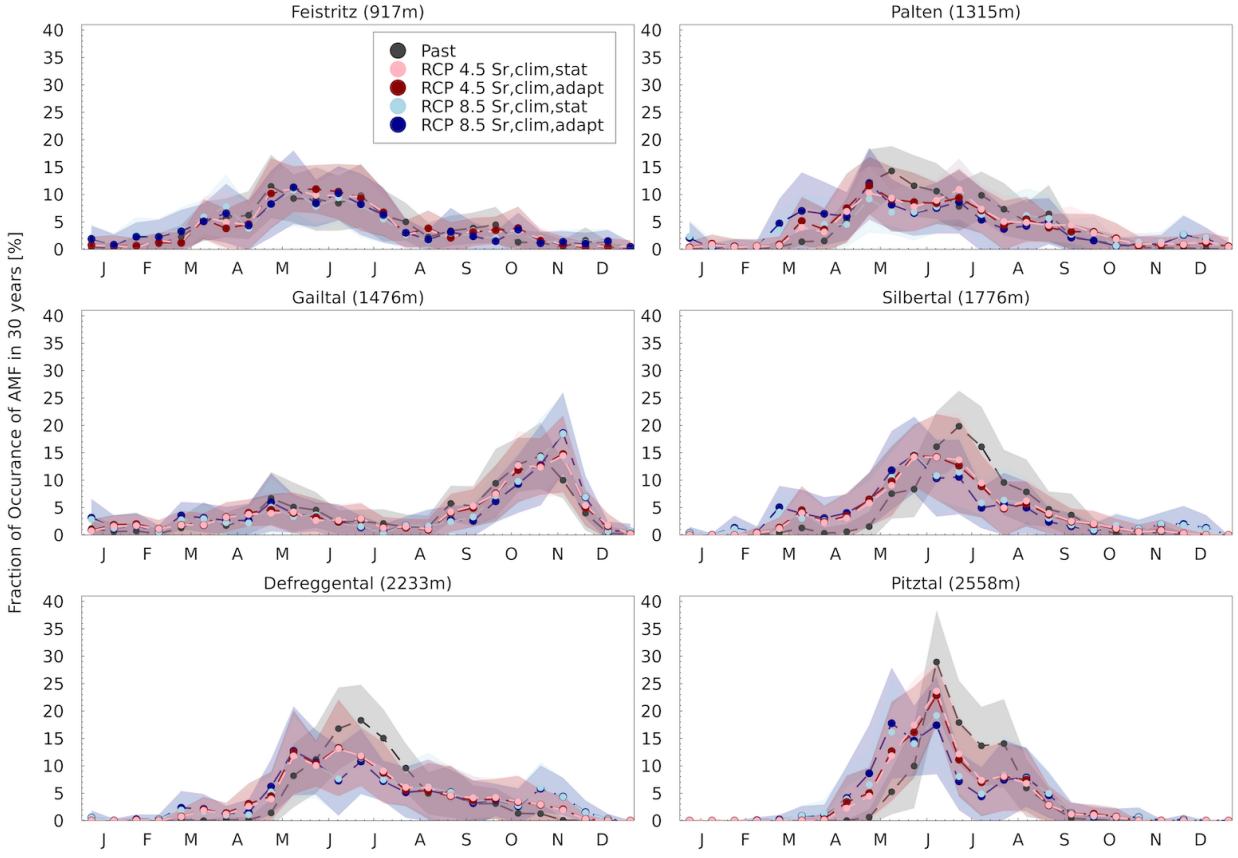

Figure 15: Simulated mean fraction of occurrences of AMF in 30 years, using a time window of 15 days, for 14 climate scenarios and 2 RCPs, using the climate based stationary and adaptive model. Results obtained from models featuring $S_{R,clim,stat}$ and $S_{R,clim,adapt}$ are respectively depicted in pink and red for RCP 4.5 and light blue and blue for RCP 8.5. Uncertainty bands of ± 1 std are shaded and lines connecting 15 day periods are used to allow for better visualisation.

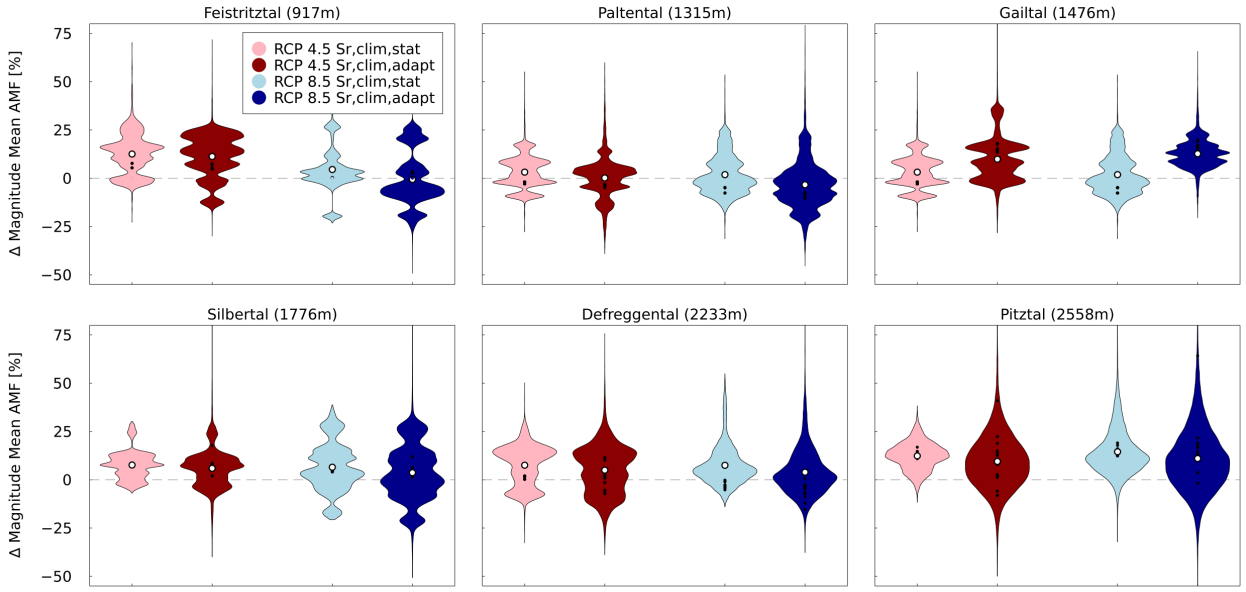

Figure 16: Relative change in average magnitude of AMF, averaged over 30 years, using 14 climate scenarios and two RCPs, for respectively the climate based stationary and adaptive model. Results obtained from models featuring $S_{R,clim,stat}$ and $S_{R,clim,adapt}$ are respectively depicted in pink and red for RCP 4.5 and light blue and blue for RCP 8.5.

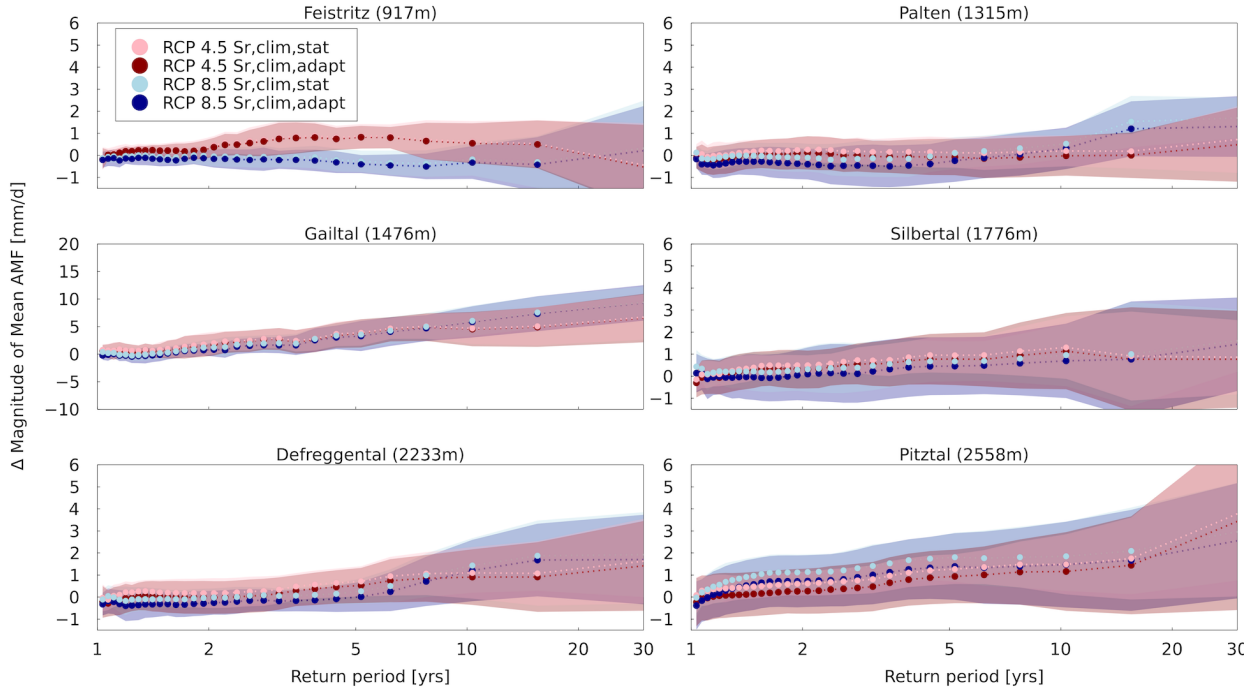

Figure 17: Simulated absolute mean change in magnitude of AMF in relation to return period, for 14 climate scenarios and 2 RCPs, using the climate-based stationary and adaptive model. Results obtained from models featuring $S_{R,clim,stat}$ and $S_{R,clim,adapt}$ are respectively depicted in pink and red for RCP 4.5 and light blue and blue for RCP 8.5. Uncertainty bands of ± 1 std are shaded and mean lines are used to allow for better visualization. Note the difference in scale for the Gailtal.

4.4.5 Magnitude of High Flows

The stationary model predicts the annual average magnitude of AMF to increase by around 10% for all catchments in the future for RCP 4.5 (Figure 16). Increases in mean annual AMF are similar to increases in precipitation, which therefore suggest a causal link with precipitation. In the Paltental and Gailtal, the increase is in annual average magnitude is slightly smaller and changes with ca. 4%. These small increments in AMF magnitude can result from a strong decrease in snowmelt in May and June, which compensates for the effect of increased precipitation. For RCP 8.5 slightly smaller changes in the magnitude of AMF are encountered. This can plausibly be explained by lower snowmelt volumes, higher evaporation and increased soil storage deficits, that are associated with higher temperatures. Only in the Pitztal AMF remain stable under RCP 8.5. Likely, the maximum snowmelt contribution remains unchanged under both emission scenarios, due to the high altitude of this catchment. However, model uncertainty is rather large, with notably upward peaks, which further increases for RCP 8.5. The respective lowest (37%) and highest (93%) uncertainty bands are found in the Silbertal and the Feistritztal (RCP 4.5).
Compared to the stationary model, the adaptive model shows on average 5% lower changes in the average magnitude of AMF for both RCP-scenarios. Lower annual mean AMF magnitude likely relates to higher storage capacities and hence lower runoff during extreme events in the future. Only in the Gailtal 15% larger changes in magnitude are predicted by the adaptive model. However, results from the adaptive model show a larger spread in predicted changes in AMF, especially in the Pitztal and Silbertal where the ranges of change increase with 90% and 65% respectively for RCP 4.5. The spread is similar for RCP 8.5.
Figure 17 provides an analysis of changes in the future magnitude of Annual Maximum Flows in relation to different return periods. The stationary model shows that in general, the absolute magnitude of AMF increases consistently with higher return periods for all catchments. For relative changes, a similar pattern is found (Figure S22). For RCP 4.5, larger changes in flows with lower return periods are predicted than for RCP 8.5 and vice versa. An explanation for this could be the increase of rare but more extreme precipitation events in comparison to more frequent but less extreme events. Only in the Pitztal, a reversed pattern is observed. The most pronounced increase is predicted for the Gailtal, where flows with a return period of 30 years increase with ca. 7mm-9mm. Thereafter, the highest increases of 3.8mm are predicted in the Pitztal. On the contrary, the Feistritztal shows decreasing magnitudes for flows with a return period higher than 15 years. High flows with a return period of 30 years are predicted to decrease -0.55mm in absolute magnitude. Hence, the lower elevation catchments show smaller increases in AMF magnitude compared to the higher elevation catchments. Furthermore, it can be seen that larger return periods go with increased uncertainty intervals. Standard deviations range between 0.5-2mm/d for yearly return periods and increase to 1.7-9mm/d for the 30 year return period, with the largest ranges of change found in the Pitztal. A similar pattern holds for relative changes. These uncertainties can be partially explained by the dependency of the evaluation of extreme events on the chosen period. Uncertainties are further increased by the natural variability in the magnitude of high flows that exceed the effects of climate change on AMF magnitude as is shown in research by Blöschl et al. (2011) and Dobler, Bürger, and Stötter (2012).
The predicted changes by the adaptive model show high similarity to the stationary model results. The adaptive model predicts consistently ca. 0.4mm (RCP 4.5) to 0.6mm (RCP 8.5) lower changes for all catchments, which corresponds to the predicted differences in mean annual AMF. Only for the Feistritztal and Silbertal, the two models show very limited differences.

4.4.6 Timing of Low Flows

Figure 18 shows the year-round distribution of timings of 7day consecutive low flows. Higher elevation catchments show a distinct maximum of low flows in winter months in the past. For lower elevation catchments the distribution in low flow events is more equally spread over the year. Hence, the maximum fraction of occurrences increases with altitude and ranges between 17% in the Feistritztal and 47% in the Gailtal. This peak in low flow occurs in between February in lower elevation catchments (Feistritztal) and March for higher elevation catchments (Pitztal).
According to the stationary model, the fraction of occurrences in winter months decreases significantly in the future, especially for RCP 8.5. On average, a 10% reduction is predicted in all catchments but the Paltental and Silbertal, where reductions equal 18% and 22% respectively. As a result, factions of occurrences become more spread out over the year, with the most decreased seasonality in the Feistritztal. In higher elevation catchments (Silbertal, Defreggental, Pitztal) the fraction of occurrences tends to move towards earlier moments in the year, and thereby the number of months experiencing substantial low flows increases. In the past, the largest fraction of low flows occurs in February and March. In the future, this moves from January to March, which is possibly related to the earlier onset of the snowmelt season, shifting the start of

minimum flows from February to January. In lower elevation catchments an increase in low flow incidents is predicted in the autumn. The highest increase is found in the Paltental, where 13% of the low flow events are experienced in autumn. Likely this relates to decreased summer precipitation and increased evaporation rates. Hence, deficits in the root zone increase, resulting in a longer storage duration and later discharge release.
The adaptive model shows a very close resemblance to the stationary model concerning timing, magnitude and spread. This corresponds to findings of Bouaziz et al. (2021) that also found model-induced changes in 7 day low flows close to zero.

4.4.7 Magnitude of Low Flows

Figure 19 shows a remarkable positive change in annual lowest flows as predicted by the stationary model. This translates to an increased magnitude of median low flows. Increases become more pronounced for RCP 8.5 in high elevation catchments. In low elevation catchments, the change in low flows is either stable or reduces slightly in comparison to RCP 4.5. Overall, the largest change occurs in the Defreggental, where the median magnitude of low flows experience a 35% change for RCP 4.5 and 62% for RCP 8.5. In the Feistritztal, the change is below 10% for RCP 4.5 and 0% for RCP 8.5.

The spread in magnitude of low flows reveals that the direction of change is uncertain for low flows in the Feistritztal, Paltental and Gailtal. The spread further increases for RCP 8.5, which ranges between 80% (Paltental) and 240% (Pitztal). The adaptive model results show a high resemblance with the stationary model predictions. However, predictions are on average 1-5% lower for RCP 4.5, and differences increase further for RCP 8.5. Hence future low flows, as predicted by the adaptive model, are smaller in magnitude. This could be related to increased values of the climate-based adaptive root zone storage capacity parameters, resulting in

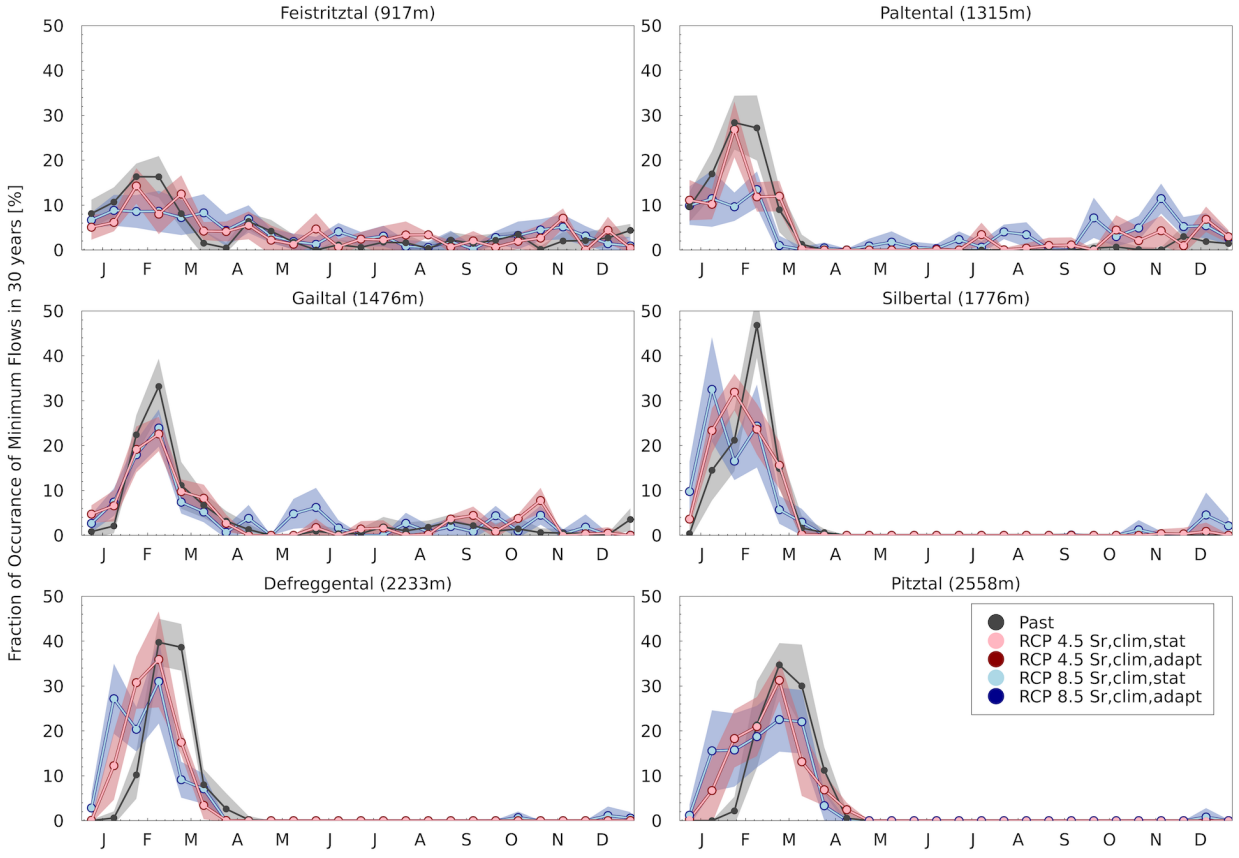

Figure 18: Simulated mean fraction of occurrences of yearly lowest 7day consecutive flow in 30 years, using time windows of 15 days, for 14 climate scenarios and 2 RCPs, using the climate-based stationary and adaptive model. Results obtained from models featuring $S_{R,clim,stat}$ and $S_{R,clim,stat}$ are respectively depicted in pink and red for RCP 4.5 and light blue and blue for RCP 8.5. Uncertainty bands of ± 1 std are shaded and lines in between 15 day periods are used to allow for better visualization.

slightly higher water retention in the root zone and a decrease in runoff volumes. Also for the adaptive model, the Defreggental shows the highest flow increase of 30% and 55% for the respective emission scenarios. In the Feistritztal the least change is encountered of 10% and -5% respectively. For all catchments the range of model results increases compared to the stationary model, resulting in ranges between 110% and 240% for RCP 8.5. Therefore the sign and magnitude of change are highly dependent on the climate projection used.

As a second analysis, the influence of changes in precipitation on low flows is examined using the Q90 to precipitation ratio. This is the discharge that is exceeded 90% of the time over precipitation and is depicted in the bottom row of Figure 19. It can be seen that the pattern of changes in the Q90/P ratio is broadly consistent with the changes in the magnitude of low flows for the different emission scenarios. The Q90 to P ratio increases in the future, with more pronounced changes for RCP 8.5 in high elevation catchments and similar or slightly reduced changes in lower elevation catchments. This pattern corresponds to changes in annual 7day low flows. However, the relative increase in Q90/P is smaller compared to the relative increase in yearly minimum flows. The Pitztal shows the highest increase in Q90/P (55%, RCP 8.5), whilst in both the Feistritztal and Gailtal negative changes of respectively -4% and -1% in Q90/P are predicted for RCP 8.5. This corresponds to a decrease of 8% resp. 4% in Q90/P compared to RCP 4.5 and is likely caused by an annual increase of precipitation, whilst the magnitude of Q90 flow remains stable. The latter can result from increased evaporation rates and decreased summer precipitation, resulting in a higher dependency on summer Q90 flows in the future. Uncertainty bands increase for RCP 8.5 and range between 60% (Paltental) and 225% (Pitztal). A similar pattern is found for absolute changes (Figure S23)

The adaptive model predicts a lower median change in Q90/P. Differences with the stationary model are in between 0% and 6% for RCP 4.5, which are experienced in the Feistritztal and Paltental respectively. For RCP 8.5 modelled spread increases up to 10% in the Paltental. The adaptive model shows a slightly higher spread compared to the stationary model, with uncertainty bands of RCP 8.5 predictions ranging between 82% (Paltental) and 225% (Pitztal). However, for both models, the spread in Q90/P is smaller than the spread in the predicted change of magnitude of low flows.

Thirdly, the severity of low flows in the future is examined based on the monthly deficit in flows, using Q90 as a threshold for the past and future. Figure 20 shows a clear relationship between monthly deficits and altitude. The higher elevation catchments experience hardly any deficits from May to November, both for the Past and Future. This can relate to both a decreased snow storage volume and higher precipitation amounts experienced in future winters, with increasing winter discharges and decreased deficits as a result. For the lower elevation catchments, however, the number of months with deficits increases. The Feistritztal even

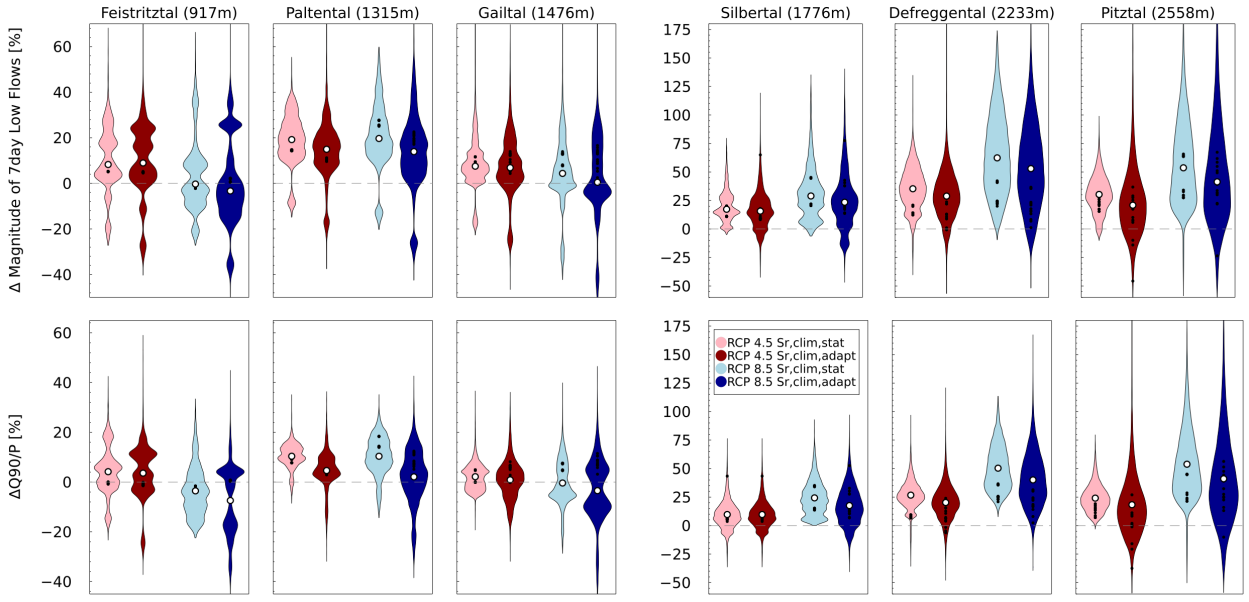

Figure 19: Relative change in average magnitude of low flows (1st row) and in ratio of Q90 to precipitation (2nd row). Results obtained from models featuring $S_{R,clim,stat}$ and $S_{R,clim,adapt}$ are respectively depicted in pink and red for RCP 4.5 and light blue and blue for RCP 8.5. Note the different scales for low and high elevation catchments.

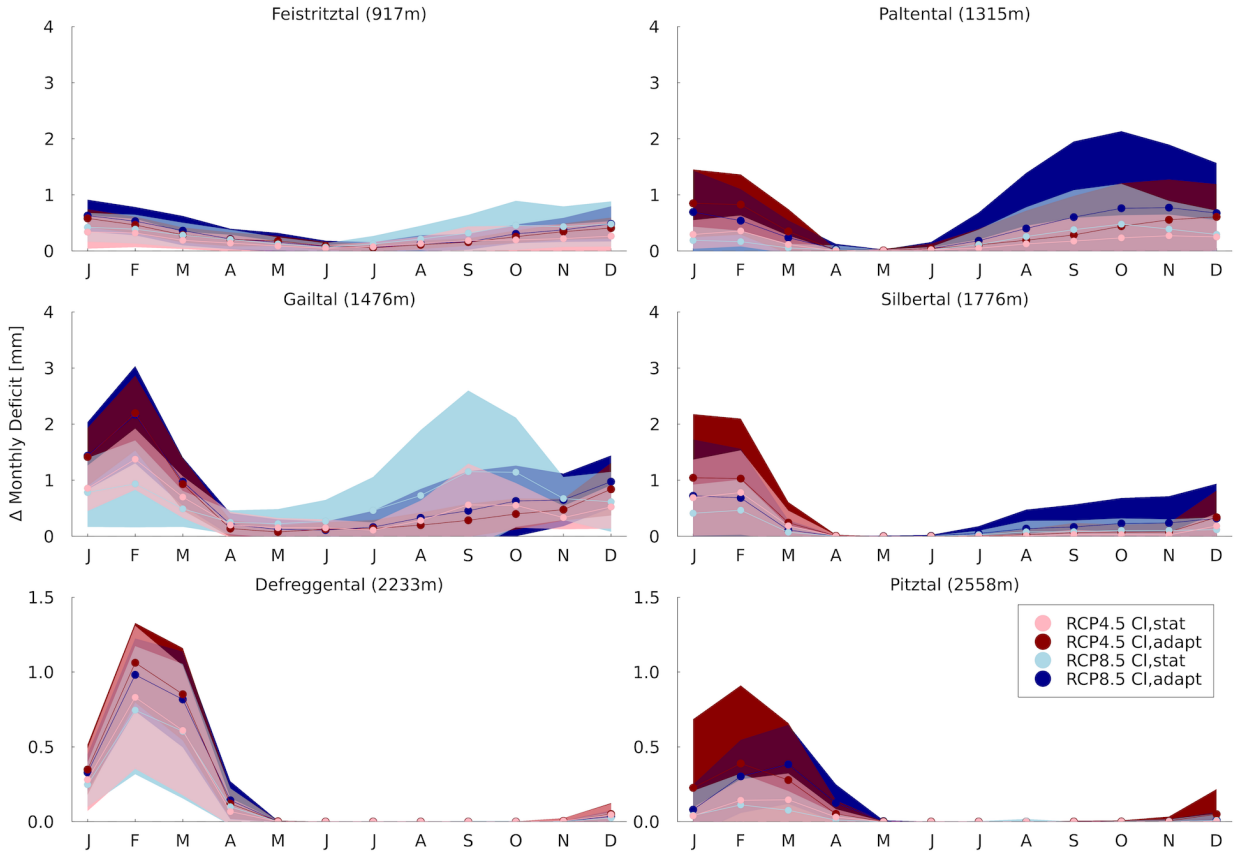

Figure 20: Monthly deficits based on the Q90 threshold for the past and under 2 emission scenarios in the future, using the climate based stationary and adaptive model. Results obtained from models featuring $S_{R,clim,stat}$ and $S_{R,clim,stat}$ are respectively depicted in pink and red for RCP 4.5 and light blue and blue for RCP 8.5.

experiences deficits every month. The stationary model predicts decreases in the magnitude of monthly deficits in the winter months for all catchments. This effect is especially pronounced for RCP 8.5. The maximum increase of drought in the winter occurs in the Gailtal and (1.4 mm/d), contrasting to only 0.2mm/d increase in the Pitztal. Thereby deficits increase in later months for catchments at higher mean elevation. Overall the number of months with an increasing deficit is largest for lower elevation catchments, in which deficits increase every month. For higher elevation catchments seasonality increases, with peak increases in deficits occurring in November to May.

The adaptive model shows higher changes in deficit compared to the stationary model. The difference in model results is persistent throughout the entire year and increases with the magnitude of drought. For RCP 8.5 this difference is larger, with maximum offset found in February in the Gailtal (1.4mm), coinciding with the highest predicted drought increase. The least difference is encountered in January in the Feistritztal (0.4mm). In other months the model projections are rather consistent, except for a remarkable higher estimation of drought by the stationary model occurring in June to December in the Gailtal. Higher median annual deficit volumes were also found by Bouaziz et al. (2021), albeit that the found changes in this study are smaller. Likely increases in deficit are the result of an increased length of low flow period under root zone adaption, as minimal streamflow remains similar.

Apart from higher drought predictions, the adaptive model also predicts an increase in model spread. This is most pronounced at the peak droughts and can range up to a 1.8mm difference in drought projection in the Gailtal, depending on the climate model used.

5 Broader Implications

Our results show broadly consistent model predictions for the climate-based stationary and adaptive model. Although the root zone storage capacity of both forest and grass changes significantly in the future, respectively with 0-100% and 25-45%, accounting for this in model

parameters only results in a limited decrease of predicted streamflow. The adaptive model shows differences in annual mean streamflow close to zero. Monthly discharges can differ up to -10% depending on the season. A similar pattern is found for seasonal runoff coefficients, whereas changes in the annual runoff coefficient lie around -5%. Annual maximum flows are predicted -5% lower, whereas changes in 7day consecutive low flows and fractions of occurrences of respectively high and low flows remain close to zero for all catchments.

The found differences are in general slightly smaller in the Feistritztal (1-2%), but larger in the higher elevation catchments. This pattern corresponds to the predicted magnitude of change between past and future streamflow in these catchments.

Although less pronounced, our findings point in the same direction of change as previously conducted studies that implemented vegetation dynamics in hydrological models. Bouaziz et al. (2021) found reductions in annual mean (-7%), annual maximum (-5%) and 7day low (0%) flows when exchanging calibrated root zone storage capacity parameters for climate-based adaptive estimates. Also, Merz et al. showed the static parameter model to overestimate mean annual and maximum streamflow by respectively +15% and +35%. Similarly, Duethmann et al. and Speich, Lischke, and Zappa showed static model overestimation to reduce by roughly a third, resp. 6x, when accounting for vegetation dynamics. According to changes in vegetation, evaporation rates were found to increase with +4% (Bouaziz et al., 2021) and +70% Merz et al. (2011), which shows that vast disagreement can occur in model representation of relevant processes in the future. Although no such disagreement was found in this study, a similar pattern of change could be distinguished: Runoff coefficients were found to decrease, inferring higher evaporation rates.

The results of this study suggest that the estimated change in root zone storage capacity is small enough to have only a limited influence on future streamflow in the selected study catchments. This is plausible as past and future climate-based parameters are covered within the range of calibration parameters (Appendix B.2), which are used as the basis for the climate-based parameter sets and also showed to reasonably describe past streamflow with only limited spread.

However, larger increments in future root zone storage capacity are likely to induce a higher offset between adaptive and stationary model results. At these locations, accounting for future changes in S_R would still be relevant for more reliable streamflow predictions. To illustrate, the Paltental shows the most pronounced changes in the root zone storage capacity between past and future, which results in relatively high differences in predicted stationary and adapted model results. Similarly, more pronounced differences in streamflow are found by Bouaziz et al. and (Merz et al., 2011) in response to larger increases in root zone storage capacity of +34% and +67% under a 2K warming scenario. However, it should be noted that both studies apply to average over multiple catchments with a large climatic gradient, which influences the magnitude of change in root zone storage capacity. This also becomes evident from Merz et al. (2011), who showed that averaging over only the relatively humid catchments results in lower increases of +46%.

The six studied catchments are all relatively humid (Figure 5) and are therefore characterized by shallow hydrologically active root zones (Merz & Blöschl, 2004). Also, the potentially adverse effects of increased precipitation and temperature limit the increments in the root zone storage capacity. Hence, to obtain a more general conclusion of the advantages and limitations of this approach, the methodology should be further explored in the context of arid catchments, with potentially higher increases in root zone storage capacity and a more pronounced impact on streamflow under climate change.

In addition, other factors could contribute to the only limited difference found in model results. First of all, this study focuses on the isolated development of the root zone storage capacity. It is, however, likely that changes in root zone storage capacity will influence other system characteristics, that alter the liquid water input and in turn the root zone storage capacity. Merz et al. account for this in a coupled simulation of a land surface and hydrological model, partially explaining the higher differences in modelled streamflow. In further research, it would hence be interesting to investigate the effect of changes in S_R on other model parameter dynamics and hence on future predictions of streamflow. The same applies to the use of the Budyko framework. Several iterations could be applied to account for the influence of root-zone storage dynamics on long-term streamflow. Thirdly, this study determines increases in the root zone storage capacity averaged over 30 years. Thereby, a potential weakening of the increasing trend over time is disregarded, which would be interesting to look into for further research.

Finally, it should be reminded that this study is an exploratory analysis of the potential impacts of including non-stationarity in the root-zone storage capacity parameter on hydrological model results. The findings of this study suggest that the changes in root zone storage capacity, following the assumptions that vegetation adapts its root zone to water deficits of certain return periods, are small enough to have very little influence on streamflow predictions. This indicates that changes in the root zone are not necessary to account for in the representative model parameter to reasonably de-

scribe streamflow. However, the results only count for the studied areas, under the stated assumptions and in careful consideration of uncertainties and limitations.

5.1 Uncertainty & Limitations

The main uncertainties in this study originate from the used approach, applied scope and advised climate data. Firstly, this study quantifies changes in modelled hydrological response, whilst relying on the combined use of the water balance method and a parameterized Budyko framework. As both methods face several assumptions, deliberate application is required.

Namely, the water balance method is founded on the assumptions that vegetation adapts its root-zone storage capacity towards changes in climate. In addition, future changes in long-term mean runoff are estimated from a parameterized Budyko equation, which assumes that the catchment specific parameter ω represents biophysical features of the catchments and changes in response to changed aridity. However, recent work of Reaver, Kaplan, Klammler, and Jawitz (2020) and Berghuijs et al. (2020) illustrates the need for careful and considerate application of the parameterized Budyko equation in changing systems. Furthermore, our study builds upon the assumption that vegetation will - and has had the time to - adapt towards prevailing climate conditions and does so in compliance with the dynamic equilibrium described by the Budyko framework. Credence to this approach is lent since Gentine et al. (2012) showed that vegetation eventually adapts to suffice water needs, which is likely reflected in the scattered pattern of catchments worldwide plotting around the Budyko curve (Troch et al., 2013). Yet, considering the unprecedented scale and rate of current climate change (Gleeson et al., 2020), it is unclear how ecosystems will cope with these changed conditions. In line with this, the assumed return period of droughts that can be bridged through root zone adaptation in the future, faces uncertainty and can have a considerable effect on the calculated future root zone storage capacity. The severity of influence depends on the magnitude of the used return period, as follows from the logarithmic shape of the GEV distribution.

Secondly, the focus of this study is limited to climate-induced changes in the root-zone storage capacity. However, climate change is likely to impact other aspects of catchment functioning (Seibert & van Meerveld, 2016). Firstly, ecosystems might be reducing or increasing their water use to water availability (Zhang et al., 2001). Secondly, increased CO_2 concentrations are likely to induce vegetation water-saving responses and increased productivity through fertilization (Keenan et al., 2013; Van der Velde et al., 2014; Ukkola et al., 2016; Jaramillo et al., 2018).

Additionally, changes in maximum interception storage (Calder, Reid, Nisbet, & Green, 2003) are not explicitly considered in the estimation of the adapted root-zone storage capacities. However, Bouaziz et al. (2020) showed impacts to be relatively minor, which is in line with the sensitivity analysis presented in Appendix A.2. Furthermore, both natural and human-induced Land Use and Land Cover (LULC) changes have been disregarded in the study. Although LULC processes are slow and current changes will only become apparent in decades and centuries to come, they can have a significant influence on hydrological responses (Jaramillo & Destouni, 2014) and reflect in vertical movements in the Budyko space (Bouaziz et al., 2018). However, future LULC developments face uncertainty and remain problematic to quantify in a meaningful way.

For this reason, long-term observed climate data is used to determine the ω-parameter. This parameter represents catchment conditions in the past and is in turn used to estimate the partitioning of water fluxes in the future. Due to time constraints, the Fu-curves are currently estimated based on one data point. In future research, a more robust estimate could be obtained by using multiple long-term climate indices as input. Furthermore the plausibility of an observation-based ω-parameter that is used to represent future conditions, could be checked and improved through iteration. Thereby a climate adapted Fu-curve can be estimated from the runoff coefficient obtained from the climate based adaptive hydrological model.

Thirdly, this study faces uncertainties of climate projections and observation data.

The results of this study rely on climate projections that invoke a large spread in modelled parameter estimates and streamflow predictions. Depending on the climate projection used, differences in projected streamflow can range up to 50%. Previous studies identify the use of multi-GCM projection as the main driver of spread in future hydrological runoff predictions (Addor et al., 2014; Her et al., 2019). Thereby the spread resulting form multi-GCM projections is commonly an order of magnitude larger than spread invoked by hydrological model uncertainties. This is in line with the significantly smaller spread in $S_{R,clim}$ estimates that is found when using observed instead of modelled climate data. Therefore, uncertainty in predicted runoff behaviour is inherent to the use of climate projections and further stresses the need to use an ensemble of climate projections in order to quantify the uncertainty introduced by climate change and limit the potential for misinterpretation.

Secondly, Hanus (2020) shows that the used projected past temperatures are lower in comparison to observed temperatures in higher elevation catchments, although

observed and modelled datasets originate from the same location. To account for this, a bias correction has been performed for the calculation of future $S_{R,clim}$. However, no correction has been applied when forcing the model with future data. Thereby the lower projected temperatures can result in increased snow accumulation and decreased runoff. Since model calibration relies on measured data and simulation data is used to predict future streamflow, this could result in larger modelled changes for both the adaptive and stationary models.

Furthermore, observed precipitation data is influenced by the limited amount of precipitation gauges used and could therefore be subject to precipitation undercatch. Possibly this contributes to the error in the position of the Pitztal in the Budyko framework and could explain precipitation and discharge mismatches in the Silbertal and Defreggental. Likely also $S_{R,clim}$ estimates for the past, and indirectly for the future, are influenced.

In addition, the choice of calculation method of potential evaporation can also reasonably influence the model results (Seiller & Anctil, 2016) and $S_{R,clim}$ estimates. Due to constraints in time and data, only the Thornthwaite method has been used. However, Li et al. (2018) advocate higher applicability of the Hargreaves method under climate change.

Lastly, the climate based parameters are inserted in existing calibration sets. This allows for baseline comparison, whilst simultaneously including some level of equifinality in the model. However, renewed model calibration will tune the ensemble of climate based parameter sets and thereby possibly result in better description streamflow and a change in future predictions.

Uncertainty during calibration is further increased through the inclusion of a loss term as a calibration parameter in the Pitztal. This parameter is required to account for the unknown amount of water that is diverted for hydropower uses but increases equifinality and hence model uncertainty. Application of the loss term also influences long-term mean runoff estimates from the Budyko framework, which reflects in root zone storage estimates.

6 Conclusion

Understanding the non-stationarity of hydrological systems in a changing climate is acknowledged as a major challenge in hydrology (Bosch, 2010). Still, a knowledge gap exists concerning the meaningful implementation of system changes in hydrological models. Process-based approaches could serve as a solution to this, due to the holistic consideration of the co-evolution of soil, climate and vegetation. Accordingly, this study provides an exploratory analysis of a top-down approach to describe non-stationarity in the root zone capacity parameter within process-based hydrological models for six catchments in the Austrian Alps. This method relies on a combination of long- and short-term water budgets and uses solely climate data to describe vegetation-climate interactions. Accordingly, root zone storage capacity parameters are estimated for the past and under 2 emission scenarios, generated from 14 different climate models, in the future.

The projected future increases in temperature and precipitation, which are particularly pronounced for high emissions (RCP 8.5), result in an increased catchment dryness and evapotranspiration. Although, climate-based ($S_{R,clim}$) parameter ranges show vast differences per catchment, root zone storage capacities are found to increase for all catchments in the future. Changes are more pronounced for forest (0-100%) than for grass (25-45%).

The climate-based parameters are subsequently implemented in a FLEX-topo hydrological model to test the plausibility of climate-based estimates by modeling past streamflow. Findings indicate that both climate-based and calibration parameter sets describe observed streamflow equally well, notwithstanding the significant reduction of parameter space for climate-based estimates. Subsequently, the verified parameter sets can be used to predict future streamflow. Here, two different models are used, which respectively use past and future climate data to establish root zone storage capacity parameters ($S_{R,clim}$). The model results are compared to investigate the effect of root zone storage adaptation on modelled streamflow. Findings show that the adaptive model results in slightly lower streamflow predictions. Differences in annual mean and extreme flows are found to be -5%, but can vary up to -10% for runoff coefficients and monthly discharges. However, the found dissimilarity is highly dependent on the catchment, time of the year, used climate model simulation and emission scenario.

Thereby, no or very little evidence is found that vegetation adaptation, following the assumptions underlying the water balance method, significantly alters the hydrological response in the studied catchments. Exchanging calibrated root zone storage capacity parameters for climate-based adaptive estimates generates broadly consistent model results in the investigated regions. This implies a low necessity to include non-stationarity in the root zone storage capacity parameter of process-based hydrological models to plausibly project streamflow in the future at the studies locations. However, more prominent differences in streamflow are expected as a result of larger increments in root zone storage capacity. Thus, to draw a broader conclusion, further research that explores this concept in different climatic regions is recommended.

References

Abermann, J., Fischer, A., Lambrecht, A., & Geist, T. (2010). On the potential of very high-resolution repeat DEMs in glacial and periglacial environments. Cryosphere, 4(1), 53–65. doi: 10.5194/tc-4-53-2010

Addor, N., Rossler, O., Köplin, N., Huss, M., Weingartner, R., & Seibert, J. (2014). Water Resources Research. , 5375–5377. doi: 10.1002/2013WR014979.Reply

Andréassian, V., Parent, E., & Michel, C. (2003). A distribution-free test to detect gradual changes in watershed behavior. Water Resources Research, 39(9), 1–11. doi: 10.1029/2003WR002081

Bavay, M., Grünewald, T., & Lehning, M. (2013). Response of snow cover and runoff to climate change in high Alpine catchments of Eastern Switzerland. Advances in Water Resources, 55(2013), 4–16. Retrieved from http://dx.doi.org/10.1016/j.advwatres.2012.12.009 doi: 10.1016/j.advwatres.2012.12.009

Berghuijs, W. R., Gnann, S. J., & Woods, R. A. (2020). Unanswered questions on the Budyko framework. (October), 5699–5703. doi: 10.1002/hyp.13958

Beven, K., & Binley, A. (1992). The future of distributed models: Model calibration and uncertainty prediction. Hydrological Processes, 6(3), 279–298. doi: 10.1002/hyp.3360060305

Blöschl, G., Bierkens, M. F., Chambel, A., Cudennec, C., Destouni, G., Fiori, A., ... Zhang, Y. (2019). Twenty-three unsolved problems in hydrology (UPH)a community perspective. Hydrological Sciences Journal, 64(10), 1141–1158. doi: 10.1080/02626667.2019.1620507

Blöschl, G., Hall, J., Parajka, J., Perdigão, R. A., Merz, B., Arheimer, B., ... Živković, N. (2017). Changing climate shifts timing of European floods. Science, 357(6351), 588–590. doi: 10.1126/science.aan2506

Blöschl, G., Viglione, A., Merz, R., Parajka, J., Salinas, J. L., & Schöner, W. (2011). Auswirkungen des Klimawandels auf Hochwasser und Niederwasser. Osterreichische Wasser- und Abfallwirtschaft, 63(1), 21–30. doi: 10.1007/s00506-010-0269-z

Boschl, A., G.; Montanari. (2010). Climate change impactsthrowing the dice? Hydrological Processes(24), 374–381. Retrieved from http://jamsb.austms.org.au/courses/CSC2408/semester3/resources/ldp/abs-guide.pdf doi: 10.1002/hyp.7574

Bouaziz, L., Aalbers, E. E., Weerts, A. H., Hegnauer, M., Buiteveld, H., Lammersen, R., ... Hrachowitz, M. (2021). The importance of ecosystem adaptation on hydrological model predictions in response to climate change. Hydrol. Earth Syst. Sci. Discuss., 2021(April), 1–39. Retrieved from https://hess.copernicus.org/preprints/hess-2021-204/%0Ahttps://hess.copernicus.org/preprints/hess-2021-204/hess-2021-204.pdf

Bouaziz, L., Thirel, G., de Boer-Euser, T., Melsen, L., Buitink, J., Brauer, C., ... Hrachowitz, M. (2020). Behind the scenes of streamflow model performance. Hydrology and Earth System Sciences Discussions, 1–38. doi: 10.5194/hess-2020-176

Bouaziz, L., Weerts, A., Schellekens, J., Sprokkereef, E., Stam, J., Savenije, H., & Hrachowitz, M. (2018). Redressing the balance: Quantifying net intercatchment groundwater flows. Hydrology and Earth System Sciences, 22(12), 6415–6434. doi: 10.5194/hess-22-6415-2018

Brunner, M. I., Melsen, L. A., Newman, A. J., Wood, A. W., & Clark, M. P. (2020). Future streamflow regime changes in the United States: Assessment using functional classification. Hydrology and Earth System Sciences, 24(8), 3951–3966. doi: 10.5194/hess-24-3951-2020

Buytaert, W., & Beven, K. (2009). Regionalization as a learning process. Water Resources Research, 45(11), 1–13. doi: 10.1029/2008WR007359

Calder, I. R., Reid, I., Nisbet, T. R., & Green, J. C. (2003). Impact of lowland forests in England on water resources: Application of the Hydrological Land Use Change (HYLUC) model. Water Resources Research, 39(11), 1–10. doi: 10.1029/2003WR002042

Coron, L., Andréassian, V., Perrin, C., Lerat, J., Vaze, J., Bourqui, M., & Hendrickx, F. (2012). Crash testing hydrological models in contrasted climate conditions: An experiment on 216 Australian catchments. Water Resources Research, 48(5). doi: 10.1029/2011WR011721

Criss, R. E., & Winston, W. E. (2008). Do Nash values have value? Discussion and alternate proposals. Hydrological Proces, 22(May 2008), 2723–2725. Retrieved from http://jamsb.austms.org.au/courses/CSC2408/semester3/resources/ldp/abs-guide.pdf doi: 10.1002/hyp.7072

de Boer-Euser, T., McMillan, H., Hrachowitz, M., Winsemius, H., & Savenije, H. (2016). Influence of soil and climate on root zone storage capacity. Journal of the American Water Resources Association, 5(3), 2–2. Retrieved from doi:10.1002/2015WR018115.%0AReceived doi: 10.1111/j.1752-1688.1969.tb04897.x

Dobler, C., Bürger, G., & Stötter, J. (2012). Assessment of climate change impacts on flood hazard potential in the Alpine Lech watershed. Journal of Hydrology, 460-461, 29–39. Retrieved from http://dx.doi.org/10.1016/j.jhydrol.2012.06.027 doi: 10.1016/j.jhydrol.2012.06.027

Donohue, R. J., Roderick, M. L., & McVicar, T. R. (2012). Roots, storms and soil pores: Incorporating key ecohydrological processes into Budyko's hydrological model. Journal of Hydrology, 436-437, 35–50. Retrieved from http://dx.doi.org/10.1016/j.jhydrol.2012.02.033 doi: 10.1016/j.jhydrol.2012.02.033

Duethmann, D., Bloschl, G., & Parajka, J. (2020). Why does a conceptual hydrological model fail to correctly predict discharge changes in response to climate change? Hydrology and Earth System Sciences, 24(7), 3493–3511. doi: 10.5194/hess-24-3493-2020

Dwarakish, G. S., & Ganasri, B. P. (2015). Impact of land use change on hydrological systems : A review of current modeling approaches Impact of land use change on hydrological systems : A review of current modeling approaches. Cogent Geoscience, 1(1). Retrieved from http://dx.doi.org/10.1080/23312041.2015.1115691 doi: 10.1080/23312041.2015.1115691

Efstratiadis, A., & Koutsoyiannis, D. (2010). Une décennie d'approches de calage multi-objectifs en modélisation hydrologique: Une revue. Hydrological Sciences Journal, 55(1), 58–78. doi: 10.1080/02626660903526292

Euser, T., Winsemius, H. C., Hrachowitz, M., Fenicia, F., Uhlenbrook, S., & Savenije, H. H. (2013). A framework to assess the realism of model structures using hydrological signatures. Hydrology and Earth System Sciences, 17(5), 1893–1912. doi: 10.5194/hess-17-1893-2013

Fenicia, F., Savenije, H. H., & Avdeeva, Y. (2009). Anomaly in the rainfall-runoff behaviour of the Meuse catchment. Climate, land-use, or land-use management? Hydrology and Earth System Sciences, 13(9), 1727–1737. doi: 10.5194/hess-13-1727-2009

Finger, D., Vis, M., Huss, M., & Seibert, J. (2015). The value of multiple data set calibration versus model complexity for improving the performance of hydrological models in mountain catchments. Water Resources ResearchRes., 51, 1939–1958. doi: 10.1002/2014WR015712.

Fu, B. (1981). On the calculation of the evaporation from land surface (Vol. 5) (No. 1). ((in Chinese))

Gao, H., Hrachowitz, M., Schymanski, S. J., Fenicia, F., Sriwongsitanon, N., & Savenije, H. H. (2014). Climate controls how ecosystems size the root zone storage capacity at catchment scale. Geophysical Research Letters, 41(22), 7916–7923. doi: 10.1002/2014GL061668

Gao, J., Holden, J., & Kirkby, M. (2015). A distributed TOPMODEL for modelling impacts of land-cover change on river flow in upland peatland catchments. Hydrological Processes, 29(13), 2867–2879. doi: 10.1002/hyp.10408

Gentine, P., D'Odorico, P., Lintner, B. R., Sivandran, G., & Salvucci, G. (2012). Interdependence of climate, soil, and vegetation as constrained by the Budyko curve. Geophysical Research Letters, 39(19), 2–7. doi: 10.1029/2012GL053492

Gharari, S., Hrachowitz, M., Fenicia, F., Gao, H., & Savenije, H. H. (2014). Using expert knowledge to increase realism in environmental system models can dramatically reduce the need for calibration. Hydrology and Earth System Sciences, 18(12), 4839–4859. doi: 10.5194/hess-18-4839-2014

Gleeson, T., Wang-Erlandsson, L., Porkka, M., Zipper, S. C., Jaramillo, F., Gerten, D., ... Famiglietti, J. S. (2020). Illuminating water cycle modifications and Earth system resilience in the Anthropocene. Water Resources Research, 56(4), 1–24. doi: 10.1029/2019WR024957

Hall, D. K., & Riggs, G. A. (2016). Modis/terra snow cover daily l3 global 500m sin grid, version 6. https://www.nasa.gov/nh/pluto-the-other-red-planet. (NASA National Snow and Ice Data Center Distributed Active Archive Center.., Retrieved 2020-05-16, from https://doi.org/10.5067/MODIS/MOD10A1.006)

Hanus, S. (2020). Effects of Climate Change on Runoff Dynamics in Alpine Catchments. , 45.

Her, Y., Yoo, S. H., Cho, J., Hwang, S., Jeong, J., & Seong, C. (2019). Uncertainty in hydrological analysis of climate change: multi-parameter vs. multi-GCM ensemble predictions. Scientific Reports, 9(1), 1–22. Retrieved from http://dx.doi.org/10.1038/s41598-019-41334-7 doi: 10.1038/s41598-019-41334-7

Hrachowitz, M., Fovet, O., Ruiz, L., Euser, T., Gharari, S., Nijzink, R., ... Gascuel-Odoux, C. (2014). Process consistency in models: The importance of system signatures, expert knowledge, and process complexity. , 5375–5377. doi: 10.1002/2013WR014979

Hrachowitz, M., Stockinger, M., Coenders-gerrits, M., Ent, R. V. D., Lücke, A., & Stumpp, C. (2020). Reduction of vegetation-accessible water storage capacity after deforestation affects catchment travel time distributions and increases young water fractions in a headwater catchment. , i, 1–47.

Hrachowitz, M., & Weiler, M. (2011, 5). Uncertainty of precipitation estimates caused by sparse gauging networks in a small, mountainous watershed. Journal of Hydrologic Engineering, 16, 460-471. doi: 10.1061/(asce)he.1943-5584.0000331

IPCC. (2019). Climate Change and Land: an IPCC special report on climate change, desertification, land degradation, sustainable land management, food security, and greenhouse gas fluxes in terrestrial ecosystems. Technical report, 35–74.

IPCC. (2021). AR6 WGI Report - Chapter 8: Water cycle changes. AR 6(August 2021). doi: 10.21513/2410-8758-2017-2-13-25

Jaramillo, F., Cory, N., Arheimer, B., Laudon, H., Van Der Velde, Y., Hasper, T. B., ... Uddling, J. (2018, jan). Dominant effect of increasing forest biomass on evapotranspiration: Interpretations of movement in Budyko space. Hydrology and Earth System Sciences, 22(1), 567–580. doi: 10.5194/hess-22-567-2018

Jaramillo, F., & Destouni, G. (2014, dec). Developing water change spectra and distinguishing change drivers worldwide. Geophysical Research Letters, 41(23), 8377–8386. doi: 10.1002/2014GL061848

Jochen Schenk, H. (2005). Vertical Vegetation Structure Below Ground: Scaling from Root to Globe. Progress in Botany, 66, 341–373. doi: 10.1007/3-540-27043-4_14

Keenan, T., Hollinger, D., Bohrer, G., Dragoni, D., Munger, W., Schmid, H. P., & Richardson, A. (2013). Increase in forest water-use efficiency as atmospheric carbon dioxide concentrations rise. Nature, 499(7458), 324–327. doi: 10.1038/nature12291

Lambrecht, A., & Kuhn, M. (2007). Glacier changes in the Austrian Alps during the last three decades, derived from the new Austrian glacier inventory. Annals of Glaciology, 46, 177–184. doi: 10.3189/172756407782871341

Levia, D. F., Creed, I. F., Hannah, D. M., Nanko, K., Boyer, E. W., Carlyle-Moses, D. E., ... Bruen, M. (2020). Homogenization of the terrestrial water cycle. Nature Geoscience, 13(10), 656–658. doi: 10.1038/s41561-020-0641-y

Li, Z., Yang, Y., Kan, G., & Hong, Y. (2018). Study on the applicability of the Hargreaves potential evapotranspiration estimation method in CREST distributed hydrological model (version 3.0) applications. Water (Switzerland), 10(12), 1–15. doi: 10.3390/w10121882

Mader, H., Steidl, T., & Wimmer, R. (1996). Abflussregime Österreichischer Fliessgewässer; Beitrag zu einer bundesweiten Fließgewässertypologie. Monograhien Bundesumweltamt, 82(August), 192pp. Retrieved from http://www.umweltbundesamt.at/fileadmin/site/publikationen/M082z.pdf

Merz, R., & Blöschl, G. (2004). Regionalisation of catchment model parameters. Journal of Hydrology, 287(1-4), 95–123. doi: 10.1016/j.jhydrol.2003.09.028

Merz, R., Parajka, J., & Blöschl, G. (2011). Time stability of catchment model parameters: Implications for climate impact analyses. Water Resources Research, 47(2). doi: 10.1029/2010WR009505

Mianabadi, A., Davary, K., & Pourreza-bilondi, M. (2020). Budyko framework ; towards non-steady state conditions. Journal of Hydrology, 588(February), 125089. Retrieved from https://doi.org/10.1016/j.jhydrol.2020.125089 doi: 10.1016/j.jhydrol.2020.125089

Milly, P. C., Betancourt, J., Falkenmark, M., Hirsch, R. M., Kundzewicz, Z. W., Lettenmaier, D. P., & Stouffer, R. J. (2008). Climate change: Stationarity is dead: Whither water management? Science, 319(5863), 573–574. doi: 10.1126/science.1151915

Milly, P. C. D., & Dunne, K. A. (2011). On the Hydrologic Adjustment of Climate-Model Projections : The Potential Pitfall of Potential Evapotranspiration. , 15(1). doi: 10.1175/2010EI363.1

Nash, J. E., & Sutcliffe, J. V. (1970). River flow forecasting through conceptual models part I - A discussion of principles. Journal of Hydrology, 10(3), 282–290. doi: 10.1016/0022-1694(70)90255-6

Nijzink, R., Hutton, C., Pechlivanidis, I., Capell, R., Arheimer, B., Freer, J., ... Hrachowitz, M. (2016). The evolution of root-zone moisture capacities after deforestation: A step towards hydrological predictions under change? Hydrology and Earth System Sciences, 20(12), 4775–4799. doi: 10.5194/hess-20-4775-2016

Prenner, D., Hrachowitz, M., & Kaitna, R. (2019). Trigger characteristics of torrential flows from high to low alpine regions in Austria. Science of the Total Environment, 658, 958–972. Retrieved from https://doi.org/10.1016/j.scitotenv.2018.12.206 doi: 10.1016/j.scitotenv.2018.12.206

Reaver, N., Kaplan, D., Klammler, H., & Jawitz, J. (2020). Reinterpreting the Budyko Framework. Hydrology and Earth System Sciences Discussions(November), 1–31. doi: 10.5194/hess-2020-584

Sankarasubramanian, A., Wang, D., Archfield, S., Reitz, M., & Vogel, R. M. (2020). HESS Opinions : Beyond the long-term water balance : evolving Budyko ' s supply demand framework for the Anthropocene towards a global synthesis of land-surface fluxes under natural and human-altered watersheds. , 1975–1984.

Savenije, H. H. (2010). HESS opinions "topography driven conceptual modelling (FLEX-Topo)". Hydrology and Earth System Sciences, 14(12), 2681–2692. doi: 10.5194/hess-14-2681-2010

Savenije, H. H., & Hrachowitz, M. (2017). HESS Opinions "catchments as meta-organisms - A new blueprint for hydrological modelling". Hydrology and Earth System Sciences, 21(2), 1107–1116. doi: 10.5194/hess-21-1107-2017

Schenk, R., J.; Jackson. (2002). The Global Biogeography of Roots. Ecological Monographs, 72(3), 311–328.

Seibert, J., & van Meerveld, H. J. (2016). Hydrological change modeling: Challenges and opportunities. Hydrological Processes, 30(26), 4966–4971. doi: 10.1002/hyp.10999

Seiller, G., & Anctil, F. (2016). How do potential evapotranspiration formulas influence hydrological projections ? Hydrological Sciences Journal, 61(12), 2249–2266. Retrieved from http://dx.doi.org/10.1080/02626667.2015.1100302 doi: 10.1080/02626667.2015.1100302

Speich, M. J., Lischke, H., & Zappa, M. (2018). Testing an optimality-based model of rooting zone water storage capacity in temperate forests. Hydrology and Earth System Sciences, 22(7), 4097–4124. doi: 10.5194/hess-22-4097-2018

Stephens, C. M., Lall, U., Johnson, F. M., & Marshall, L. A. (2021, jan). Landscape changes and their hydrologic effects: Interactions and feedbacks across scales (Vol. 212). Elsevier B.V. doi: 10.1016/j.earscirev.2020.103466

Stephens, C. M., Marshall, L. A., & Johnson, F. M. (2019, dec). Investigating strategies to improve hydrologic model performance in a changing climate. Journal of Hydrology, 579. doi: 10.1016/j.jhydrol.2019.124219

Switanek, B. M., Troch, A. P., Castro, L. C., Leuprecht, A., Chang, H. I., Mukherjee, R., & Demaria, M. C. (2017). Scaled distribution mapping: A bias correction method that preserves raw climate model projected changes. Hydrology and Earth System Sciences, 21(6), 2649–2666. doi: 10.5194/hess-21-2649-2017

Troch, P. A., Carrillo, G., Sivapalan, M., Wagener, T., & Sawicz, K. (2013). Climate-vegetation-soil interactions and long-term hydrologic partitioning: Signatures of catchment co-evolution. Hydrology and Earth System Sciences, 17(6), 2209–2217. doi: 10.5194/hess-17-2209-2013

Ukkola, A. M., Prentice, I. C., Keenan, T. F., Van Dijk, A. I., Viney, N. R., Myneni, R. B., & Bi, J. (2016). Reduced streamflow in water-stressed climates consistent with CO2 effects on vegetation. Nature Climate Change, 6(1), 75–78. doi: 10.1038/nclimate2831

Van der Velde, Y., Vercauteren, N., Jaramillo, F., Dekker, S. C., Destouni, G., & Lyon, S. W. (2014). Exploring hydroclimatic change disparity via the Budyko framework. Hydrological Processes, 28(13), 4110–4118. doi: 10.1002/hyp.9949

Vormoor, K., Lawrence, D., Heistermann, M., & Bronstert, A. (2015). Climate change impacts on the seasonality and generation processes of floods ndash; Projections and uncertainties for catchments with mixed snowmelt/rainfall regimes. Hydrology and Earth System Sciences, 19(2), 913–931. doi: 10.5194/hess-19-913-2015

Wagener, T. (2007). Advanced Bash-Scripting Guide An in-depth exploration of the art of shell scripting Table of Contents. Hydrological Processes, 21(September 2007), 3233–3236. Retrieved from http://jamsb.austms.org.au/courses/CSC2408/semester3/resources/ldp/abs-guide.pdf doi: 10.1002/hyp.6873Can

Wang-Erlandsson, L., Bastiaanssen, W. G., Gao, H., Jägermeyr, J., Senay, G. B., Van Dijk, A. I., ... Savenije, H. H. (2016). Global root zone storage capacity from satellite-based evaporation. Hydrology and Earth System Sciences, 20(4), 1459–1481. doi: 10.5194/hess-20-1459-2016

Xing, W., Wang, W., Zou, S., & Deng, C. (2018). Projection of future runoff change using climate elasticity method derived from budyko framework in major basins across china (Vol. 162) (No. September 2017). Elsevier. Retrieved from https://doi.org/10.1016/j.gloplacha.2018.01.006 doi: 10.1016/j.gloplacha.2018.01.006

Yates, S. K., D. (1994). Potential evapotranspiration methods and their impact on the assessment of river basin runoff under climate change. International Institute for Applied Systems Analysis.

Young, A. R., Round, C. E., & Gustard, A. (2000). Spatial and temporal variations in the occurrence of low flow events in the uk (Vol. 4) (No. 1). doi: 10.5194/hess-4-35-2000

Zekollari, H., Huss, M., & Farinotti, D. (2019). Modelling the future evolution of glaciers in the European Alps under the EURO-CORDEX RCM ensemble. Cryosphere, 13(4), 1125–1146. doi: 10.5194/tc-13-1125-2019

Zhang, L., Dawes, W. R., & Walker, G. R. (2001). Response of mean annual evapotranspiration to vegetation changes at catchment scale. Water Resources Research, 37(3), 701–708. doi: 10.1029/2000WR900325

Zhang, L., Hickel, K., Dawes, W. R., Chiew, F. H., Western, A. W., & Briggs, P. R. (2004). A rational function approach for estimating mean annual evapotranspiration. Water Resources Research, 40(2), 1–14. doi: 10.1029/2003WR002710

Acknowledgements

While writing this, I can finally look back on what has been almost a year of research. During my master's in Water Management and Environmental Engineering, I knew very soon that I wanted to complete my thesis in the field of hydrological modelling. Still, when I decided on this topic, I knew that writing this thesis would be quite challenging. But, wasn't that exactly what I was looking for? Getting the most out of this graduation work and proving myself what I had learned during my studies at the Delft University of Technology. I can say now, that the past months have learned me a lot. My analytical and academic proficiency has improved and I quite surprised myself with my hacker skills. But most of all, I have learned a lot about myself: About keeping work and life in balance and the importance of not always raising the bar, but being satisfied instead. And that is exactly where I am now: Satisfied, happy and proud!

It goes without saying that I could not have achieved the same result without the help of several individuals in my professional and personal environment. Therefore I would like to grab this opportunity to express my gratitude to them.
To start, I would like to thank my committee members. In particular thanks to you Markus, for your close involvement with this study. Our meetings always provided me with a fresh perspective and renewed my motivation to get the most out of this work, not the least because of your positive attitude and enthusiasm. Furthermore, thanks to Harry, Gerrit, and Marie-Claire, for making the time to supervise this research and giving valuable feedback for improvement. Besides that, I would like to thank Sarah, for providing the base model, guiding me through the code, and letting me bother you with all my questions. You helped me to kick start the project and your work has been a great inspiration to me.

On a more personal note, I would like to thank my parents (mom) for all the mental support in the times that I did not entirely enjoy and/or have faith in this study anymore. Also thanks to you Noa, for your sisterly advice, sober perspective, and of course your license to prescribe the required anti-shingles medication.
A big thanks to you Ruben for putting up with a dragon for the past eleven months. You always dealt with my mood swings and provided me with/joined me in the most intense running schedule I have ever committed to. However, it managed to take my mind of this work and inspired me to finally run my first marathon in Rotterdam (2022). And, lastly, of course, thanks for borrowing your laptop!

Concerning that matter, I could not have completed this study without the material support of three extra computers. Therefore, I'd also like to thank Ivar for lending me your 8-Core super laptop and using your linguistic talent to review my research. Thanks to Lennart for your visual eye and Robbert too for listening to my weekly update during Roti-Monday.
Thanks to the boys of the Azaleastraat: Auke, for providing a desktop and introducing me to TeamViewer - which is indispensable if you have to run four computers. Still, I enjoyed the frequent visits to your place! Also thanks to Yannick for reading my final version extracting the pain points from this study.
Lastly, I would like to give a really big thanks to my friends, who have always given me a safe and fun working environment. First of all, my "study mates", for not taking graduating too seriously and making me laugh a lot! I'd like to thank Vera in particular for being my soulmate in this three years of master and let me prove that "zaakchicks" can be fun!!!
Thanks to the Giants, for rowing the Ringvaart Regatta with me. It was great to have another commitment than solely writing this thesis.
Also a big thanks to Fleur, for being my more or less graduate coach. Your project management skills inspired me and helped me a lot in working through this research.
Lastly, since this study was mainly conducted from home (thank you too, Mark & Hugo), I would like to thank my roommates from the C.P. Tielestraat and Stateway for all the nice study breaks and for forcing me to chill in the evenings.

It may have taken some time and effort, but I am really happy with the outcome. Enjoy reading!

Magali

Supplementary Material to

Investigating potential effects of including root zone storage capacity adaptation on modelled streamflow dynamics in a future changing climate

for obtaining a masters degree in Water Management & Environmental Engineering, TU Delft

Magali Ponds 4355792

Contents

A Supplementary material to Methods

A.1 Method: Process Scheme

	1. BUDYKO	2. WATER BALANCE	3. GEV	4. HBVMODEL
AIM	Project long term mean runoff	Determine future annual maximum root zone storage deficits	Determine the maximum root zone storage capacity for forest and grass	Test the influence of a climate adaptive root zone storage capacity on future modelled streamflow
EXPLANATION	A. Determine observed position of catchment in Budyko space p_{obs} using P_{op} and T_{op} B. Calculate catchment specific parameter $\omega_{obs.}$ C. Find future position p_{fut} using P_{fut}, T_{fut} and ω_{obs} D. Determine runoff coefficient and future long term mean runoff $\bar{Q}_{fut}$	A. Calculate daily effective precipitation timeseries using 300 different I_{max} values B. Calculate daily evapotranspiration timeseries, scaled to long term $\overline{E_R}$ estimate C. Calculate timeseries for cumulative root zone storage deficit D. Make yearly timeseries of annual maximum root zone storage deficits	A. Use Gumble Extreme Value distribution to calulate root zone storage deficit corresponding to return periods of 2 and 20 years for forest and grass respectively B. Select minimum and maximum $S_{r,def}$ values for each vegetation type and timeframe to create parameter ranges C. Correct parameter ranges for potential bias in climate models D. Correct parameter ranges for share of vegetated area in catchment	A. Calibrate (C) model using $1{\cdot}10^6$ Monte Carlo Samples. Select best 300 C parameter sets B. Create Climate-Based (CB) parametersets by replacing Sr,C with Sr,Cl. For each parametersets 10 random samples from the Cl-parameter range are taken, resulting in 3000 parametersets C. Investigate model perfomance for modelling observed streamflow using C- and Cl- parametersets respectively D. Compare modelled future streamflow using Sr,Cl,obs and Sr,Cl,fut, to assess the influence of an climate-adapted root zone storage parameter on runoff projections.
	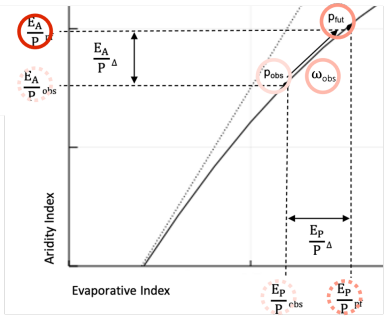	$P_E(t) = P(t) + M(t) - E_T(t) - \frac{dS_i(t)}{dt}$ $\overline{E_R} = \overline{P_E} - \bar{Q}$ $E_R(t) = (E_P(t) - E_I(t)) \cdot \frac{\overline{E_R}}{(\overline{E_P} - \overline{E_I})}$ $S_{R,def}(t) = \min \int_{T_0}^{T_1} (P_E(t) - E_R(t))\, dt$	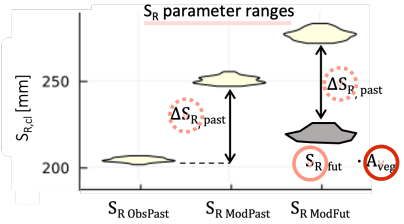	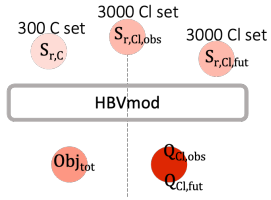
ASSUMPTIONS	• Budyko framework captures long term partitioning of water fluxes • The Fu equation manages to capture catchment specific influences in parameter ω • Catchment specific parameter remains constant over time	• Vegetation dynamicly adapts its root zone to prevailing climate conditions in order to bridge dry spells of a certain return period • 300 I_{max} values have shown to result in a stable range for Sr,def	• Forest root zone adaptation is assumed to bridge droughts with a T_{forest}=20 years, for grass T_{grass}=2 years. • T_{rip}=T_{grass} • Bare zone has static root zone storage, ranging between 1-50mm	• $S_{R,def,frorest} > S_{R,def,grass} > S_{R,def,rip} > S_{R,def,bare}$ • Equifinality is included in Cl-parameter sets by increasing sample size to 10.

Figure S1: Process scheme of method adopted in the research

A.2 Sensitivity analysis of number of I_{max} values used on S_r parameter range

Figure S2 shows the dependency of different I_{max} values on the found S_R parameter ranges for forest and grass respectively. To limit this influence, random samples I_{max} can be used. As can be seen, S_R ranges change when using less than 300 I_{max} values, but remains rather stable when using more than 300 values. 300 different I_{max} values have hence been identified as a threshold for stable parameter range in S_R.

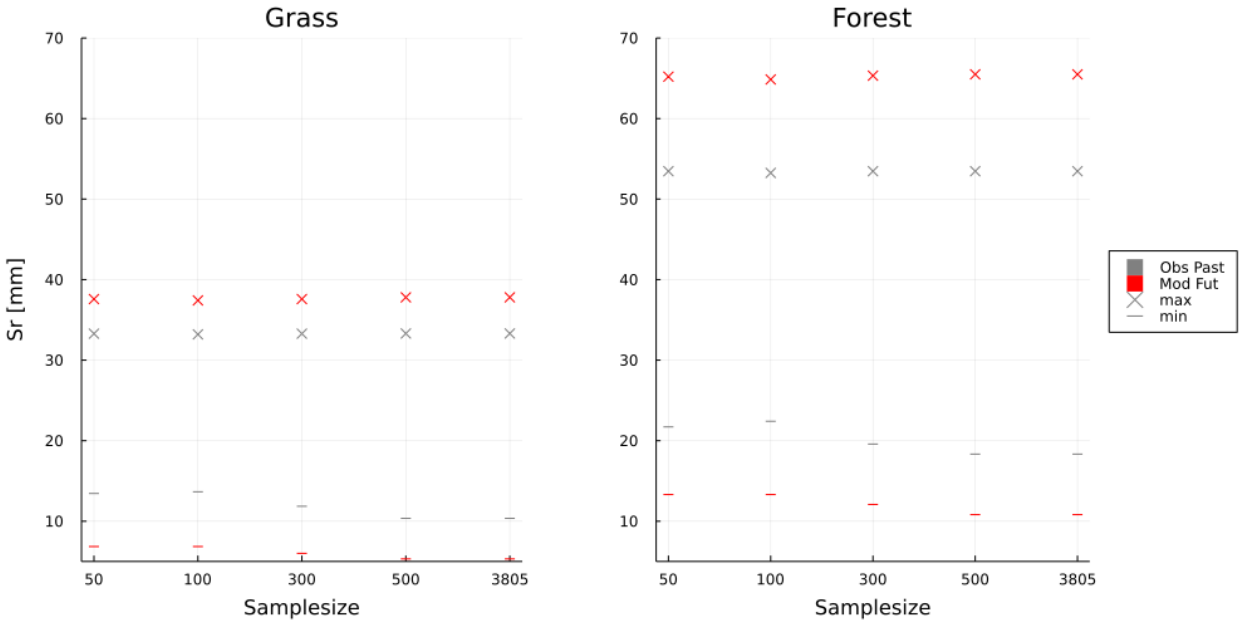

Figure S2: Sensitivity analysis of number of I_{max} samples used on the found spread in water balance estimates of S_R

A.3 Bias correction climate models

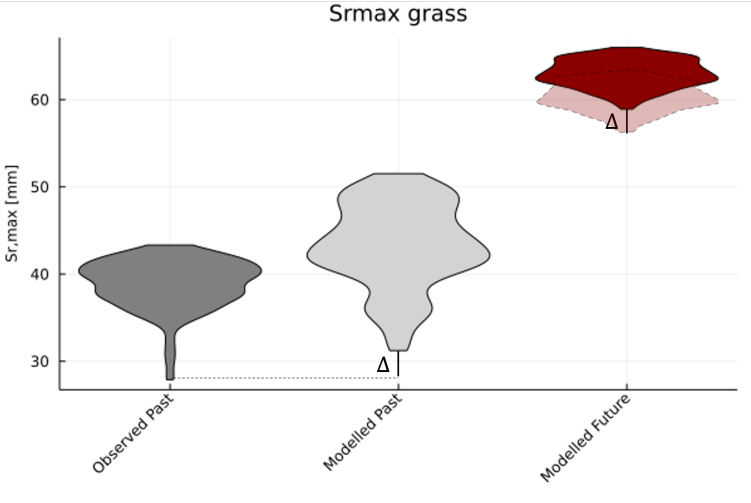

Figure S3: Correction for potential climate biases in modelled Sr parameter ranges

The use of climate model data involves uncertainties and potential biases. To limit this, an ensemble of regional climate model simulations has been deployed. However, a formal correction of climate model data, as it might alter the relations between climate variables[1]. Instead, to account for potential biases in the used climate models, a climate correction has been performed as is proposed in the work of Bouaziz et al.[2] and shown in Equation 1 & Figure S3. Here, the bias is defined as the difference in S_R estimates derived from observed and simulated climate data. It should be noted that observed climate data is considered as the best available estimate of current-day climate conditions. Hence, observed historic S_R estimates are applied in model simulations and modelled future S_R values are scaled accordingly. Hence, for every used Regional Climate Model (RCM) and emission scenario (RCP), the 'bias' in simulated historic storage deficits are subtracted from future storage deficit, derived with RCM simulations.

$$S_{R,cor,fut,min} = S_{R,obs,min} + \Delta(S_{R,mod,fut,min} - S_{R,mod,past,min}) \tag{1}$$

[1] U. Ehret et al. "HESS Opinions "should we apply bias correction to global and regional climate model data?"". In: Hydrology and Earth System Sciences 16.9 (2012), pp. 3391–3404. ISSN: 10275606. DOI: 10.5194/hess-16-3391-2012.

[2] L J E Bouaziz et al. "The importance of ecosystem adaptation on hydrological model predictions in response to climate change". In: Hydrol. Earth Syst. Sci. Discuss. 2021.April (2021), pp. 1–39. ISSN: 1812-2116. URL: https://hess.copernicus.org/preprints/hess-2021-204/%0Ahttps://hess.copernicus.org/preprints/hess-2021-204/hess-2021-204.pdf.

B Supplementary Results

B.1 Catchment mean changes in the Budyko space

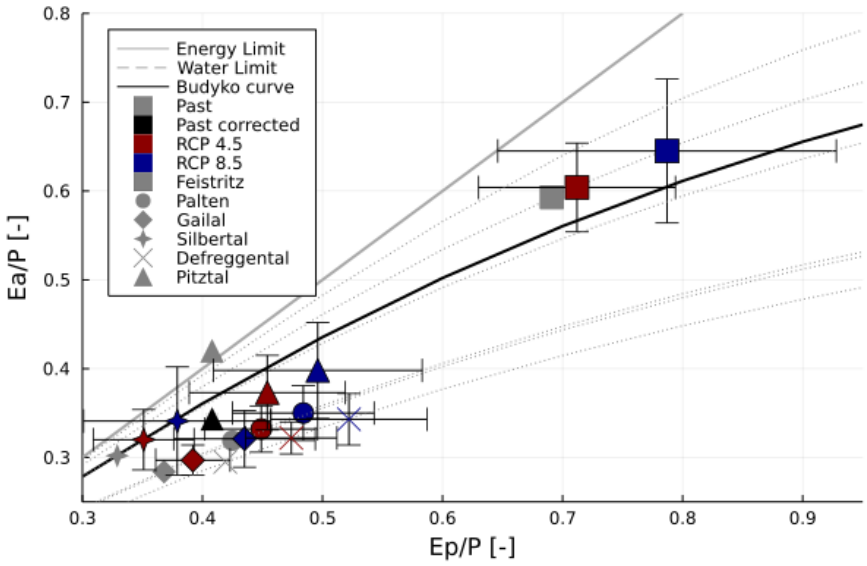

Figure S4: The mean location of the study catchments in the Budyko space in the past and under two emission scenarios at the end of the 21st century. Fu curves are represented by the dashed lines. Error bars indicate minimum and maximum movements, originating from different climate projections.

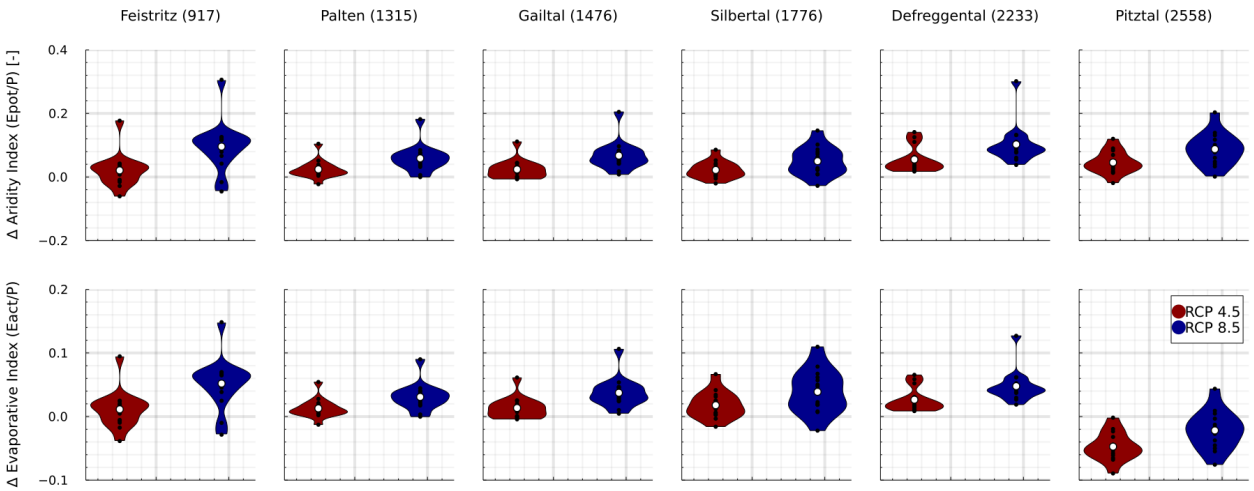

Figure S5: The mean changes in Aridity and Evaporative Index of the study catchments in the past and under two emission scenarios at the end of the 21st century, using 14 climate model.

B.2 Waterbalance estimated parameter ranges of S_r

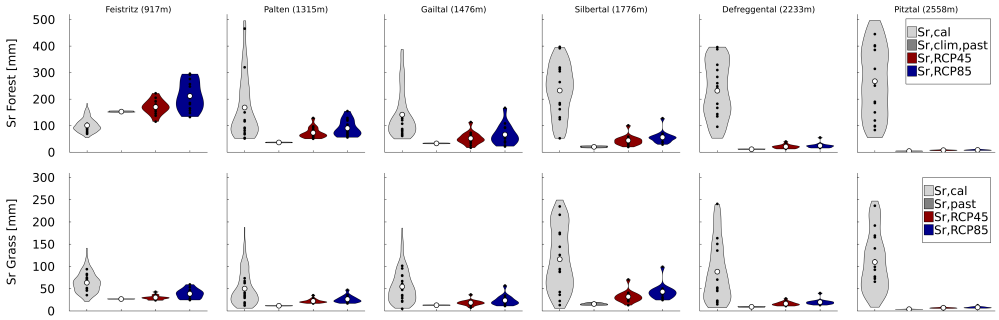

Figure S6: Parameter ranges obtained from calibration (light grey) and from the water-balance method, using observed climate data (grey) and for 14 different RCMs using RCP4.5 (red) and RCP 8.5 (blue)

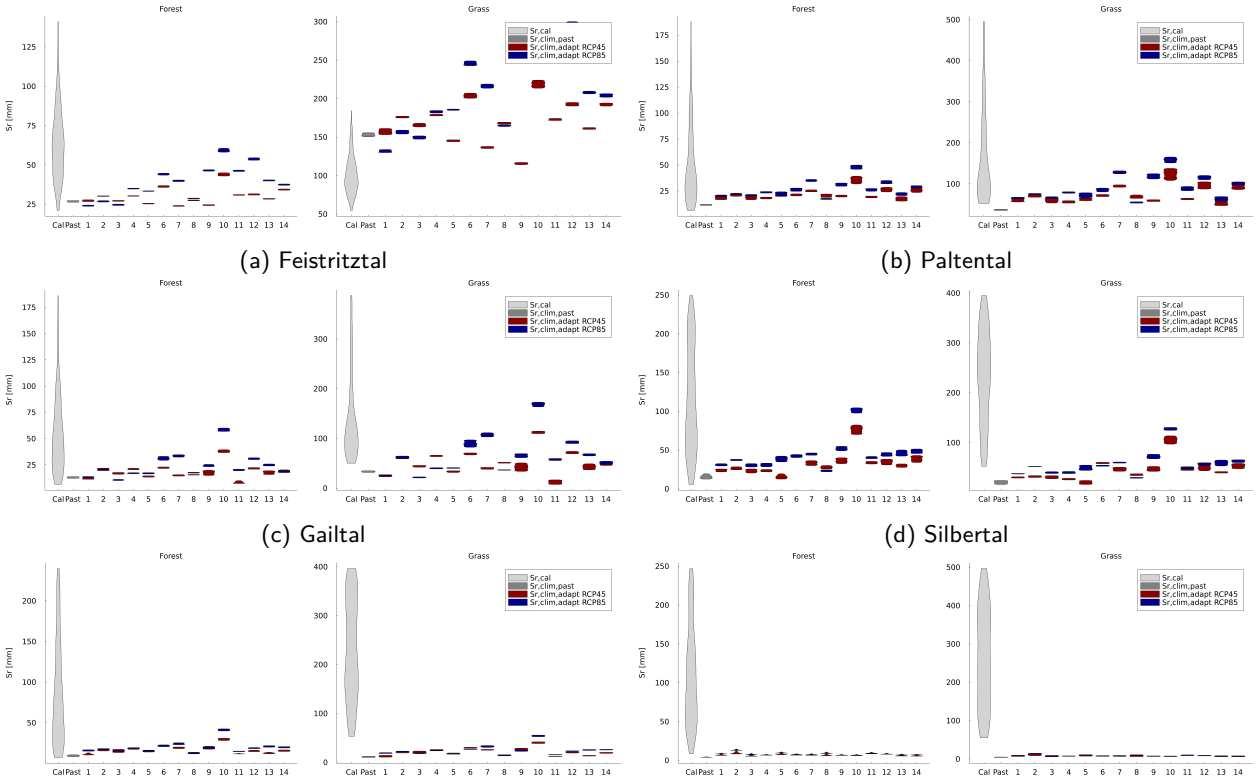

(a) Feistritztal

(b) Paltental

(c) Gailtal

(d) Silbertal

(e) Defreggental

(f) Pitztal

Figure S7: Obtained ranges of root zone storage capacity for each catchment, obtained through calibration (Cal) or computed with the water balance method using respectively observed past (Past) or simulated climate data from 2 RCPs and 14 RCMs (ID numbers)

B.3 Calibration & Evaluation

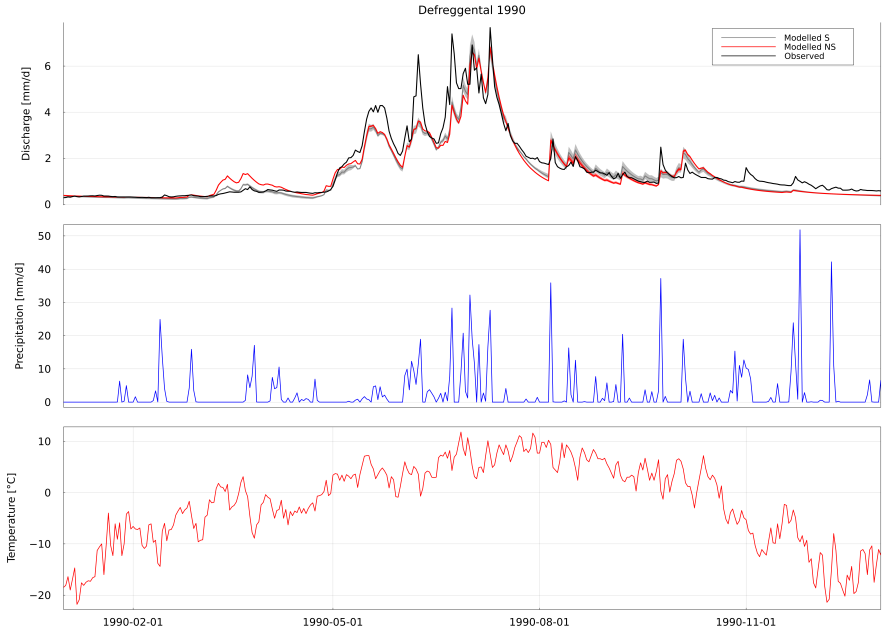

(a)

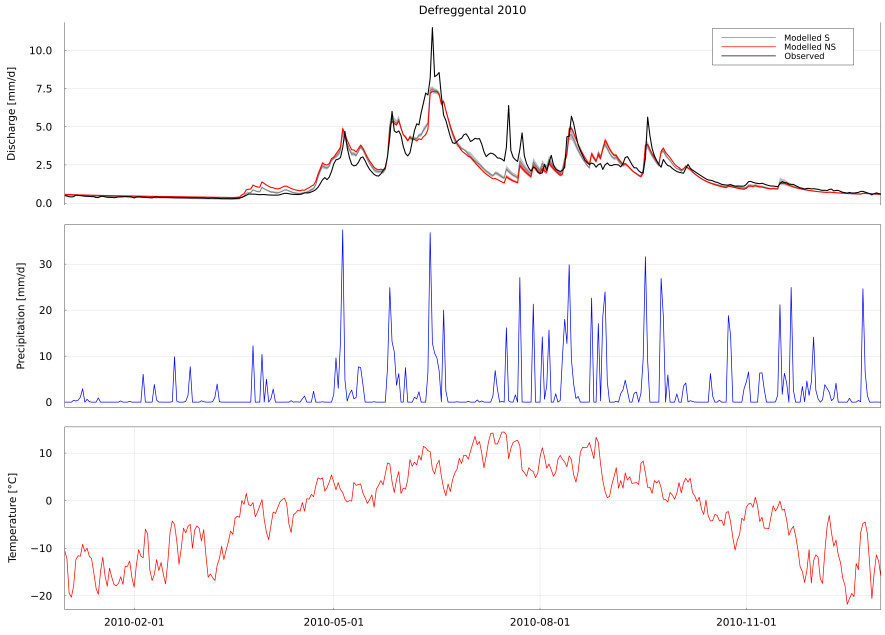

(b)

Figure S9: Comparison of measured and both calibrated and climate-based modelled runoff in the Defreggental, also showing the corresponding temperature and precipitation. The solid lines indicate mean modelled runoff using the best parameter sets, shaded areas show the range of best parameter sets

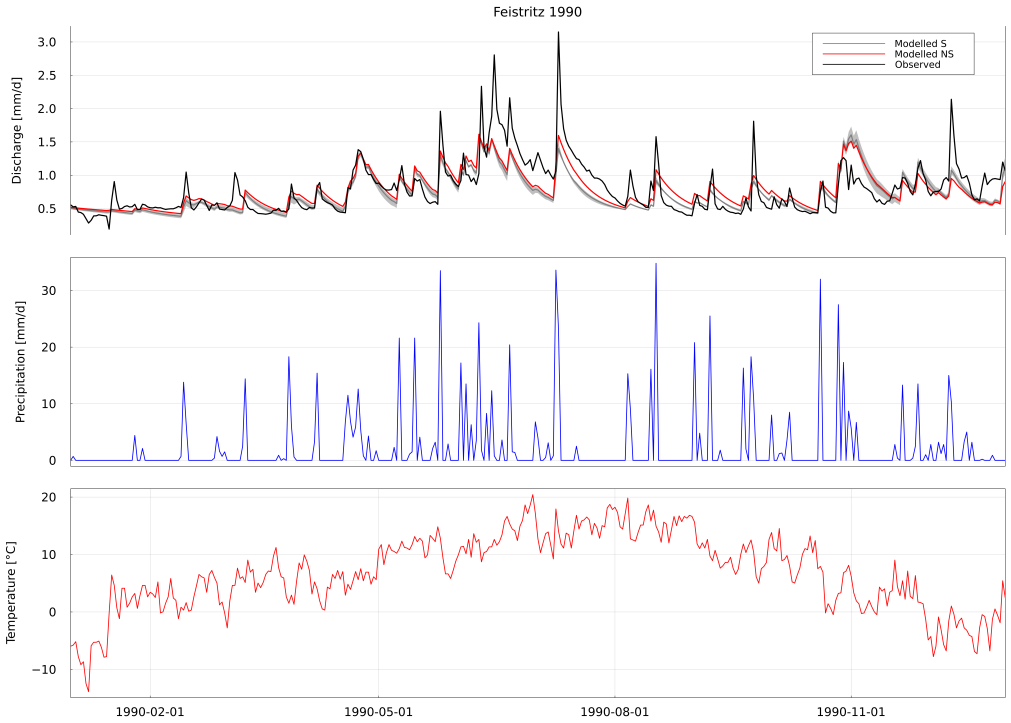

(a)

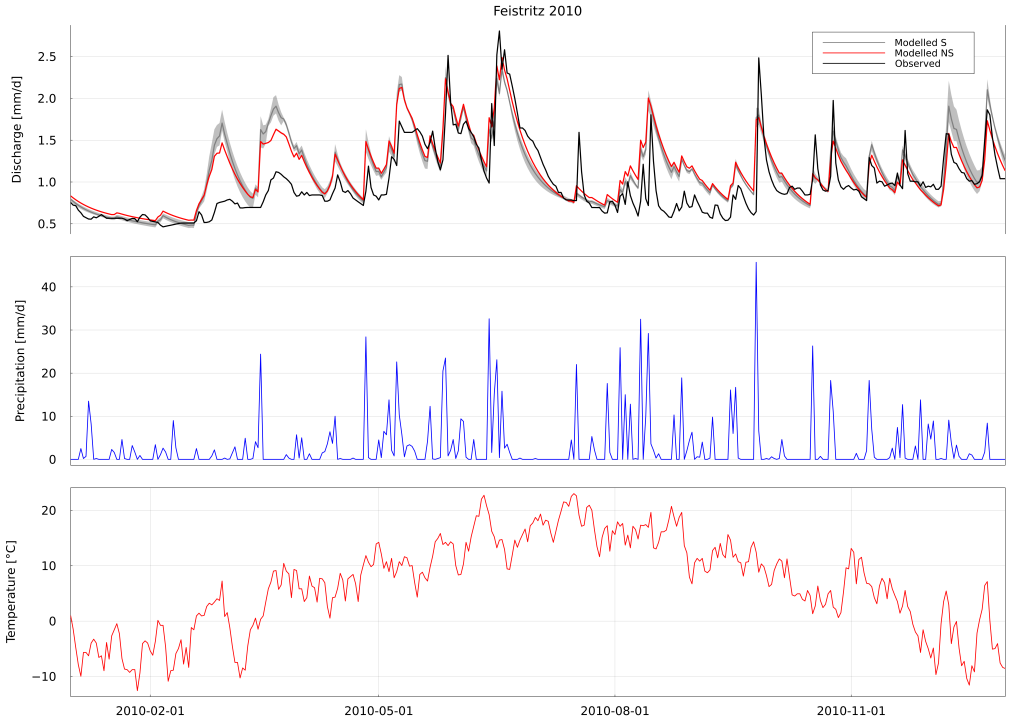

(b)

Figure S11: Comparison of measured and both calibrated and climate-based modelled runoff in the Feistritztal, also showing the corresponding temperature and precipitation. The solid lines indicate mean modelled runoff using the best parameter sets, shaded areas show the range of best parameter sets

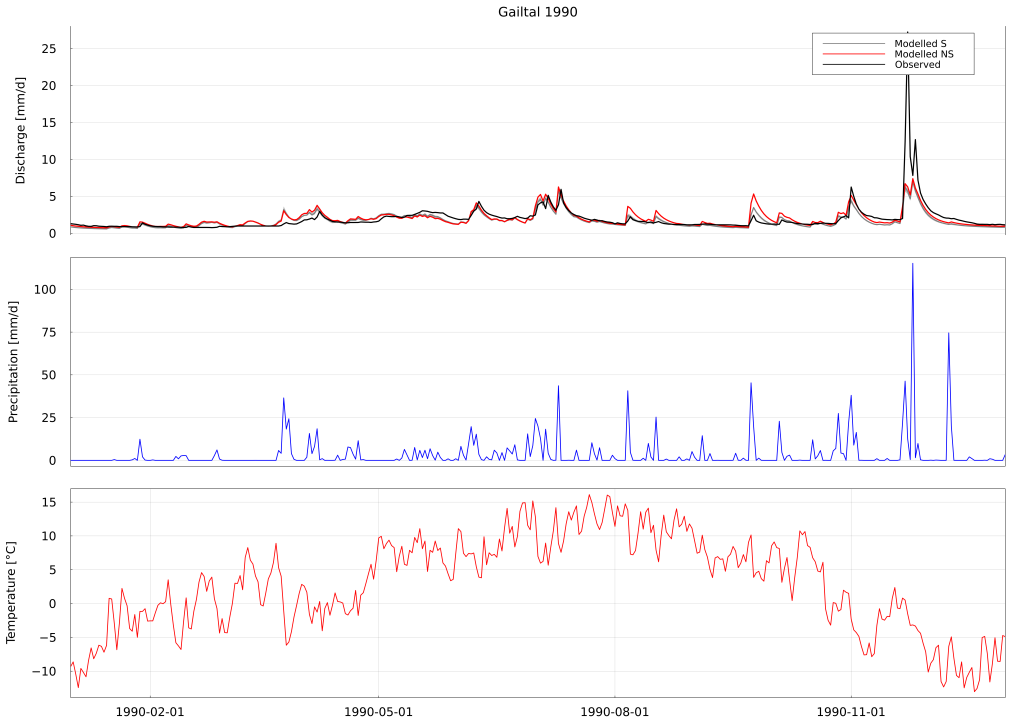

(a)

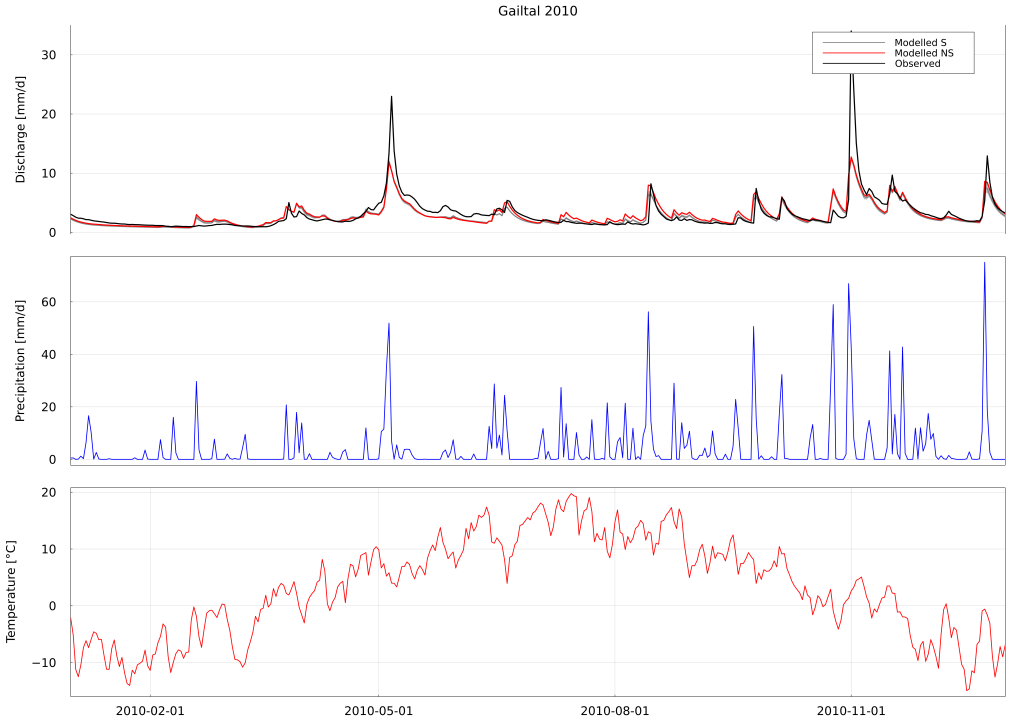

(b)

Figure S13: Comparison of measured and both calibrated and climate-based modelled runoff in the Gailtal, also showing the corresponding temperature and precipitation. The solid lines indicate mean modelled runoff using the best parameter sets, shaded areas show the range of best parameter sets

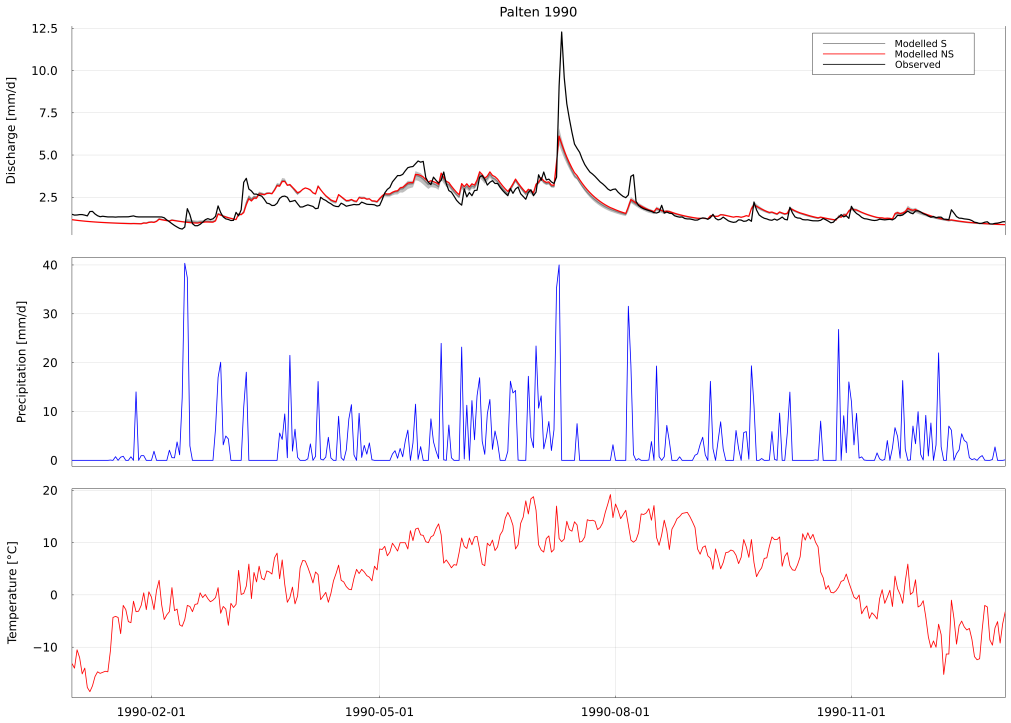

(a)

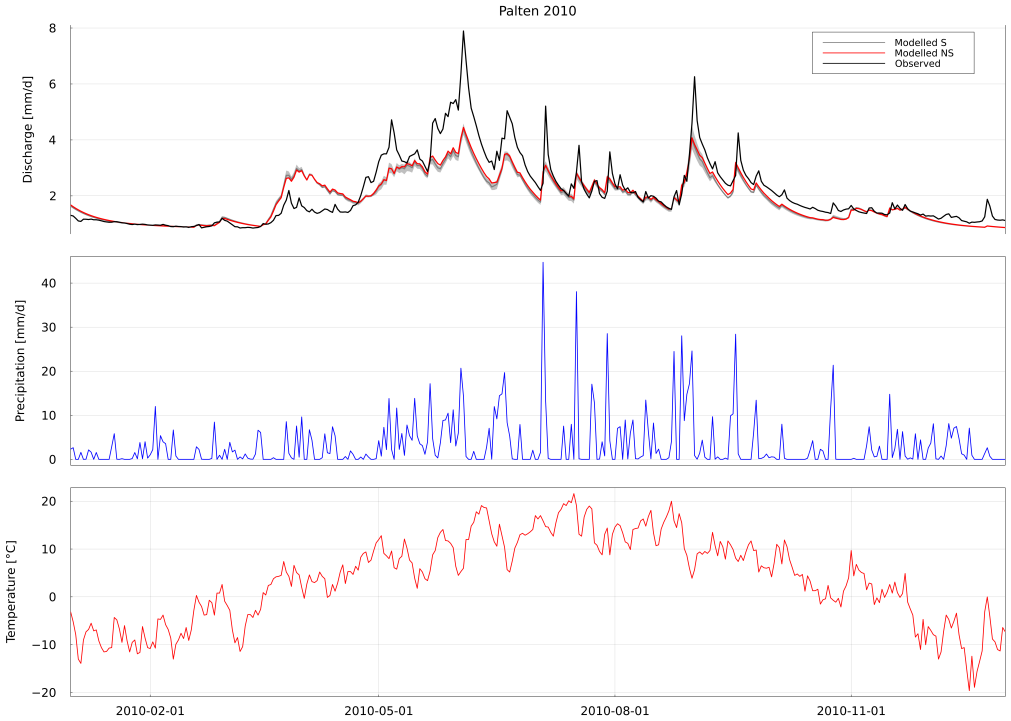

(b)

Figure S15: Comparison of measured and both calibrated and climate-based modelled runoff in the Paltental, also showing the corresponding temperature and precipitation. The solid lines indicate mean modelled runoff using the best parameter sets, shaded areas show the range of best parameter sets

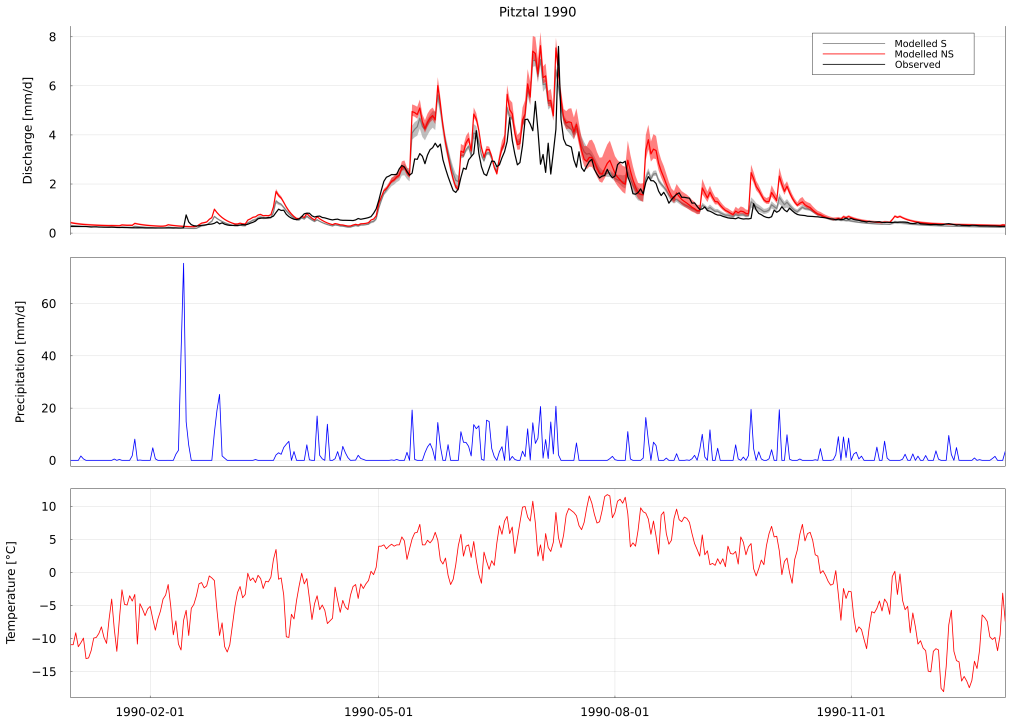

(a)

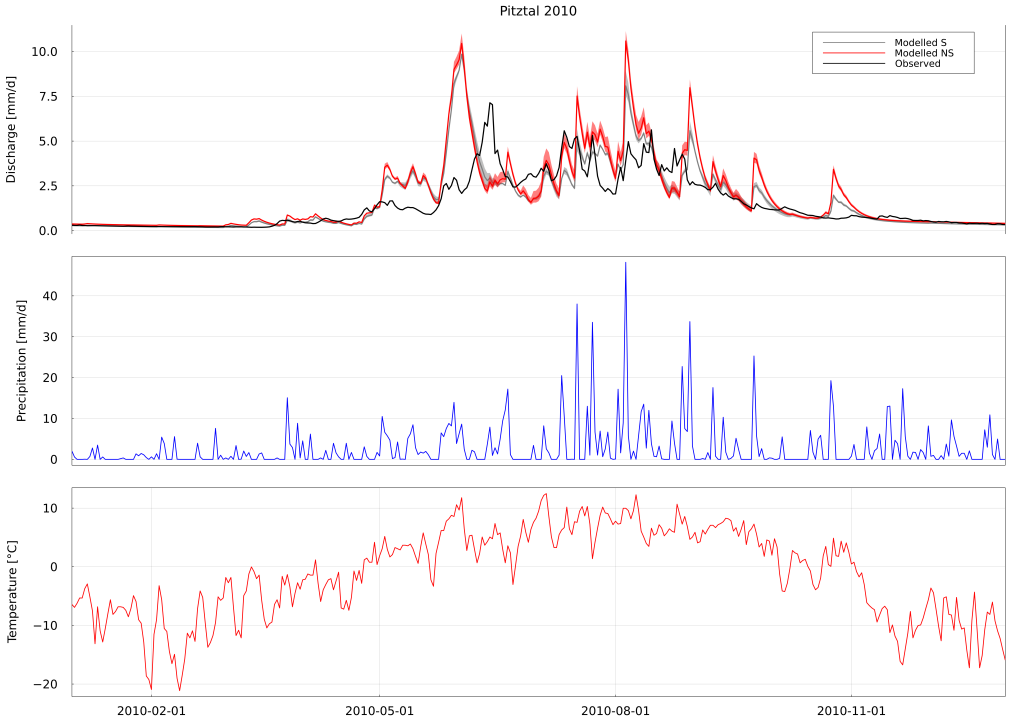

(b)

Figure S17: Comparison of measured and both calibrated and climate-based modelled runoff in the Pitztal, also showing the corresponding temperature and precipitation. The solid lines indicate mean modelled runoff using the best parameter sets, shaded areas show the range of best parameter sets

B.4 Predicted Future Streamflow

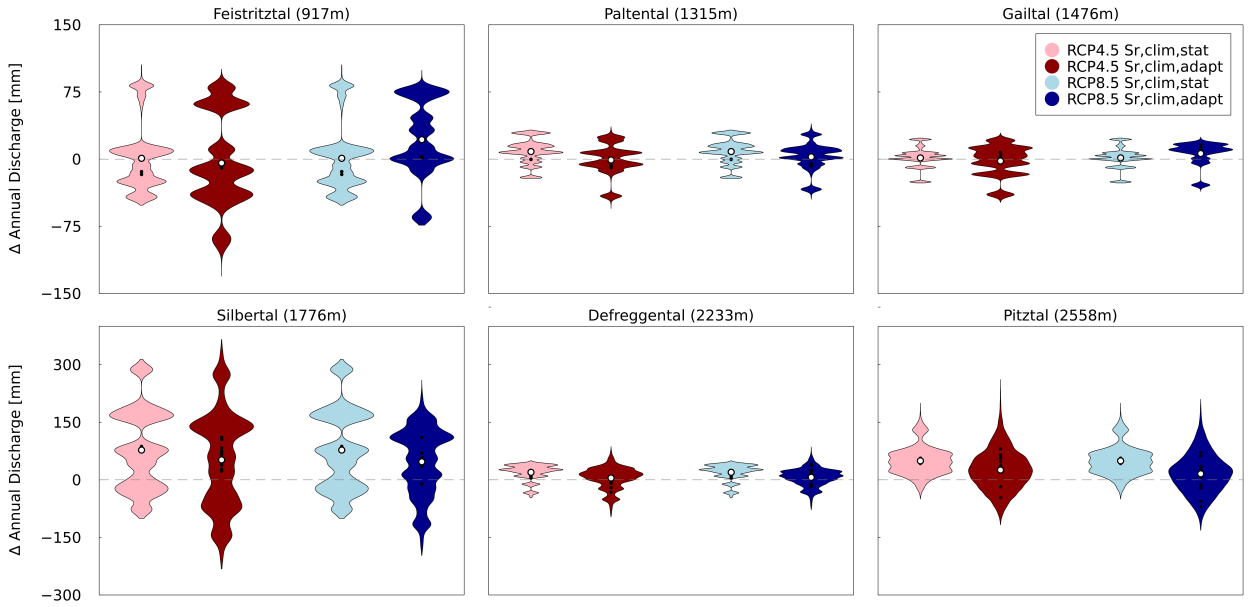

Figure S18: Absolute changes in mean annual discharge for all catchments, using both $S_{R,clim,stat}$ (light) and $S_{R,clim,stat}$ (dark), for all 14 climate simulations and RCPs. RCP 4.5 is coloured in red and RCP 8.5 in blue.

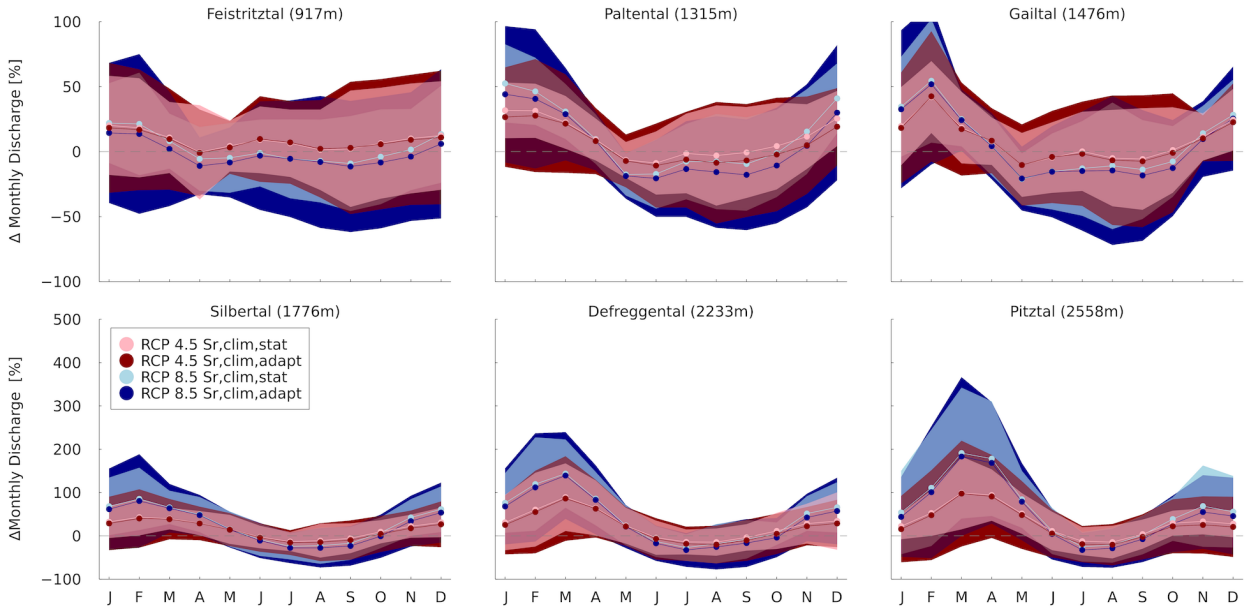

Figure S19: Relative changes in mean monthly discharge, for 14 climate scenarios and 2 RCPs, using the climate-based stationary and adaptive model. Results obtained from models featuring $S_{R,clim,stat}$ and $S_{R,clim,stat}$ are respectively depicted in pink and red for RCP 4.5 and lightblue and blue for RCP 8.5.

Table S1: Simulation mean occurance of average timing of AMF over 30years,±1 std, dates refer to mean date in the past

	Model	Past	Date	RCP 4.5	RCP 8.5	Change RCP 4.5	Change RCP 8.5
Feistritztal	clim,stat	162±10	June 11	163±15	145±30	+1 days	-17days
Feistritztal	clim,adapt	162±10	June 11	165±15	151±26	+3 days	-11days
Paltental	clim,stat	174±9	June 23.	173±19	168±26	-1 days	-6 days
Paltental	clim,adapt	174±9	June 23.	167±20	151±25	-7 days	-23 days
Gailtal	clim,stat	273±22	September 30.	294±15	308±17	+21 days	+35 days
Gailtal	clim,adapt	273±21	September 30.	296±19	307±47	+23 days	+34 days
Silbertal	clim,stat	193±9	July 11.	177±11	170±16	-16 days	-23 days
Silbertal	clim,adapt	193±9	July 11.	174±13	162±19	-19 days	-31 days
Defreggental	clim,stat	196±10	July 14.	191±16	198±20	-5 days	+2 days
Defreggental	clim,adapt	196±10	July 14.	188±16	193±21	-8 days	-3 days
Pitztal	clim,stat	189±7	July 7.	179±11	175±14	-10 days	-14 days
Pitztal	clim,adapt	189±7	July 7.	177±11	172±14	-12 days	-17 days

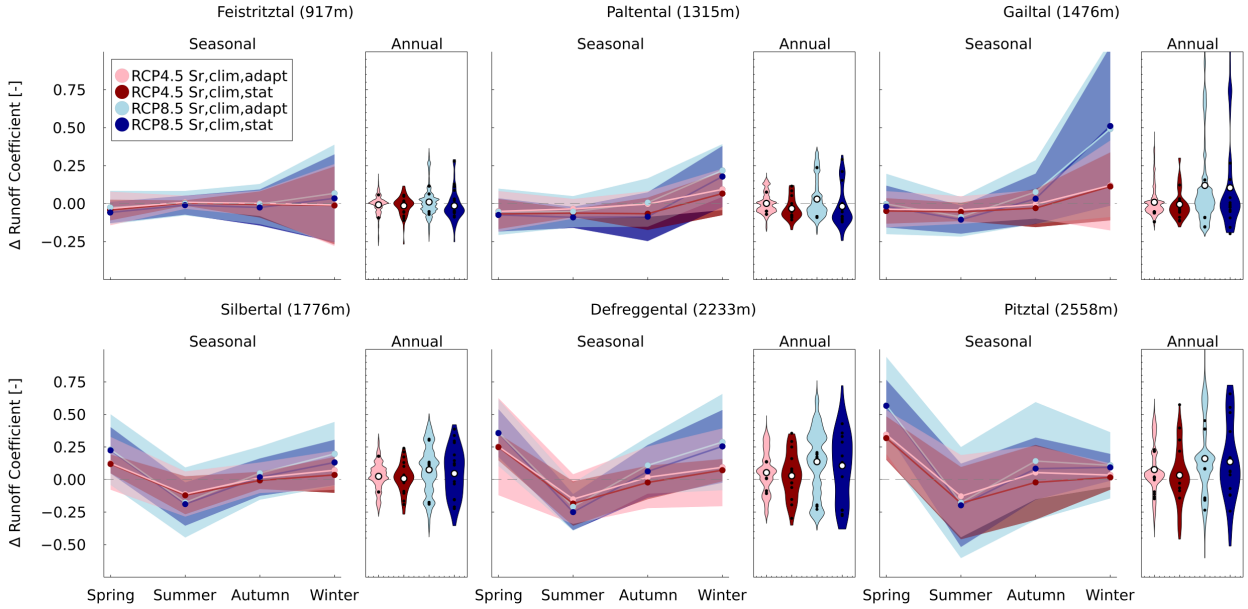

Figure S20: Relative changes in 30 years average seasonal runoff coefficient, for 14 climate scenarios and 2 RCPs, using the climate-based stationary and adaptive model. Results obtained from models featuring $S_{R,clim,stat}$ and $S_{R,clim,stat}$ are respectively depicted in pink and red for RCP 4.5 and light blue and blue for RCP 8.5.

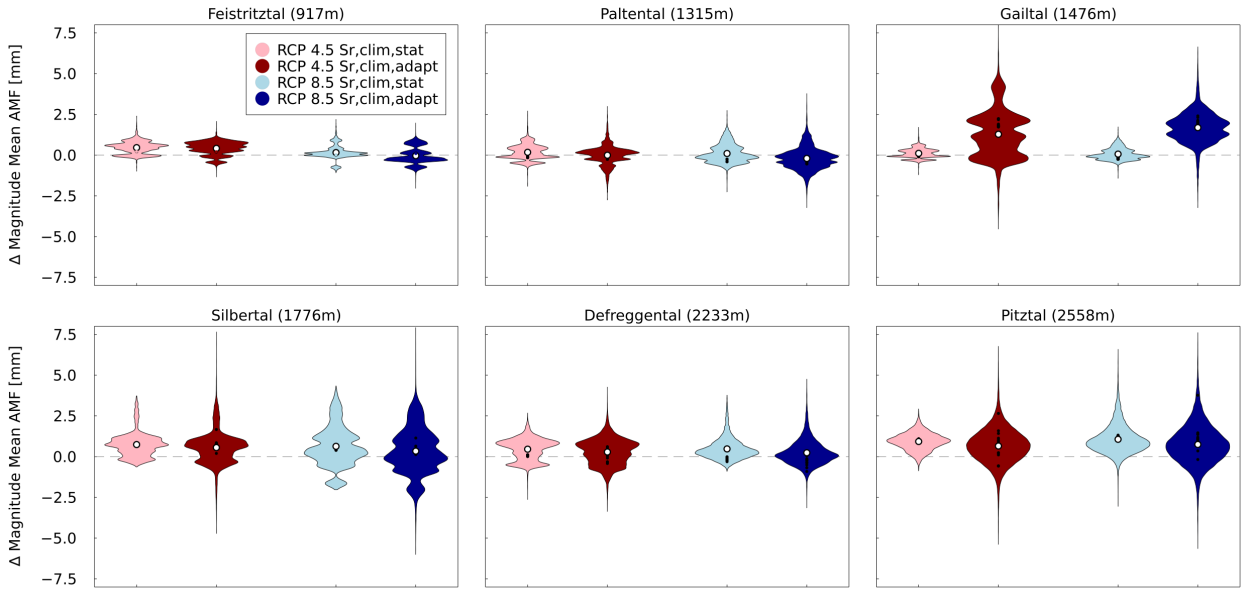

Figure S21: Absolute change of average magnitude of AMF over a 30 year time period, for 14 climate scenarios and 2 RCPs, using the climate-based stationary and adaptive model. Results obtained from models featuring $S_{R,clim,stat}$ and $S_{R,clim,stat}$ are respectively depicted in pink and red for RCP 4.5 and light blue and blue for RCP 8.5.

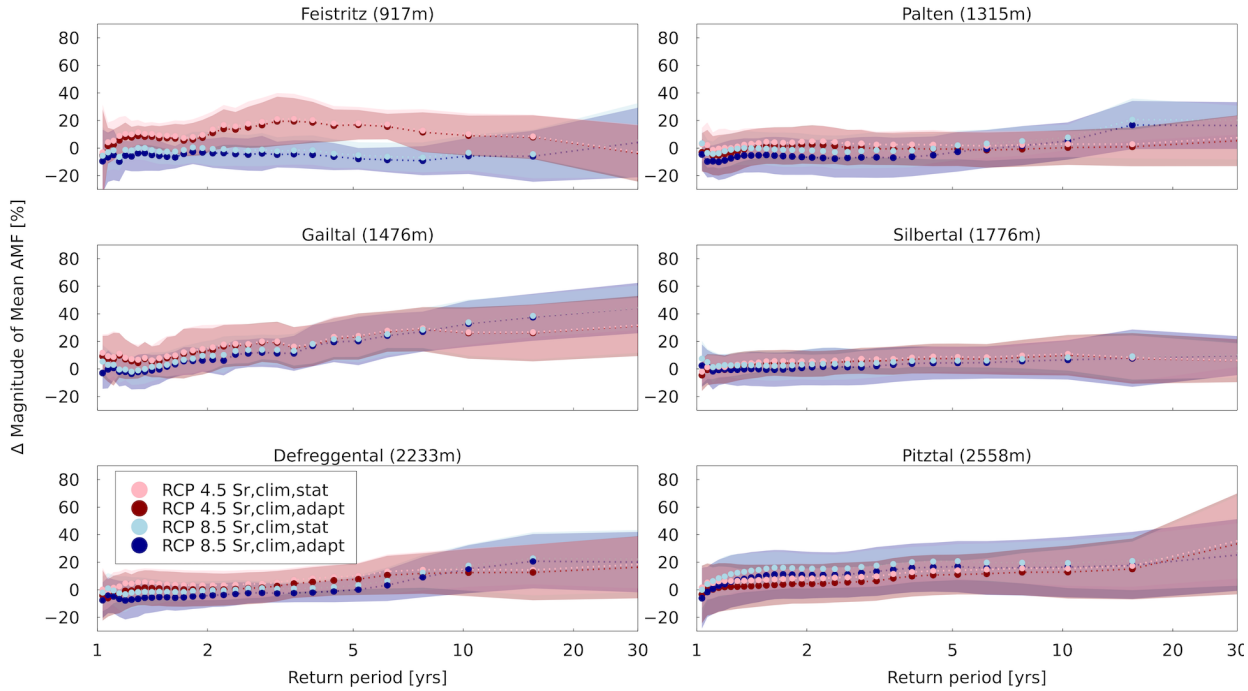

Figure S22: Simulated mean relative change in magnitudes of AMF in relation to the return period, for 14 climate scenarios and 2 RCPs, using the climate-based stationary and adaptive model. Results obtained from models featuring $S_{R,clim,stat}$ and $S_{R,clim,stat}$ are respectively depicted in pink and red for RCP 4.5 and light blue and blue for RCP 8.5.Uncertainty bands of 1 std are shaded and mean lines are used to allow for better visualisation. Note the difference in scale for the Gailtal.

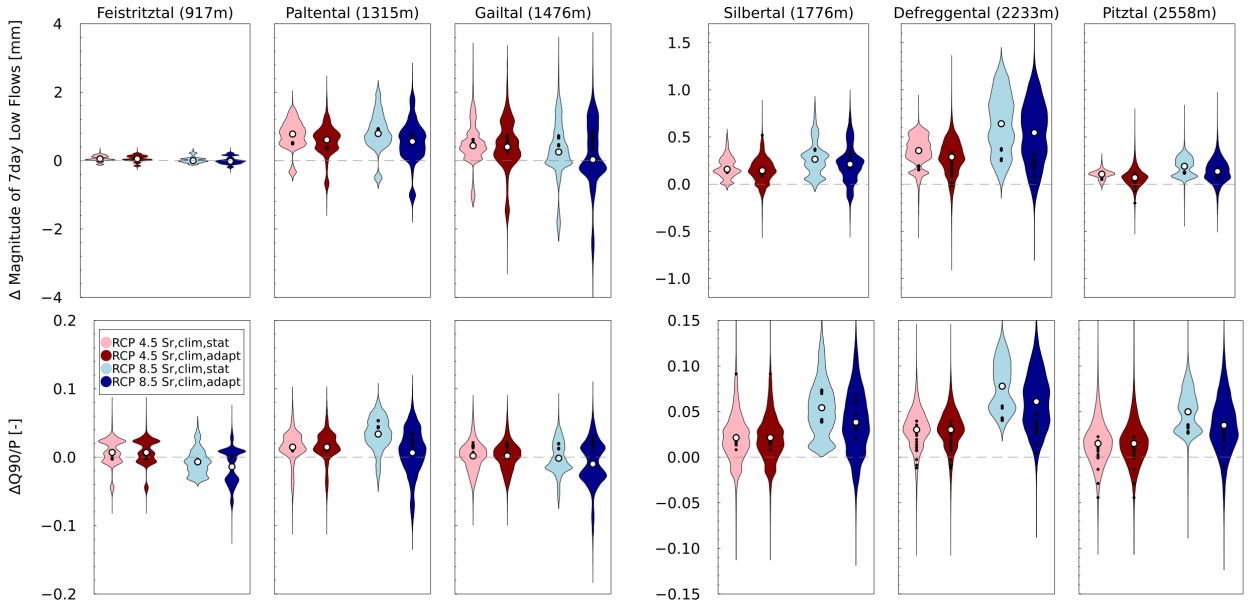

Figure S23: Absolute change of average changes in 7 day consecutive low flows and Q90 to P ratio. Results are averaged over 14 climate scenarios and 2 RCPs. Results obtained from models featuring $S_{R,clim,stat}$ and $S_{R,clim,stat}$ are respectively depicted in pink and red for RCP 4.5 and light blue and blue for RCP 8.5.